LBNL-39128
UC-404

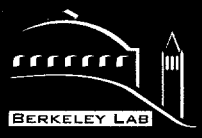

ERNEST ORLANDO LAWRENCE
BERKELEY NATIONAL LABORATORY

In Situ Toughened SiC Ceramics with Al-B-C Additions and Oxide-Coated SiC Platelet/SiC Composites

J. Cao
Materials Sciences Division

August 1996
Ph.D. Thesis

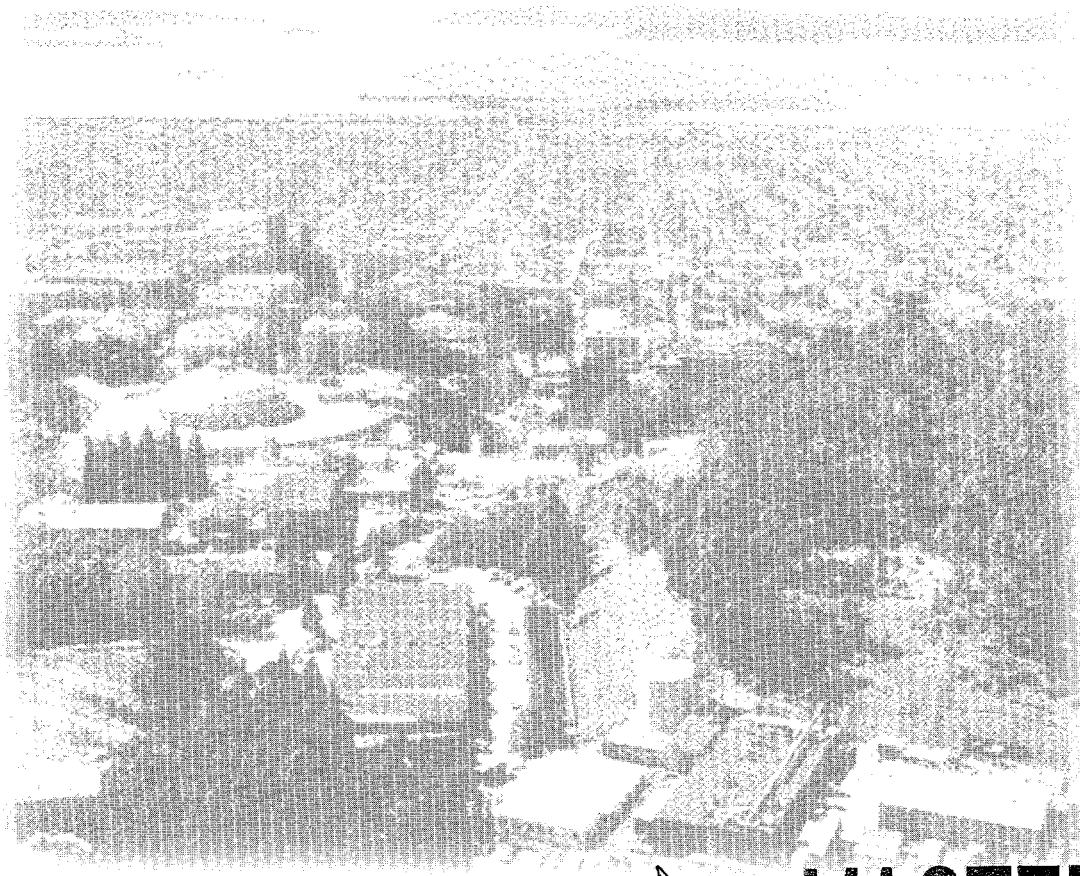

LBNL-39128

In Situ Toughened SiC Ceramics with Al-B-C Additions and Oxide-Coated SiC Platelet / SiC Composites

Jianjun Cao

(Ph.D. Thesis)

Department of Materials Science and Mineral Engineering
University of California, Berkeley
and
Materials Sciences Division
Lawrence Berkeley National Laboratory
University of California
Berkeley, CA 94720-1760

Fall, 1996

Work supported by the Director, Office of Energy Research, Office of Basic Energy Sciences, Materials Sciences Division of the U.S. Department of Energy under Contract No. DE-AC03-76SF00098.

In Situ Toughened SiC Ceramics with Al-B-C Additions and Oxide-Coated SiC Platelet / SiC Composites

by

Jianjun Cao

B.E. (Tsinghua University) 1986
M.Eng. (Tsinghua University) 1988

A dissertation submitted in partial satisfaction of the

requirements for the degree of

Doctor of Philosophy

in

Engineering -- Materials Science and Mineral Engineering

in the

GRADUATE DIVISION

of the

UNIVERSITY of CALIFORNIA, BERKELEY

Committee in charge:

Professor Lutgard C. De Jonghe, Chair
Professor Robert O. Ritchie
Professor Claudia P. Ostertag

Fall 1996

Abstract

In Situ Toughened SiC Ceramics with Al-B-C Additions and

Oxide-Coated SiC Platelet / SiC Composites

by

Jianjun Cao

Doctor of Philosophy in Materials Science and Mineral Engineering

University of California, Berkeley

Professor Lutgard C. De Jonghe, Chair

This work aimed at fabrication and characterization of high toughness SiC ceramics through the applications of *in situ* toughening and SiC platelet reinforcement. The processing-microstructure-property relations of hot pressed SiC with Al, B, and C additions (designated as ABC-SiC) were investigated. Through a liquid phase sintering mechanism, dense SiC was obtained by hot pressing at a temperature as low as 1700°C with 3 wt% Al, 0.6 wt% B, and 2 wt% C additions. These sintering aids also enhanced the β-to-α (3C-to-4H) phase transformation, which promoted SiC grains to grow into plate-like shapes. Under optimal processing conditions, the microstructure exhibited high-aspect-ratio plate-shaped grains with a thin (< 1 nm) Al-containing amorphous grain boundary film.

The mechanical properties of the toughened SiC and the composites were evaluated in comparison with a commercial Hexoloy SiC under identical test conditions.

The R-curve behavior was examined using the strength-indentation load relationship and compared with that directly measured using precracked compact tension specimens. The *in situ* toughened ABC-SiC exhibited much improved flaw tolerance and a significantly rising R-curve behavior. A steady-state toughness in excess of 9 $MPam^{1/2}$ was recorded for the ABC-SiC in comparison to a single valued toughness below 3 $MPam^{1/2}$ for the Hexoloy. Toughening in the ABC-SiC was mainly attributed to grain bridging and subsequent pullout of the plate-shaped grains. The high toughness ABC-SiC exhibited a bend strength of 650 MPa with a Weibull modulus of 19; in comparison, the commercial SiC showed a bend strength of 400 MPa with a Weibull modulus of 6.

Higher fracture toughness was also achieved by the reinforcement of SiC platelets, encapsulated with alumina, yttria, or silica, in a SiC matrix. The coating prevented sintering reaction between the platelets and the matrix, enhanced densification of the composites, and more importantly provided a weak interface which promoted crack deflection and platelet pullout. The composite with alumina-coated platelets in a fine-grained matrix showed higher toughness than the corresponding monolithic material. Coupled toughening from coated-platelet reinforcement and matrix grain bridging resulted in a toughness of 8 $MPam^{1/2}$. However, tailoring the microstructure to achieve coupled toughening was limited by the processing temperature at which the oxide coating remained stable.

In Situ Toughened SiC Ceramics with Al-B-C Additions and Oxide-Coated SiC Platelet / SiC Composites

TABLE of CONTENTS

ACKNOWLEDGMENTS

I would like to express my gratitude to my advisor, Professor Lutgard C. De Jonghe, for his guidance. His remarkable knowledge in many different scientific fields is very inspiring.

My gratitude also goes to Professor Robert O. Ritchie for being the chairman of my Qualifying Examination Committee, for his reviewing and comments on the manuscript, and for his supervision on mechanics in my research. Also to be thanked is Professor Claudia P. Ostertag for being on my Qualifying Examination Committee, reviewing this manuscript, and helpful discussions and comments on my research. Special thanks goes to Dr. Warren J. MoberlyChan for his advise, invaluable discussion on my research, and critically reading part of the manuscript.

Members of the De Jonghe research group and the Ritchie research group, especially Chris J. Gilbert, Mani Gopal, Mark Sixta, Tyrone D. Mitchell, and Jay P. Daniel are thanked for their suggestions, assistance, and friendship. Proofreading and comments on the manuscript by Mani Gopal, Mark Sixta, and Tim Perham are high appreciated. I am also grateful to Brain Dalgleish and James Wu for their assistance on sample preparation at the beginning of this work.

I thank Dr. Warren J. MoberlyChan for providing the TEM pictures and AES spectra; Mr. Chris J. Gilbert for allowing me to use his data and very helpful discussions on toughening mechanisms; Mr. Mark Sixta for providing a specimen for the oxidation study; and Marianna Y. Niu for providing a TEM picture. Regents Fellowship and Earl C. Anthony Fellowship from U. C. Berkeley is acknowledged for providing a stipend plus tuition for the 1995/96 academic year.

So many thanks go to my wife, Yanping Ma, and daughter, Emily L. Cao for their love and support.

PART I. BACKGROUND and OBJECTIVES

CHAPTER 1

BACKGROUND and OBJECTIVES

1-1. SILICON CARBIDE CERAMICS

Advanced structural ceramics provide higher strength and superior oxidation resistance than metals at elevated temperatures, as well as low density and low thermal expansion. Such properties assume a great deal of importance in applications such as advanced aerospace systems, highly efficient power generation systems, and heat exchangers, etc.[1,2] Ceramic components can potentially be used to build automotive engines with high fuel efficiency and less pollution. The major drawback of ceramics, however, is their low fracture toughness, meaning that these materials have a low tolerance to crack-like defects. In particular, silicon carbide generally has better high temperature properties than most other advanced ceramics (e.g., Si_3N_4 and Al_2O_3). Furthermore, the raw materials to make silicon carbide are relatively inexpensive compared to silicon nitride and therefore the final products may be cost-competitive.[3] SiC ceramics have been used in applications where the properties of high hardness, high stiffness, creep resistance, high thermal conductivity, low coefficient of thermal expansion, and good chemical stability are of primary value. The physical and mechanical properties of SiC ceramics are summarized in Table 1-1.[4-9]

Historically, SiC has been used for heating elements and as an abrasive. This material is also suitable for seals, bearings, nozzles, liners, and cutting tools. More

recently, SiC has been applied in electronic packaging and semiconductor processing equipment. The brittle nature of SiC in the conventional form, typically with a fracture toughness of 2-3 $MPam^{1/2}$, however, has limited its widespread application.

In recent years, a considerable amount of work has been devoted to improve the fracture toughness of silicon carbide.[10-14] Essentially, the approaches to produce toughened SiC materials can be divided into *in situ* toughening and particulate reinforcement, with an increased interest nowadays in the former practice.

Table 1-1. Properties of Silicon Carbide (after references 4-9)

Theoretical density (g/cm^3)	3.21
Lattice constant (A)	β-SiC, a = 4.36
	α-SiC, a = 3.08
	c = 2.52 x n*
Young's modulus (GPa)	390 - 460
Hardness (GPa)	24 - 25
Bend strength (MPa)	300 - 1000
Fracture toughness ($MPam^{1/2}$)	2 - 9
Poisson's ratio	0.21
Coefficient of thermal expansion (1/°C)	4.4 - 4.9 x 10^{-6} (mean for 25-2000°C)
Thermal conductivity (W/cm °C)	5 (at 0°C)
Electron bandgap (eV)	3C: 2.2
	6H: 2.9
electron mobility (cm^2/Vs)	3C: 1000
	6H: 200 - 300

* Number of close-packed layers in a unit cell.

1-2. POLYTYPISM in SiC

The Si and C atoms in SiC form strong covalent bonds. The atomic arrangement is based on a tetragonal grouping of carbon atoms with a silicon atom at the center. SiC crystals have layered structures of the tetrahedra; variations in the one-dimensional stacking sequence of the parallel layers produce numerous polytypes. By convention, SiC is classified into the β- and α-phases. The β phase has a cubic lattice, with a stacking sequence in the classical ABC notation as ···ABCABC···. The β phase is also denoted as the *3*C-polytype (Ramsdell notation) where the number 3 stands for 3 layers in a unit cell and the following letter C represents the cubic crystal structure. The α phase can be either hexagonal (H) or rhombohedral (R). Common α phases are 6H with the stacking sequence of ···ABCACB···, 4H with stacking sequence of ···ABAC···, and 15R with stacking sequence of ···ABCBACABACBCACB···. Each unit layer of structure (e.g., "A") represents a closed-packed layer of Si atoms with one C above each Si at a distance of 1.89 angstrom. Therefore, notations such as ···AαBβCγ AαBβCγ··· for the 3C-SiC has also been adapted in the literature. Fig. 1-1 shows 3C(β)-, 2H(α)-, and 6H(α)-SiC unit cells.[15]

Over 40 polytypes in SiC have been identified, some of which contain hundreds of layers in a unit cell with the c-axis lattice parameter (unit cell height) over 100 nm.[15] As the local bonding of Si and C atoms (the first-nearest -neighbor relationship) is the same in all polytypes, the energy differences among them are small. However, the β phase is

generally believed to be the low temperature phase, while the α phase is stable at high temperatures. Practically, the β phase transforms to the α phase at high temperatures, but the α phase does not transform back to the β phase at low temperatures probably due to kinetics. It is also noted that the stability of a polytypes is very sensitive to impurities such as aluminum, boron, and nitrogen. With B and C doping, the β (3C) phase transforms to the α (6H) phase typically at temperatures greater than 2000°C.[3,16] Aluminum lowers the onset temperature of the phase transformation.[8,17,18] In this study, as will be shown later, 3C-SiC with 3 wt% Al-0.6 wt% B-2 wt% C additions was found to begin transforming to 4H-SiC at a temperature as low as 1700°C.

As the energy differences among the various stacking sequences are small, stacking faults and microtwins are common in SiC single crystals and powders. Typically these planar faults form on one set of the close-packed {111} planes in the β phase and parallel to the basal plane in the α phase.

1-3. SYNTHESIS of SiC

Silicon carbide does not exist in large quantities in nature. It was accidentally discovered in 1891 by E. G. Acheson, who latter developed a method to synthesize SiC powder.[5] A mixture of silica and coke were electrically heated to very high temperatures (~2600°C at the core) to produce SiC chiefly by the chemical reaction:

$$SiO_2 + 3\ C \rightarrow SiC + 2\ CO \qquad (1\text{-}1)$$

The product was then ground, refined, and classified to produce SiC powders for a variety of applications.

Acheson's method has been used in mass-production for many years, and is still the major technique to produce SiC powders on commercial scales. α-SiC is obtained by processing at high temperatures (typically 2200°C to 2600°C). Fine β-SiC powder is synthesized by reacting a mixture of high-purity silica powder and carbon black in the temperature range of 1500-1800°C. Sol-gel methods have been used to prepare a uniform mixture of silicon and carbon; after reaction at high temperatures, high quality SiC powders are made.[20-22]

Gas phase synthesis routes produce fine, pure SiC powder.[3, 23-25] SiH_4 or $SiCl_4$ reacts with hydrocarbons such as CH_4, often in the presence of a plasma, to produce SiC powders by reactions such as the following:

$$SiCl_4 + CH_4 \rightarrow SiC + 4\ HCl \qquad (1\text{-}2)$$

Thermal decomposition of CH_3SiCl_3, $(CH_3)_4Si$, or polycarbosilane forms SiC by reactions such as:

$$CH_3SiCl_3 \rightarrow SiC + 3\ HCl \qquad (1\text{-}3)$$

Single crystal SiC in dimensions of millimeters can be synthesized by the Acheson's method. Larger single crystals are made by sublimation of high quality polycrystalline SiC and condensation on a seed.[26,27] Polished SiC wafers up to 60 mm in diameter were commercially available in 1993.[28] Chemical vapor deposition (CVD) homoepitaxial SiC films on the (0001) basal plane of 6H substrates have been well studied. The "off-axis" angle played an essential role in the growth of films at relatively low temperatures, such as 1400°C.[29] At relatively large tilt angles, grown films assumed the 6H stacking sequence of the substrate. At smaller tilt angles, nucleation of 3C-SiC occurred on the terraces and formed 3C-SiC films.

1-4. PROCESSING SiC CERAMICS

Although the strong covalent nature of the Si-C bond is responsible for the high elastic modulus, hardness, strength, and chemical stability of SiC, this covalent bond is also responsible for the processing difficulties of this material. Since pure SiC can't be densified at any temperature even with an applied external pressure, the additions of sintering aids are necessary for densification. The thermodynamic driving force for sintering is to eliminate free surfaces in the powder compact at the expense of generating grain boundaries. Densification proceeds by transporting mass from areas of particle contact to the pores via bulk and/or grain boundary diffusion. Evaporation-condensation and surface diffusion, on the other hand, cause powder coarsening and pore growth. In pure SiC, the difference in thermodynamic free energy between surfaces and grain boundaries is small and so is the driving force for sintering. Kinetically, the self-diffusivity

of SiC is low. As a consequence, sintering additives have to be used that raise the driving force for densification and/or promote mass transport. The most commonly used sintering aids are boron-carbon, first discovered by Prochazka in 1975.[30,31] Commercial SiC materials are typically doped with B and C. The carbon addition is believed to reduce the native oxide present on the SiC powders, thereby raising the surface energy; the boron is expected to segregate at the grain boundaries and therefore lowers the grain boundary energy. Tanaka pointed out that a certain amount of carbon was required regardless of the oxygen content in the starting SiC powders, suggesting that carbon might also participate in lowering the grain boundary energy.[32] The additions of B and C together would significantly raise the driving force for sintering. Furthermore, amorphous grain boundary films were observed in B and C doped SiC.[32,33] Grain boundary diffusivity would be expected to increase in the presence of an amorphous grain boundary film. Many reports in the literature, however, claimed that the grain boundaries in B and C doped SiC were free of amorphous materials. With the additions of B and C, SiC was typically sintered at temperatures greater than 2000°C.

To overcome the sintering difficulties in the solid state, liquid-phase sintering techniques are developed to fabricate SiC ceramics. Sintering additives, such as Al_2O_3, Y_2O_3, MgO, or a combination of these oxides, are used to form a liquid phase at the sintering temperatures, providing a path for enhanced mass transport. The liquid-phase sintering of SiC can be described by a solution-reprecipitation process.[34] During heating, reaction of the sintering additives with the native oxide on the SiC particles forms a liquid. For example, Fig. 1-2 shows an equilibrium phase diagram among Al_2O_3-Y_2O_3- SiO_2,

where the lowest melting point of an eutectic is ~ 1350°C. With only a small amount of SiO_2, a liquid forms at temperatures of 1700-1800°C[35] (Oxide-added SiC are typically sintered at temperatures ≥ 1850°C[10,11]). During liquid-phase sintering, initial densification proceeds by particle rearrangement induced by the capillary forces from the newly formed liquid. Further densification is achieved by a solution-reprecipitation mechanism. Due to the capillary pressure, the material at the points of particle contact dissolves into the liquid-phase and precipitates out at the pores. The densification rate is controlled by the amount of the liquid phase, the wettability of the liquid on SiC, the solubility of SiC in the liquid, and size of the SiC particles.

The additions of aluminum and its compounds in SiC also promote densification by the liquid phase sintering mechanism.[36,37] The combination of Al, B, and C has been extremely effective, providing enhanced densification particularly at lower sintering temperatures.[38] The phase relations among SiC-Al_4C_3-B_4C are shown in Fig. 1-3, where the $Al_8B_4C_7$ is a liquid at 1800°C.[39]

1-5. OBJECTIVES of THIS STUDY

The objectives of this study are to fabricate and characterize high toughness silicon carbide materials. Two approaches are taken, namely *in situ* toughening and reinforcement with coated-SiC platelets.

There has been considerable interest in recent years to toughen SiC ceramics. *In situ* toughened SiC materials were developed to achieve a microstructure akin to that of toughened Si_3N_4.[3,4] Through the additions of large amounts of Al_2O_3-Y_2O_3 (YAG)[10,40] or Al_2O_3,[11,41] SiC was sintered under carefully controlled atmospheres to obtain a microstructure containing plate-like grains. These materials exhibited toughness twice that of conventional B and C doped SiC. The processing difficulties, however, caused poor reproducibility of these oxide-containing toughened materials. In addition, the SiC ceramics with substantial amounts of YAG displayed poor strength properties.[10] It was also demonstrated that TiB_2[42] and TiC[13,43] particle reinforcement in SiC raised the fracture toughness to ~ 6 $MPam^{1/2}$. These composites utilized the coefficient of thermal expansion (CTE) mismatch to generate a compressive hoop stress and a tensile radial stress around the particles, causing crack deflection and an increase in fracture toughness. However, at elevated temperatures the internal stresses were relieved by creep, with a corresponding degradation of the mechanical properties.[44]

In this study, *in situ* toughened SiC was prepared by hot pressing with Al, B, and C additions. Optimization of the processing conditions was aimed at producing high-aspect-ratio grains with weak grain boundaries. The sintering additives were chosen to obtain full densification at relatively low temperatures and to promote the β-to-α phase transformation. Formation of the α phase, with a hexagonal crystal structure, caused growth of highly elongated grains. An amorphous grain boundary phase was the by-product of liquid-phase sintering. As the Al, B, and C were added in relatively low

concentrations compared to the YAG-doped SiC, high toughness and high strength were expected to be achieved simultaneously. Sintering behaviors, microstructural development and control, mechanical properties, and oxidation behavior were studied, with an emphasis on the understanding of processing-microstructure-property relationships.

SiC composites reinforced with oxide-encapsulated SiC platelets were also investigated with the aim to achieve high toughness. The SiC platelet was an ideal reinforcing phase to provide matching CTE and apparent chemical compatibility. Without a protective barrier, however, exaggerated growth of the platelets and strong bonding between the matrix and the platelets might occur. Therefore, fabrication of useful SiC platelet/SiC composites required a means of protecting the platelets. Production of an interfacial phase could protect the integrity of the platelets during sintering and hopefully achieve a weak bonding between the platelets and the matrix. A weak interface would promote crack deflection and/or debonding and pullout. The isolation of the platelets from the matrix was accomplished by the encapsulation of the platelets with an appropriate oxide prior to incorporation in the β-SiC powder (matrix). A slurry coating technique was used to coat the platelets with alumina or yttria. In addition to the reinforcement of a fine-grained β-SiC matrix with oxide-coated SiC platelets, efforts were also made to combine the toughening effects from platelet reinforcement and *in situ* toughening in the matrix.

1-6. REFERENCES

[1]E. G. Butler and M. H. Lewis, "Prospects For Ceramics In Airborne Gas Turbine Engines," 4th International Symposium on Ceramic Materials and Components for Engines, Ed. R. Carlsson, T. Johansson, and L. Kahlman, Elsevier Applied Science, pp. 32-49, 1992.

[2]H. E. Helms and P. J. Haley, "Emerging Ceramic Components For Automotive Gas Turbines," Third International Symposium on Ceramic Materials and Components for Engines, Ed. V. J. Tennery, pp. 1347-64, 1988.

[3]M. Srinivasan, "The Silicon Carbide Family of Structural Ceramics," in Structural Ceramics, Edited by J. B. Wachtman, Jr., Treatise on Materials Science and Technology, Vol. 29, pp. 99-159, Academic Press, Inc., 1989.

[4]Y. Inomata, "Crystal Chemistry of Silicon Carbide," in Silicon Carbide Ceramics--1, Edited by S. Somiya and Y. Inomata, Elsvier Applied Science, NY, NY, pp.1-11, 1991.

[5]K.Yamada and M. Mohri, "Properties and Applications of Silicon Carbide Ceramics," in Silicon Carbide Ceramics--1, Edited by S. Somiya and Y. Inomata, Elsvier Applied Science, NY, NY, pp.13-44, 1991.

[6]Morton Advanced Materials, "CVD Silicon Carbide," Technical Bulletin #107, 1994.

[7]J. A. Powell, P. G. Neudeck, L. G. Matus, and J. B. Petit, "Progress in silicon carbide semiconductors technology," in Wide Band Gap Semiconductors, MRS Symposium Proceedings (Boston, Massachusetts, 1991), Ed. by T. D. Moustakas, J. I. Pankove, and Y. Hamakawa, vol. 242, p. 495-505.

[8]J. J. Cao, W. J. MoberlyChan, L. C. De Jonghe, C. J. Gilbert, and R. O. Ritchie, "*In Situ* Toughened Silicon Carbide With Al-B-C Additions," J. Am. Ceram. Soc., **79** [2] 461-69 (1996).

[9]G. V. Srinivasan, S. K. Lau, and R. S. Storm, "High Temperature Hexoloy™ SX Silicon Carbide, Final Report," $ORNL_{91}$-SG341/1, (1991).

[10]N. P. Padture and B. R. Lawn, "Toughness Properties of a Silicon Carbide with an *in situ* Induced Heterogeneous Grain Structure," J. Am. Ceram. Soc., 77 [10] 2518-22 (1994).

[11]K. Suzuki, "Pressureless-Sintered Silicon Carbide with Addition of Aluminum Oxide," in Silicon Carbide Ceramics--2. Edited by S. Somiya and Y. Inomata, Elsvier Applied Science, NY, NY, pp.162-82, (1991).

[12]S. S. Shinozaki, "Unique Microstructural Development in SiC Materials with High Fracture Toughness," MRS Bulletin, **20** [2] 42-5 (1995).

[13]G. Wei and P. Becher, "Improvements in Mechanical Properties in SiC by the Addition of TiC Particles," J. Am. Ceram. Soc., **67** [8] 571-74 (1984).

[14]Y. Ohya, M. J. Hoffmann, and G. Petzon, "Sintering of *in-situ* Synthesized SiC-TiB_2 Composites with Improved Fracture Toughness," J. Am. Ceram. Soc., **75** [9] 2479-83 (1992)

[15]A. R. Verma and R. Krishna, Polymorphism and Polytypism in Crystals, John Wiley and Sons, Inc., (1966).

[16]A. H. Heuer, G. A. Fryburg, L. U. Ogbuji, T. E. Mitchell, and S. Shinozaki, "$\beta \rightarrow \alpha$ Transformation in Polycrystalline SiC: I, Microstructural Aspects," J. Am. Ceram. Soc., **61** [9-10] 406-12 (1978).

[17]S. Shinozaki, J. Hangas, K. Maeda, and A. Soeta, "Enhanced Formation of 4H Polytype in Silicon Carbide Materials," in Silicon Carbide'87, J. D. Cawley and C. E. Semler Ed., Ceramic Transactions, Vol. 2, pp. 113-21, (1987).

[18]R. M. Williams, B. N. Juterbock, S. Shinozaki, C. R. Peters, and T. J. Whalen, "Effects of Sintering Temperatures on the Physical and Crystallographic Properties of β-SiC," Am. Ceram. Soc. Bull., **64** [10] 1385-89 (1985).

[19]Y. Tajima and W. D. Kingery, "Solubility of Aluminum and Boron in Silicon Carbide," J. Am. Ceram. Soc., **65** [2] C27-29 (1982).

[20]D. A. White, S. Oleff, R. D. Broyer, P. A. Budinger, and J. R. Fox, "Preparation of Silicon Carbide From Organosilicon Gels: I, Synthesis and Characterization of Precursor Gels," Adv. Cer. Matls., **2** [1] 45-52 (1987).

[21]D. A. White, S. Oleff, and J. R. Fox, "Preparation of Silicon Carbide From Organosilicon Gels: II, Gel Pyrolysis and SiC Characterization," Adv. Cer. Matls., **2** [1] 53-59 (1987).

[22]J. Y. Choi, D. K. Kim, and C. H. Kim, "Synthesis of Monodisperse, Spherical Si_3N_4 / SiC Composite Powder from Alkoxides by Sol-Gel Process and Heat Treatment," Paper No. SVIIP-9-96, 98th Annual Meeting of the American Ceramic Society, Indianapolis, Ind, 1996.

[23]M. Endo and N. Urasato, "Preparation and Sintering Properties of Ultrafine Silicon Carbide Powder Obtained by Vapor Phase Reaction," in Silicon Carbide Ceramics--1, Edited by S. Somiya and Y. Inomata, Elsvier Applied Science, NY, NY, pp.119-147, 1991.

[24]J. Hojo, "Sintering Behavior of Ultrafine Silicon Carbide Powder," in Silicon Carbide Ceramics--1, Edited by S. Somiya and Y. Inomata, Elsvier Applied Science, NY, NY, pp.149-168, 1991.

[25]T. Hirai and M. Sasaki, "Silicon Carbide Prepared by Chemical Vapor Deposition," in Silicon Carbide Ceramics--1, Edited by S. Somiya and Y. Inomata, Elsvier Applied Science, NY, NY, pp.77-98, 1991.

[26]Y. M. Tairov and V. F. Tsvetkov, "Investigation of growth progress of ingots of silicon carbide single crystal," J. Crystal Growth, 43 (1978) 209-12.

[27]D. L. Barrett, et al, "Growth of large SiC single crystals," J. Crystal Growth, 128 (1993) 358-62.

[28]H. M. Hobgood, et al, "Large diameter 6H-SiC crystal growth for microwave device applications," in Silicon Carbide and Related Materials, Proceedings of the Fifth Conference (Washington, DC), Ed. by M. G. Spencer, et al, Inst. Phys. Conf. Ser. No. 137, pp. 7-12, (1993).

[29]H. Matsunami, "Progress in SiC epitaxy ---- present and future," ibid., p. 45-50.

[30]S. Prochazka and R. M. Scanlan, "Effect of Boron and Carbon on Sintering of SiC," J. Am. Ceram. Soc., 58[1-2]72 (1975).

[31]S. Prochazka, "The Role of Boron and Carbon in Sintering of Silicon Carbide," Special Ceramics, Vol. 6, pp. 171-181, (1975).

[32]H. Tanaka, "Sintering of Silicon Carbide," in Silicon Carbide Ceramics--1, Edited by S. Somiya and Y. Inomata, Elsvier Applied Science, NY, NY, pp.213-238, (1991).

[33]W. J. MoberlyChan, unpublished material, (1995).

[34]W. D. Kingery, "Densification during Sintering in the Presence of a Liquid Phase, I: Theory," J. Appl. Phys., **30** [3] 301-06 (1959).

[35]M. A. Mulla and V. D. Krstic, "Low-Temperature Pressureless Sintering of β-Silicon Carbide with Aluminum Oxide and Yttrium Oxide Additions," Ceramic Bulletin, **70** [3] 439-443 (1991).

[36]R. Alliergro, L. B. Coffin, and J. R. Tinkepaugh, "Pressure-Sintered Silicon Carbide," J. Am. Ceram. Soc., **39** [11] 386-389 (1956).

[37]W. Bocker, R. H. Landfermann, and H. Hausner, "Sintering of Alpha Silicon Carbide with Additions of Aluminum," Powder Met. Intl., **11** [2] 83-85 (1979).

[38]B. Lin, M. Imai, T. Yano, and T. Iseki, "Hot-Pressing of Beta-SiC Powder with Al-B-C Additives," J. Am. Ceram. Soc., **69** [4] C-67-C-68 (1986)

[39]Y. Inomata, H. Tanaka, Z. Inoue, and H. Kawabata, "Phase Relation in SiC-Al_4C_3-B_4C System at 1800°C," J. Ceram. Soc. Japan, **88** (6), 353-55 (1980).

[40]S. K. Lee and C. H. Kim, "Effects of α-SiC versus β-SiC Starting Powders on Microstructure and Fracture Toughness of SiC Sintered with Al_2O_3-Y_2O_3 Additives," J. Am. Ceram. Soc., 77 [6] 1655-58 (1994).

[41]M. A. Mulla and V. D. Krstic, "Mechanical Properties of β-SiC Pressureless Sintered with Al_2O_3 Additions," Acta Metall. Mater., **42** [1] 303-08 (1994).

[42]Y. Ohya, M. J. Hoffmann, and G. Petzon, "Sintering of in-situ Synthesized SiC-TiB_2 Composites with Improved Fracture Toughness," J. Am. Ceram. Soc., 75 [9] 2479-83 (1992).

[43]M. Janney, "Microstructural Development and Mechanical Properties of SiC and of SiC-TiC Composites," Am. Ceram. Soc. Bull., **65** [2] 357-62 (1986).

[44]B. Lin, T. Yano and T. Iseki, "High - Temperature Toughening Mechanism in SiC / TiC Composites," J. Ceram. Soc. Japan, **100** [4] 509-513 (1992).

1-7. FIGURE CAPTIONS

Fig. 1-1 Crystal structures of (a) 3C-, (b) 2H-, and (c) 6H-SiC.

Fig. 1-2 Equilibrium phase diagram between Al_2O_3-Y_2O_3-SiO_2 (after Ref. [35], Chapter 1).

Fig. 1-3 Phase relationships for the SiC-B_4C-Al_4C_3 system at 1800°C. The shaded area is the region where a liquid was formed at 1800°C (after Ref. [38], Chapter 1).

PART II. *IN SITU* TOUGHENED SILICON CARBIDE CERAMICS with Al-B-C ADDITIONS

CHAPTER 2

PROCESSING and MICROSTRUCTURAL DEVELOPMENT

2-1. INTRODUCTION

To overcome the low sinterability of SiC, the additions of sintering aids are necessary for densification. Boron and carbon are known to be effective to densify SiC at temperatures greater than 2000°C.[1] Such materials, however, exhibit poor fracture toughness both at ambient and elevated temperatures, typically of ~ 2 to 3 $MPam^{1/2}$, thus inhibiting their widespread application. In recent years, liquid-phase sintered SiC with oxide additions has received considerable attention. The added oxides, such as Al_2O_3 [2-4] and $Al_2O_3 + Y_2O_3$ [5-10] are presumed to form a liquid phase in reaction with the native SiO_2 present on the SiC particle surfaces at relatively low temperatures. For example, an equilibrium phase diagram among Al_2O_3-Y_2O_3-SiO_2 shows liquid formation at temperatures as low as 1700-1800°C with only a small amount of SiO_2 (see Fig. 1-2). Kim and Kim,[11] and later Mulla and Krstic,[6] obtained high density SiC ceramics with fine-grained microstructures by free sintering at ~ 1850°C using Al_2O_3-Y_2O_3 additives. After sintering or heat treatment at temperatures of ~ 2000°C, *in situ* toughened SiC ceramics, with fracture toughness twice as high as the conventional B and C doped SiC, were obtained with the oxide additions.[2-4,7-9] Common to these toughened materials is the formation of elongated grains which is promoted by the β-to-α phase transformation. [1-3,6-8] A major difficulty associated with sintering of the oxide-doped SiC, however, is the chemical reaction between SiC and the oxide(s) which forms gaseous products.[12,13] For

example, a green compact of a powder mixture of SiC with 10 mole % of Al_2O_3 lost 35% of the initial weight after firing at 1825°C for 4 hours, reducing the density from 58% for the green compact to a final density of only 50%.[12] To minimize this reaction and weight loss during sintering, the green compact is typically packed in a protective bed of loose SiC and Al_2O_3 powder mixture and then sealed in a thread-tight graphite or boron nitride crucible. In addition to the processing difficulties, the SiC materials with substantial amount of oxide such as YAG (yttria alumina garnet) exhibited poor strength properties.[9] Although the YAG-doped SiC exhibited improved long-crack toughness, it showed lower strength and poorer wear-resistance compared to a commercial B and C-doped SiC.[9]

In the oxide-containing SiC ceramics, the formation of elongated grains is critical to improve the fracture toughness. The β-to-α phase transformation has been known to play a major role in microstructural control. A number of studies applied α-SiC seeding to induce the phase transformation in β-SiC with YAG additives. For example, Padture used 0.5 % of α-SiC seeds in an β-SiC matrix,[8,9] Gong and Chen used 7% of α-SiC seeds.[14] Literature reports on the experimental conditions, such as the amount of oxide addition, the alumina-to-yttria ratio, the sintering temperature and time, to achieve the elongated microstructures are inconsistent. Furthermore, the microstructural characteristics of the toughened materials have not yet been fully described and understood.

The disadvantages associated with the oxide-containing *in-situ*-toughened SiC materials include the processing difficulties, inconsistent reports on sintering conditions,

poor understanding of the microstructures, and in some cases poor strength properties. In this study, non-oxide liquid-phase sintering aids are used to overcome the shortcomings associated with the oxide additives and, at the same time, to hopefully achieve better properties.

Aluminum and its compounds have long been known to aid densification in hot pressed SiC.[15] Al and its compounds alone, or with B, can also be used for pressureless sintering of SiC.[16] The combination of Al, B, and C is extremely effective, providing enhanced densification particularly at lower sintering temperatures.[17] Lin *et al.*[18] reported, in a brief communication, that β-SiC was hot pressed to 96% of theoretical density with a fine-grained microstructure at 1650°C, using 6 wt% Al metal, 1 wt% B metal, and 1 wt% C-black. Furthermore, the addition of Al has been known to lower the β-to-α phase transformation temperature. Shinozaki and coworkers[19-21] studied the enhanced 3C-to-4H phase transformation in β-SiC with 1.5 wt% Al, 1.2 wt% B, and 4 wt% C additions. The low sintering temperatures, coupled with the enhanced β-to-α phase transformation, not only reduce manufacturing costs, but also make microstructural control easier.

Liquid-phase sintered SiC with Al, B, and C additions offers great potential to achieve superior mechanical properties, especially the fracture toughness. These sintering additives can possibly assist the formation of a microstructure, akin to that of *in situ* toughened Si_3N_4 ceramics, with highly elongated grains and weak grain boundaries. However, the mechanical properties of *in situ* toughened SiC using Al, B, and C sintering

additives have not been reported in the literature. The objectives of this work are to obtain and characterize *in situ* toughened microstructures in Al, B, and C doped SiC. The sintering additives of Al, B, and C are first optimized in terms of enhancing densification and forming the desirable microstructure. The β-to-α phase transformation and microstructural evolution were investigated using a number of analytical techniques. The foci of this chapter are to analyze the microstructures and to investigate the effects of the processing conditions, namely sintering additives, hot pressing temperatures and time, on the microstructures. Mechanical properties and oxidation behavior will be discussed in Chapters 3 and 4, respectively.

2-2. EXPERIMENTAL PROCEDURE

2-2.1. Material Production

A flow chart of the experimental procedures is shown in Fig. 2-1. Submicron β-SiC[i] was wet mixed in toluene with Al[i], B[ii], and Apiezon wax[iii]. Referring to the sintering additives, the materials were designated as ABC-SiC. The Al-metal constituted from 1 to 6 wt% of the powder, while the boron content was kept at 0.6 wt% and the wax at 4 wt%. The Apiezon wax, which served both as a carbon source upon pyrolysis and as a binder, was first dissolved in toluene with the assistance of a magnetic stirrer on a hot plate. The appropriate amounts of SiC, Al, and B powders were then added to the solution. The mixture was agitated for 5-10 minutes using a power ultrasonic probe[iv].

[i] BSC-21, Ferro Co., Cleveland, OH.
[i] H-3 and H-10, Valimet, Stockton, CA.
[ii] Callery Chemical Co., Callery, PA.
[iii] Biddle Instruments, Plymouth Meeting, PA.
[iv] SONICATOR Ultrasonic Processor, Model W-375.

This 375 watts, 20 KHz ultrasonic processor had sufficient power to mix approximately ~ 40 grams of powders in ~ 200 mL toluene. Larger batches were divided, ultrasonically agitated separately, and then mixed in a larger beaker. The powder mixtures were stir-dried in air, and re-ground in a mortar and pestle and screened through a 200 mesh sieve. Green compacts of 38.1 mm in diameter and approximately 6 mm in height were prepared by uniaxial compression at 35 MPa in a metal die set.

The green compacts were hot pressed in graphite dies lined with graphite foil (the dies and foils were sprayed with BN), at temperatures between 1700°C and 1950°C, for 15 minutes up to 4 hours, at 50 MPa, under flowing argon. Three specimens, separated by graphite spacers, were made in each run. In a hot pressing experiment, the chamber was first pumped down. Temperature was slowly raised under manual control to 400°C, and held at this temperature overnight in vacuum to bake the furnace and to burn out the organics and moisture in the specimen. The chamber was then back-filled with Ar. Further heating and cooling rates of 10°C / minute were program controlled. The temperature was monitored by an W-Rh thermocouple below ~ 1300°C and by a double wavelength pyrometer sighting on the graphite die at higher temperatures. The accuracy of the pyrometer was checked by melting pure Pt in the furnace. The pressure was applied at approximately 1 MPa / minute when the temperature reached 1000°C. It was released 5 minutes before the end of the soaking at the same rate.

2-2.2. Microstructural Characterization

The surfaces of the hot pressed pellets were grounded off by ~ 500 μm using a surface grinder with a diamond wheel. Densities of the specimens were determined by Archimedes' method in distilled water. Performed on polished surfaces, X-ray diffraction (XRD) tracings were carried out in the 2θ range between 20 to 50 degrees, with a speed of 0.05° / minute and a time constant of 1 second. Peak intensities were determined by integrating the areas under the peaks. The relations listed in Table 2.1, proposed by Ruska *et al.*,[23] were used to quantify the polytypes of SiC.

Table 2-1. Equations to calculate the volume fractions of SiC polytypes[23]

15R		6H		4H		3C		Peak	d(nm)
3.2a			+	9.9c			=	A	0.266
11.2a	+	19.4b					=	B	0.263
26.0a			+	38.9c			=	C	0.257
31.1a	+	59.2b	+	25.1c	+	100.0d	=	D	0.251
		18.1b	+	34.1c			=	E	0.235
2.4a	+	6.5b			+	13.1d	=	F	0.217

Microstructures of the hot pressed materials were revealed by boiling specimens in Murakami's reagent -- 10 g of NaOH and 10 g of $K_3Fe(CN)_6$ in 100 mL H_2O -- for 45 to 100 minutes, and characterized using an optical microscope (OM) and a scanning electron microscope (SEM). Some specimens were heavily etched in a molten salt mixture of KOH and KNO_3 at 500°C for 8 hours to expose the shapes of the SiC grains in 3-D and the interlocking nature of the plate-shaped grains. SEM micrographs of polished surfaces with

no conductive coatings, imaged with ≤ 8 KeV incident electron beam, provided additional contrast to distinguish secondary phases. Energy dispersive spectroscopy (EDS), X-ray mapping (wavelength dispersive spectroscopy, WDS), and Auger electron spectroscopy (AES) were employed to analyze the compositions of the secondary phases. Through collaboration, conventional and high resolution transmission electron microscopy (TEM and HR-TEM) was performed to study phase distribution, grain morphology, grain boundaries, and crystal structures. Compositional information of the grain boundary phase was obtained from AES spectra acquired of intergranular fracture surfaces.

2-3. EXPERIMENTAL RESULTS AND DISCUSSIONS

2-3.1. Sintering Aids

2-3.1a Carbon Yield from Wax Pyrolysis

The apiezon wax served as a binder and as a carbon source to aid sintering. The yield of carbon from pyrolysis of the wax was first investigated. Green compacts of SiC powders and 5 wt% wax were prepared by uniaxial compression at 35 MPa, and heat treated in flowing Ar at various temperatures. The results are shown in Table 2-2. Decomposition of the wax was found to be complete after heating at 400°C for 1 hour (specimen #2), and yielded ~ 50% carbon. Further heating of specimen #2 at 500°C for 3 hours did not change its weight (specimen #5).

Table 2-2. Carbon Yield from Pyrolysis of the Apiezon Wax

Experiment run	Heating (Temp./Time)	Initial weight of wax (g) in a specimen	Weight loss (g)	"carbon" yield (%)
1	300°C/1 h	0.065	0.018	72.3
2	400°C/1 h	0.065	0.033	49.2
3	400°C/2 h	0.065	0.032	50.8
4	500°C/1 h	0.065	0.032	50.8
5	400°C/1 h + 500°C/3 h	0.065	0.031	52.3

2-3.1b Aluminum Content and Particle Sizes

The densities of the silicon carbides, hot pressed at 1700°C and at 1900°C respectively, have been plotted versus the added contents of the atomized aluminum powder in Figure 2-2. The combination of Al, B, and C as sintering additives has evidently been effective for densification. When hot pressed at 1700°C, the silicon carbides reached nearly full density (~ 99% TD) with 3 wt% Al addition. This processing temperatures was ~300°C lower than the typical densification temperatures for SiC. By processing at 1900°C, only 1 wt% Al was sufficient to densify the material.

X-ray diffraction spectra from the polished surfaces of the SiC ceramics, with 3% Al-0.6% B-2% C additions, hot pressed at various temperatures are shown in Fig. 2-3a, together with the spectrum of the β-SiC starting powder. After processing at 1700°C for 1 hour, the SiC remained mainly as the β-phase (3C); however, the peak broadness was significantly reduced from that of the original powders, indicating that the β-phase grains

had grown. At higher hot-pressing temperatures, the materials had increasing amounts of α (4H) phase. After hot pressing at 1950°C, the relative XRD intensities of this specimen had a near perfect match with those of a 4H-SiC standard,[23] indicating first that the β-to-α (3C-to-4H) phase transformation was essentially complete and secondly that the 4H-SiC grains were randomly oriented. No other SiC polytypes (*e.g.*, 6H or 15R) were evident at any temperature. Fig. 2-3b shows the volume fraction of the transformed 4H-phase, determined by Ruska's method,[23] as a function of the hot pressing temperature. These results are also listed in Table 2-3. Upon doping with 3 wt% Al, the 3C-SiC began to transform to 4H-SiC at ~1700°C. When processed for 1 hour at 1780°C, 1900°C, and 1950°C, the materials contained 20%, 75%, and 100% 4H-SiC, respectively. On the other hand, in a material with 1 wt% Al this phase transformation did not occur even at 1900°C for 1 hour (Fig. 2-3b). In addition to the dependence on temperature and the Al content, the volume fraction of the α phase was also related to the soaking time. For example, the material with 3 wt% Al exhibited 100% 4H-SiC after processing at 1900°C for 4 hours. From the above observations, we know that the addition of Al not only enhanced densification but also promoted the β-to-α phase transformation.

Fig. 2-4a is an SEM micrograph showing a polished surface, normal to the hot pressing direction, of a SiC sample containing 6 wt% atomized aluminum powders with a nominal size of 3 microns. The grayish background is SiC, while the darker and brighter regions indicate secondary phases. This contrast is likely to originate from the differences in conductivity of the various phases, as all contrast vanished when a thin conductive gold

coating was applied to the surface. Backscattering electrons might also contribute to the difference in the contrasts, although the SEM image was taken under the secondary electron mode. Fig. 2-4b exhibits a polished cross-section of the same material, where the secondary phases are elongated, suggesting that during hot pressing these secondary-phase regions are easily deformed, and likely to be in a liquid form. Fig. 2-5 shows a similar SEM picture of a polished cross-section of a sample doped with 6 wt% Al powders of 10 micron size, where the secondary phases are bigger than those in Fig. 2-4b. In both cases, the sizes of the secondary phases are comparable to the sizes of the original atomized aluminum powders. The amount of secondary phase regions also correlates well with the Al content. More studies on compositions and crystal structures of the secondary inclusions are presented later in section 2-3.3 of this chapter.

Table 2-3. Processing Conditions and SiC Polytypes

Material	Starting powder	Sintering aides	Hot-press conditions	SiC polytypes
B1	#100(3C)	3Al-0.6B-2C	1700°C/1h	*100(3C), <1(4H)
B2	100(3C)	3Al-0.6B-2C	1780°C/1h	80(3C), 20(4H)
B3	100(3C)	3Al-0.6B-2C	1900°C/1h	25(3C), 75(4H)
B4	100(3C)	3Al-0.6B-2C	1900°C/4h	100(4H)
B5	100(3C)	3Al-0.6B-2C	1950°C/1h	100(4H)
A1	99.5(3C), 0.5(6H)	3Al-0.6B-2C	1900°C/15 min.	30(3C), 40(4H), 30(6H)
C1	100(3C)	1Al-0.6B-2C	1900°C/1h	100(3C)

Weight percentages of the starting powder of each SiC polytypes as indicated in parentheses.

* Volume percentage calculated based on XRD using the method by Ruska *et al.*[23]

In order to obtain a more homogeneous material, smaller sizes and low concentrations of aluminum addition would be desirable. On the other hand, sufficient aluminum was necessary to improve the sinter-ability at relatively low temperatures and to enhance the β-to-α transition. Three wt% of Al of nominal size of 3 μm, the smallest commercially available, was chosen as a sintering aid for further microstructural and property evaluations.

2-3.2. Microstructural Evolution

Figures 2-6a through 2-6d show SEM micrographs of the green compact, and heavily etched specimens hot pressed at 1700°C, 1780°C, and 1900°C, respectively. After etching in a molten-salt mixture at 500°C for 8 hours, the polished surfaces of specimens had been removed and therefore the three-dimensional morphologies of grains were exposed. In the SiC hot pressed at 1700°C, the grains were mostly equiaxed with the larger ones being slightly elongated. The average grain size was larger than the initial powder, consistent with the XRD data where the peak width was significantly reduced. Upon hot pressing at 1780°C, the grains started to grow into plate-like shapes. In the specimens hot pressed at 1900°C, the plate-shaped grains grew and exhibited an increased aspect ratio.

In Fig. 2-6c, the plate-shaped grains began to impinge on each other. Further elongation of these grains was impeded in the areas of impingement. In other radial directions where impingement did not occur, the grains continued to elongate. Therefore,

the plate-shaped grains formed a 3-D interlocking network (Fig. 2-6d). Formation of the grain interlocks is further illustrated in Fig. 2-7. When two plate-shaped grains intersected edge by edge, growth of the grains in length created a grain interlock, as is shown in Figures 2-7a; when the edge of one grain intersected the broad surface of another grain, further thickening of the later grain into the surrounding β-SiC formed an imprint on it, as is illustrated in Fig. 2-7b and experimentally observed in Fig. 2-8. As an aside, such grain interlocks are expected to inhibit grain boundary sliding, thereby improving high temperature creep properties; however, by restricting the pullout of grains, they are also to limit the fracture toughness.

In order to better understand a microstructure, multiple characterization tools and etching techniques are required. Fig. 2-6b through 2-6d display well the grain shapes. Such heavily etched surfaces, however, may not represent the true distribution of the grain sizes because smaller grains are more readily removed during etching. On the other hand, TEM pictures and optical and SEM micrographs of lightly etched surfaces, such as the ones shown in Figures 2-9a and 2-9b for the ABC-SiC hot pressed at 1900°C for 1 hour, provide only 2-D sections. From Fig. 2-9 alone, the SiC grains may be mistaken as needle-shaped. A previous report on an oxide-doped SiC misinterpreted the SiC grains as "rod-shaped" from SEM micrographs of polished surfaces.[12]

For plate-shaped grains, their thickness on a cross-section are exaggerated except those being sectioned normal to the plate. Conversely, the length or diameter of a grain is underestimated because the grain is typically not sectioned through its middle. As a

consequence, the aspect ratios determined from two dimensional measurements tend to underestimate the true aspect ratios. Therefore, quantitative assessment of the grain size and aspect ratios is difficult. One way is to measure the thickness of the thinnest plate and the length of the longest plate in each micrograph. Kim *et al.*[24] measured the sizes of elongated SiC grains in this manner. This approach, however, assumed the grains were monosized, which might not be true. In this study, a more averaged measurement was taken. Cross-sectional grain length, grain width, and aspect ratios were measured for at least 100 grains in multiple TEM images and SEM micrographs of lightly etched surfaces, and the results are listed in Table 2-4. The highest apparent aspect ratio of 9 is achieved by hot pressing at 1900°C for 4 hours (specimen B4). The true aspect ratios are believed to be at least twice these value for the highly elongated microstructures. Transmission optical microscopy of thin foil specimens of material B4 showed numerous grains having aspect ratios ≥ 30. It was also noted that numerous small grains (< 0.2 μm) were observed in the microstructures for silicon carbides processed at 1700°C and 1780°C. Because these small grains were not believed to contribute to toughening, they were not included in the measurements reported in Table 2-4.

The microstructural evolution was related to the 3C-to-4H phase transformation. The material hot pressed at 1700°C exhibited a microstructure comprised of β-SiC grains with an average grain size substantially larger than that of the initial particle size, indicating grain growth of the β-SiC powders (Fig. 2-6a and 2-6b). Considering the

isotropic property of the cubic crystal structure, one might expect the β-SiC grains to grow in a perfectly equiaxed manner. However, many of the β-SiC grains, especially the

Table 2-4. Processing Conditions and Microstructural Results of the Hot-Pressed ABC-SiC Materials

Material	Hot-press Temp.	Density (g/cm^3)	SiC Grain Size		
			Length(μm)	Width(μm)	Aspect ratio
B1	1700°C/1h	3.19	1.0 (0.5)*	0.4 (0.2)	2.8 (0.9)
B2	1780°C/1h	3.19	2.7 (0.9)	0.7 (0.3)	4.0 (1.4)
B3	1900°C/1h	3.18	5.5 (2.4)	0.7 (0.2)	7.6 (2.3)
B4	1900°C/4h	3.18	8.9 (2.9)	1.0 (0.3)	9.0 (2.9)
B5	1950°C/1h	3.18	13.3 (3.6)	2.6 (0.9)	5.4 (1.6)
Hexoloy[#]	N/A[+]	3.14	~5	~5	~1

Note: * Data in the parentheses indicate standard deviation.

[#] Commercial SiC (Hexoloy SA) from Carborundum, Niagara Falls, NY.

[+] Sintering temperature was not reported.

larger ones, exhibited a small elongation typically with aspect ratios ~ 2 (Fig. 2-6b, also see Fig. 3a in reference [25]). This was because of the fact that the initial powders contained twins and stacking faults on one set of the closed packed {111} planes, providing anisotropy to the crystal structure. After hot pressing at temperatures greater than 1700°C, the 3C-to-4H phase transformation took place, and at the same time the grains grew into plate-like shapes with increasing aspect ratios. Such grains were determined to be initially of a dual crystal structure (*i.e.*, partially 3C and partially 4H in one grain). Fig. 2-10a exhibits an TEM micrograph of the material hot pressed at 1780°C

for 1 hour, where 3 types of grains are shown. Some were very fine (submicron) β-SiC grains. Larger β phase grains had grown to 1-2 microns with a small elongation along the direction of the stacking faults. The other grains were much larger with higher aspect ratios, as represented by the grain nearly at the center of Fig. 2-10a. Figures 2-10b through 2-10d show selected area diffraction (SAD) patterns of the three sequential regions of the grain, as marked in Fig. 2-10a. The upper portion of the grain had an 4H (α) crystal structure with a straight grain boundary. The lower portion had an 3C (β) crystal structure with faceted grain boundaries. Electron diffraction from the middle portion of the grain (Fig. 2-10c) showed (111) twinning of the β phase and streaking due to a high density of stacking faults. This middle region of the grain might be regarded as a conversion from the 3C to the 4H stacking sequence (see section 2-3.6 for discussions on the phase transformation mechanisms). The α phase, due to its anisotropic crystal structure, grew preferentially in the basal plane, i.e., to increase length of the grain. In order to minimize interface energy in the system, lengthening of the α phase pulled the β phase within the same grain to grow together with it (see schematics in Fig. 2-17). The α/β interface within a single grain was perfectly coherent, and therefore had minimal energy. In fact, this interface was nothing more than a change in stacking sequence of the basal planes. The coherent $\{111\}_\beta//(0001)_\alpha$ interface were suggested to have energies several orders of magnitude less than random β/α interfaces.[26] Co-growth of the α+β phases was energetically favorable because it eliminated generation of the high energy α/β random grain boundaries.[26] Thickening of the grain was believed to be caused by a ledge

mechanism, and was controlled by the kinetics of nucleation of new monolayers on the flat upper surface of the grain, which was suggested to be slow.

The ABC-SiC hot pressed at 1900°C for 1 hour contained 75% of 4H phase and 25% of 3C phase from XRD analysis (Fig. 2-3). The microstructure of this material is displayed in Fig. 2-9. TEM studies showed that the highly elongated grains comprised of mainly 4H-SiC with partial 3C-SiC. After hot pressing at 1900°C for 4 hours, the phase transformation was nearly complete; the material exhibited the highest aspect ratio. Further grain growth in the α phase, through an Ostwald ripening mechanism, reduced the aspect ratios of the grains. The material processed at 1950°C had larger grains with lower aspect ratios. The driving force for growth (lengthening) was reduced in a coarse microstructure. On the other hand, thickening was controlled by the nucleation rate of monolayers on the flat surface, which was proportional to the surface area. Larger plate-like grains tended to thicken faster because of the higher nucleation rate for new monolayers.

2-3.3. Secondary Phases and Grain Boundary Phases

Ceramic materials generally use sintering aids and contain secondary phases. For example, *in situ* toughened Si_3N_4 ceramics typically incorporate ~ 10% of yttria plus alumina additives.[27,28] The more recently developed *in situ* toughened SiC materials often contain 10-20% of YAG (alumina + yttria) or alumina additions.[3-11] The amount of sintering aids in ABC-SiC is relatively minimal; however, a careful characterization of the

secondary phases can be helpful to understand the microstructural evolution and the material's performance. Three categories of "secondary phases" have been observed in the ABC-SiC according to their geometries. On the smallest scale is the presence of an amorphous grain boundary film (≤ 1 nm). The intermediate size secondary phases are crystalline "triple points", residing at larger triple junctions of the SiC grains.[29,30] Bulk secondary phases exhibit dimensions comparable to the size of the Al powders, as have been previously discussed.

Fig. 2-11 is an HR-TEM image showing two neighboring SiC grains and a thin (≤ 1 nm) amorphous grain boundary film. The amorphous grain boundary phase contained Al and O as determined by AES, and by PEELS of TEM samples.[31] An example of AES spectrums is shown in Fig. 2-12a, which is acquired of a fresh intergranular fracture surface. In addition to Si and C, signals of Al and O are evident in this spectrum. After sputtering for a few seconds, however, the Al and O signals disappear (Fig. 2-12b), indicating that the Al and O segregated in the amorphous grain boundary film.

Fig. 2-13 is an SEM micrograph showing strips of triple junction material on a fracture surface. This micrograph images a flat surface of a plate-shaped SiC grain. Each strip of material represents a triple junction among the imaged SiC grain and two other SiC grains on the opposite side of the fractured specimen. It is noteworthy that, during fracture, all the triple junction materials were left on the flat surface of the imaged grain, indicating a stronger bonding between the triple junction material and the dominant SiC neighbor. Fig. 2-14 exhibits a high resolution TEM image showing that the triple junction

is crystalline, and that the crystalline triple junction has an orientation relationship with the dominant neighbor. $Al_8B_4C_7$ and Al_4O_4C are the two common phases observed at the triple junctions. In the case shown in Fig. 2-14, the orientation relation was determined to be:[29]

$$[0\bar{1}1]_{Al4O4C} // [0\bar{1}10]_{4H\text{-}SiC} \quad \text{and} \quad (100)_{Al4O4C} // (0001)_{4H\text{-}SiC}$$

The triple junctions larger than 2-3 nm in the ABC-SiC are crystallized after densification without additional heat treatment. It is, however, well known that in Si_3N_4 materials a second heat treatment is necessary to crystallize the triple junctions.[27] Crystalline triple junctions are considered beneficial to creep properties.[27]

Figure 2-15a shows an SEM micrograph of a polished surface of a hot pressed SiC containing 6wt%Al-0.6wt%B-2wt%C. The high Al content was intended to exaggerate the formation of the bulk secondary phases. The silicon carbide matrix appeared gray, while various secondary phases were relatively brighter or darker. Energy dispersive and wavelength dispersive X-ray spectroscopy (EDS and WDS) showed that the secondary phase regions contained Al and were free of Si. WDS further revealed that the bright secondary phases contained oxygen, while the dark secondary phases did not. Figures 2-15b through 2-15d show wavelength dispersive X-ray maps of Al, Si, and O, respectively, obtained on the polished surface imaged in Figure 2-15a. Auger electron spectroscopy (AES) further determined that the dark secondary phases were mainly aluminum-boron-carbides, with a few being aluminum carbides, while the bright regions were aluminum oxides and aluminum oxycarbides. Examples of the Auger electron spectra of the bulk

secondary phases are shown in Fig. 2-16. Electron diffraction and lattice imaging by TEM have confirmed the existence of these secondary phases.[29-31] Graphite inclusions, often reported in SiC with B and C additions,[20,32] were not observed in the ABC-SiC. The silicon carbides with 3 wt% Al had smaller amounts of secondary phases, with the major inclusions determined to be $Al_8B_4C_7$, minor secondary phases being Al_4O_4C, and occasionally Al_2O_3 and Al_4C_3 as determined by TEM.[29-31]

The formation of secondary phases was attributed to the sintering additives present in concentrations well above their solubility in SiC. The solubility limit reported for aluminum in 4H-SiC was 0.26 wt% and 0.50 wt% at 1800°C and 2000°C respectively, and for boron it was 0.1 wt% at 2500°C.[33]

2-3.4. Sintering Process

Sintering of the present Al, B, and C-doped SiC was believed to be a liquid phase process. A likely scenario that could be envisioned was as follows (Fig. 2-17). The metal aluminum melted at a low temperature (660°C) and established an equilibrium vapor pressure in the vicinity of the Al melt. Aluminum vapor coated the SiC particle surfaces through the connected channels in the powder compact, and reacted with the native oxide on the powder surface as well as the added carbon and boron to form a liquid grain boundary phase. Surface diffusion of Al could have also contributed to formation of the liquid phase. Due to the capillary force from the liquid film and the applied pressure, particle rearrangement occurred and achieved partial densification.[34] A liquid phase

sintering mechanism,[35] *i.e.*, a solution-reprecipitation process, caused gradual densification coupled with grain growth. At this stage, corresponding to sintering at ~ 1700°C, a fine-grained dense 3C-SiC was obtained (Fig. 2-17b). At higher sintering temperatures, the 3C-SiC began to transform to 4H-SiC, which preferentially grew in the basal plane. Elongation of the 4H portion pulled the 3C portion within the same grain to grow along with it in order to minimize surface energy, and thus formed plate-like grains containing duplex (4H + 3C) phases (Fig. 2-17c). After hot pressing at an appropriate temperature, an optimal microstructure containing high-aspect-ratio plate-shaped grains was obtained (Fig. 2-17d).

As the sintering additives, especially the Al, were present in concentrations above their solubility in SiC, secondary phases existed at grain boundaries, grain triple junctions, and isolated bulk regions (see Figures 2-11, 2-13, and 2-15, respectively). During grain growth, the liquid grain boundary film remained thin which became amorphous upon cooling after hot pressing. Accumulation of the liquid grain boundary phase (during grain growth) formed triple junction pockets, which crystallized when cooled after sintering. On the other hand, B, C, and O were presumed to transport into the aluminum melt and form bulk secondary phases. The liquid flowed, filling pores between the nearby SiC particles and engulfing many grains, as observed by TEM.[31]

Densification and grain growth were competing processes. It was critical to control the processing conditions to enhance densification prior to the occurrence of significant grain growth. Otherwise, the coarsened grains (powders) would inhibit further

densification. As discussed above, formation of α-SiC grains in a β-SiC matrix caused the α-SiC grains to grow (lengthen) rapidly. The driving force for α-SiC grains to grow, which was sum of the driving force to reduce the grain boundaries and the volume free energy by transforming the β phase to the α phase, was higher than that for growth of the β-SiC grains. The processing conditions of the ABC-SiC, described here, satisfied the requirement to have a near fully dense material first and then to evoke the β-to-α phase transformation and produce a microstructure composed of elongated grains. If the phase transformation took place before full densification, a porous SiC would result. An example of a porous SiC with highly elongated grains is shown in Fig. 2-18, where the material was prepared by hot pressing submicron β-SiC powders (B20, H. C Stark, Germany) at 2000°C for 1 hour with 0.3 wt% Al-0.6 wt% B-1.5 wt% C additions.

2-3.5. The β-to-α Transformation

The α-SiC is generally believed to be more stable than the β phase at high temperatures. The onset temperature of the β-to-α phase transformation, however, is sensitive to impurities. For example, in B and C doped SiC ceramics, the phase transformation begins at temperatures greater than 1950°C.[36-38] The addition of a small amount of metallic aluminum or aluminum compounds lowers this phase transformation temperature.[36] The onset of the β-to-α phase transformation has been reported at approximately 1800°C with 1.5wt%Al-1.2wt%B-4wt%C additions.[20,21] In the present study, 3 wt% of metallic Al with 0.6 wt% B and 2 wt% C was found to strongly promote

the β-to-α phase transformation by further lowering the onset temperature. A trace of 4H-SiC was detected at a hot pressing temperature as low as 1700°C by TEM. Hot pressing at 1780°C for 1 hour caused 20% 3C-to-4H transformation (Fig. 2-3), as determined by XRD using the method of Ruska *et al.*[23] After hot pressing at 1900°C for 1 hour, 75% 4H formed; after soaking at this temperature for 4 hours the transformation was complete. The onset temperature for the β-to-α phase transformation in the ABC-SiC is the lowest ever reported. Promotion of the phase transformation, coupled with the enhanced sinterability discussed earlier, made it easier to control the microstructure in the ABC-SiC.

It was known that boron and carbon doped β-SiC transformed to the 6H polytype at temperatures greater than 1950°C.[36] The addition of aluminum, on the other hand, enhanced the occurrence of the 4H polytype and lowered the phase transformation temperature.[16,39,40] Favored formation of the 4H polytype in Al-containing SiC had also been reported by Hamminger *et al.*[41,42] when studying the structures of several pressureless sintered SiC compositions. Shinozaki and co-workers[19-21] found that the 3C-to-4H phase transformation was enhanced by the presence of Al together with B and C. However, Shinozaki *et al.* reported that the 3C-SiC transformed to 4H-SiC through an intermediate structure of 15R, which was not observed in the present study (neither by XRD nor by TEM). The differences in crystal structures of the transformation products were believed to originate in the differences in the starting β-SiC powders. Pure crystalline β-phase powders were used here, while Shinozaki *et al.*[19-21] used powders containing 29% of a "disordered" phase. A hot pressed material (at 1900°C for 15 minutes) from β-SiC

powders seeded with 0.5 wt% of sub-micron 6H-SiC contained 30 % of 6H, 40 % of 4H, with 3C as the balance (see Table 2-3). The minimal addition of 6H seeds caused substantial 3C-to-6H transformation, or more appropriately, the growth of the 6H grains.

The mechanism(s) by which Al caused the preferential formation of the 4H crystal structure is not well understood. One speculation is that Al may have a chemical effect. Tajama and Kingery[33] determined the solubility of Al in 4H-SiC as 0.26 wt% and 0.5 wt% at 1800°C and 2000°C, respectively. Shinozaki *et al.*[22] measured 0.8 wt% Al in their 4H-SiC grains near the growing tips. Although these authors implied that Al had higher solubility in 4H-SiC than in other polytypes, no explanation was offered why the 4H structure could accommodate more Al. In the ABC-SiC, attempts to establish a difference in Al content in the 4H and 3C portions of a dual phase grain has thus far been inconclusive.[30] The other possibility is that the 4H polytype be more stable than the 6H at relatively low temperatures. The Al addition lowers the β-to-α phase transformation temperature where 4H-SiC become favored. A calculation predicted that the 4H structure was the equilibrium phase below 1950°C.[43] At higher temperature, either 3C-SiC or 4H-SiC might transform to 6H-SiC. Mitomo *et al.*[40] found that 4H-SiC partially transformed to 6H-SiC at 2200°C in the presence of Al.

The β-to-α phase transformation mechanisms in SiC have been studied extensively for many years. Numerous recent studies on SiC processing have typically referenced a series of papers by Heuer *et al.*[26,44-46] The α-SiC was said to nucleate on the existing twin

boundaries and stacking faults in the β grains. These planar defects actually offered local stacking of the α phase. A striking phenomenon was the formation of composite grains in which α plates were sandwiched between "envelopes" of the β phases. The generation and cooperative growth of these α (core) / recrystallized β (envelope) composite grains comprised the initial stage of the β-to-α phase transformation. The tips of the composite grains were flush with each other as they abutted surrounding original β grains. The basal faces of the α core were always covered by the β envelope which was coherent to the α core. Direct contact of the basal faces of the α plates with the random β grains was claimed not to exist presumably because of the very high energy of such grain boundaries. The rapid planar growth of the α/β composite grains and concomitant coarsening of the envelopes comprised of a direct transformation from the original β phase to the α phase at the tips and a "recrystalization" from the original β phase to the β envelope. The next stage of the phase transformation, i.e., thickening of the α plates into the β envelopes, proceeded by generation and motion of partial dislocations.[45]

Composite grains comprising of an α plate core with a β envelope were never observed in the ABC-SiC, although multiple specimens with various volume fractions of the α phase were extensively studied with TEM.[29,30] As discussed previously, the dual phase grains in ABC-SiC always had the α phase on one side with an atomically flat boundary and the β phase on the other side with faceted boundaries (Fig. 2-10a). MoberlyChan[30] suggested the 3C-to-4H phase transformation in the ABC-SiC be a

growth-induced transformation. At temperatures greater than 1700°C, the attachment of new unit layers on to the growing grains assumed the 4H stacking sequence, forming (β + α) dual phase grains. The thermodynamically favored α (4H) portion of the grain experienced faster growth (lengthening), which pulled the β part of the grain to grow together with it. Thickening of the dual phase grains were limited by the kinetics to generate new monolayers on the flat surfaces. Thus, a microstructure was developed with high-aspect-ratio plate-shaped grains.

2-4. CONCLUSIONS

ABC-SiC ceramics, using 3 wt% Al, 0.6 wt% B, and 2 wt% C as sintering aids, were prepared by hot pressing in the temperature range from 1700°C to 1950°C for 15 minutes to 4 hours. Sintering behavior, phase transformations, and microstructures of hot pressed silicon carbide ceramics were investigated using a number of analytical techniques, including x-ray diffraction (XRD), scanning electron microscopy (SEM), Auger electron spectroscopy (AES), and transmission electron microscopy (TEM). Dense β-SiC, with mostly very fine equiaxed grains (<1 μm) and some larger elongated grains (1-2 μm in length), was obtained by hot pressing at 1700°C, which is ~ 300°C below the common sintering temperatures for SiC. By processing at higher temperatures, the β-to-α phase transformation took place, forming initially (β + α) dual phase plate-shaped grains with at least one broad face of each dual phase grain nearly atomically flat. The α portion of the grain preferentially grew in the basal plane, and pulled the β part to grow along with it.

Thickening of the grains was believed to be controlled by the nucleation rate of monolayers on the flat surface, which was suggested to be slow. Growth of the highly elongated grains produced grain interlocks. Thus a microstructure was obtained containing an 3-D interlocking network of high-aspect-ratio plate-shaped grains. An amorphous thin grain boundary film (1 nm) and partially crystalline triple junctions were also observed. Isolated bulk secondary phases, having similar sizes as the added Al powders, was identified mainly as $Al_8B_4C_7$. Application of a two-step processing technique, i.e., to heat treat the green compact prior to densification homogenized the material.

In the ABC-SiC, the initial β-SiC transformed to 4H-SiC. No other α phase polytypes were observed. The β-to-α phase transformation was suggested to proceed by a grain growth mechanism; at temperatures where the 4H-SiC was stable, growth of grains assumed the 4H stacking sequence.

2-5. REFERENCES

[1]S. Prochazka and R. M. Scanlan, "Effect of Boron and Carbon on Sintering of SiC," J. Am. Ceram. Soc., 58[1-2] 72 (1975).

[2]K. Suzuki, "Pressureless-Sintered Silicon Carbide with Addition of Aluminum Oxide," in Silicon Carbide Ceramics--2. Edited by S. Somiya and Y. Inomata. Elsvier Applied Science, NY, NY, pp.162-82, (1991).

[3]M. A. Mulla and V. D. Krstic, "Mechanical Properties of β-SiC Pressureless Sintered with Al_2O_3 Additions," Acta Metall. Mater., **42** [1] 303-08 (1994).

[4]S. S. Shinozaki, J. Hangas, K.R. Carduner, M. J. Rokosz, K. Suzuki, and N. Shinohara, "Correlation Between Microstructure and Mechanical Properties in Silicon Carbide with Alumina Addition," J. Mater. Res., **8** [7] 1635-43 (1993).

[5]V. D. Krstic, "Optimization of Mechanical Properties in SiC by Control of the Microstructure," MRS Bulletin, **20** [2] 46-8 (1995).

[6]M. A. Mulla and V. D. Krstic, "Low-Temperature Pressureless Sintering of β-Silicon Carbide with Aluminum Oxide and Yttrium Oxide Additives," Ceram. Bull., **70** [3]339-443(1991).

[7]S. K. Lee and C. H. Kim, "Effects of α-SiC versus β-SiC Starting Powders on Microstructure and Fracture Toughness of SiC Sintered with Al_2O_3-Y_2O_3 Additives," J. Am. Ceram. Soc., 77 [6] 1655-58 (1994).

[8]N. P. Padture, "*In Situ* Toughened Silicon Carbide," J. Am. Ceram. Soc., 77 [2] 519-23 (1994).

[9]N. P. Padture and B. R. Lawn, "Toughness Properties of a Silicon Carbide with an in Situ Induced Heterogeneous Grain Structure," J. Am. Ceram. Soc., 77 [10] 2518-22 (1994).

[10]M. Omori and H. Takei, "Preparation of Presureless-Sintered SiC- Al_2O_3-Y_2O_3," J. Mat. Sci., **23**, 3744-3749 (1988).

[11]D. H. Kim and C. H. Kim, "Toughening Behavior of Silicon Carbide with Additions of Yttria and Alumina," J. Am. Ceram. Soc., **73** [5] 1431-34 (1990).

[12]A. Gadalla, M. Elmasry, and P. Kongkachuichay, "High Temperature Reactions Within SiC-Al_2O_3 Composites," J. Mater. Res., 7 [9] 2585-92 (1992).

[13]M. A. Mulla and V. D. Krstic, "Pressureless Sintering of β-SiC with Al_2O_3 Additions," J. Mat. Sci., **29,** 934-938 (1994).

[14]S. Gong and I. -W. Chen, "Processing and Properties of SiC-TiB_2 Composites," 98th Annual Meeting of the American Ceramic Society, Paper No. B-157, Indianapolis, Ind., (1996).

[15]R. Alliergro, L. B. Coffin, and J. R. Tinkepaugh, "Pressure-Sintered Silicon Carbide," J. Am. Ceram. Soc., **39** [11] 386-389 (1956).

[16]W. Bocker, R. H. Landfermann, and H. Hausner, "Sintering of Alpha Silicon Carbide with Additions of Aluminum," Powder Met. Intl., **11** [2] 83-85 (1979).

[17]H. Tanaka, "Sintering of Silicon Carbide," in Silicon Carbide Ceramics--1. Edited by S. Somiya and Y. Inomata. Elsvier Applied Science, NY, NY, pp.213-238, 1991.

[18]B. Lin, M. Imai, T. Yano, and T. Iseki, "Hot-Pressing of Beta-SiC Powder with Al-B-C Additives," J. Am. Ceram. Soc., 69 [4] C-67-C-68 (1986)

[19]S. Shinozaki, J. Hangas, K. Maeda, and A. Soeta, "Enhanced Formation of 4H Polytype in Silicon Carbide Materials," in Silicon Carbide'87, J. D. Cawley and C. E. Semler Ed., Ceramic Transactions, Vol. 2, pp. 113-21, (1987).

[20]S. Shinozaki, R. M. Williams, B. N. Juterbock, W. T. Donlon, J. Hangas, and C. R. Peters, "Microstructural Developments in Pressureless-Sintered β-SiC Materials with Al, B, and C Additions," Am. Ceram. Soc. Bull., **64** [10] 1389-93 (1985).

[21]R. M. Williams, B. N. Juterbock, S. Shinozaki, C. R. Peters, and T. J. Whalen, "Effects of Sintering Temperatures on the Physical and Crystallographic Properties of β-SiC," Am. Ceram. Soc. Bull., **64** [10] 1385-89 (1985).

[22]S. S. Shinozaki, "Unique Microstructural Development in SiC Materials with High Fracture Toughness," MRS Bull., xx [2] 42-45 (1995).

[23]J. Ruska, L. J. Gauckler, J. L. Lorenz, and H. U. Rexer, "The Quantitative Calculation of SiC Polytypes from Measurements of X-Ray Diffraction Peak Intensities," J. Mater. Sci., **14** [8] 2013-17 (1979).

[24]Y. W. Kim, K. S. Cho, and J. G. Lee, "Effect of Large α-Silicon Carbide Seed Grains on Microstructure and Fracture Toughness of Pressureless Sintered α-Silicon Carbide," Submitted to Communication of J. Am. Ceram. Soc., (1995).

[25]J. J. Cao, W. J. MoberlyChan, L. C. De Jonghe, C. J. Gilbert, and R. O. Ritchie, "*In Situ* Toughened Silicon Carbide With Al-B-C Additions," J. Am. Ceram. Soc., **79** [2] 461-69 (1996).

[26] T. E. Mitchell, L. U. Ogbuji, A. H. Heuer, "β→α Transformation in Polycrystalline SiC: II, Interfacial Energetics," J. Am. Ceram. Soc., **61** [9-10] 412-413 (1978).

[27]M. J. Hoffmann, "High-Temperature Properties of Si_3N_4 Ceramics," MRS Bull., xx [2] 28-32 (1995).

[28]Y. Goto and G. Thomas, "α to β Transformation and Microstructural Changes of Si3N4 During Sintering," pp. 157-164, in Silicon-Based Structural Ceramics. Ed. B. W. Sheldon and S. C. Donforth, Ceramic Transactions, Vol. 42, The American Ceramic Society, (1994).

[29]W. J. MoberlyChan, R. M. Cannon, L. H. Chan, J. J. Cao, C. J. Gilbert, R. O. Ritchie, and L. C. De Jonghe, "Microstructural Development to Toughen SiC," MRS Proceedings, Fall'1995.

[30]W. J. MoberlyChan, "The β-3C to α-4H Phase Transformation and Microstructural Development in SiC Hot Pressed with Al, B and C Additives," to be published.

[31]W. J. MoberlyChan, J. J. Cao, M. Y. Niu, and L. C. De Jonghe, "Toughened β-SiC Composites with Alumina-Coated α-SiC Platelets," in High Performance Composites---Commonalty of Phenomena, edited by K. K. Chawla, P. K. Liaw, and S. G. Fishman, TMS Publication, pp. 219-29, (1994).

[32]R. A. Bishop and H. K. Bowen, "Suspension Processing of Beta-SiC Powders," in Silicon Carbide'87, J. D. Cawley and C. E. Semler Ed., Ceramic Transactions, Vol. 2, pp. 157-73, (1987).

[33]Y. Tajima and W. D. Kingery, "Solubility of Aluminum and Boron in Silicon Carbide," J. Am. Ceram. Soc., **65** [2] C27-29 (1982).

[34]W. D. Kingery, H. K. Bowen, and D. R. Uhlman, Introduction to Ceramics (2nd Ed.), John Wiley and Sons, (1976).

[35]W. D. Kingery, "Densification during Sintering in the Presence of a Liquid Phase, I: Theory," J. Appl. Phys., **30** [3] 301-06 (1959).

[36]M. Srinivasan, "The Silicon Carbide Family of Structural Ceramics," in Structural Ceramics, Edited by J. B. Wachtman, Jr., Treatise on Materials Science and Technology, Vol. 29, pp. 99-159, Academic Press, Inc., (1989).

[37]A. H. Heuer, G. A. Fryburg, L. U. Ogbuji, T. E. Mitchell, and S. Shinozaki, "$\beta \rightarrow \alpha$ Transformation in Polycrystalline SiC: I, Microstructural Aspects," J. Am. Ceram. Soc., **61** [9-10] 406-12 (1978).

[38]L. U. Ogbuji, T. E. Mitchell, and A. H. Heuer, "$\beta \rightarrow \alpha$ Transformation in Polycrystalline SiC: III, Thickening of α Plates," J. Am. Ceram. Soc., **64** [2] 91-99 (1981).

[39]J. M. Bind, "Phase Transformations During Hot Pressing of Cubic SiC," Met. Res. Bull., **13** [2] 91-96 (1978).

[40]M. Mitomo, Y. Inomata, and H. Tanaka, "The influence of Aluminum on the Stability of 4H- and 6H-Silicon Carbide at 2200°C," Mater. Res. Bull., **6,** 759-64 (1971).

[41]R. Hamminger, G. Grathwohl, and F. Thummler, "Microanalytical Investigation of Sintered SiC," J. Mater. Sci., **18** [2] 353-64 (1983).

[42]R. Hamminger, G. Grathwohl, and F. Thummler, "Microanalytical Investigation of Sintered SiC, Part 2. Study of the Grain Boundaries of Sintered SiC by High Resolution Auger Electron Spectroscopy," J. Mater. Sci., **18**, 3154-3160 (1983).

[43]C. Cheng, V. Heine, and I. L. Jones, "Silicon Carbide Polytypes as Equilibrium Structures," J. Phys. Condensed Matter., **2,** 5097-5113 (1990).

[44]A. H. Heuer, G. A. Fryburg, L. U. Ogbuji, T. E. Mitchell, and S. Shinozaki, "$\beta \rightarrow \alpha$ Transformation in Polycrystalline SiC: I, Microstructural Aspects," J. Am. Ceram. Soc., **61** [9-10] 406-12 (1978).

[45]L. U. Ogbuji, T. E. Mitchell, and A. H. Heuer, "β→α Transformation in Polycrystalline SiC: III, Thickening of α Plates," J. Am. Ceram. Soc., **64** [2] 91-99 (1981).

[46]L. U. Ogbuji, T. E. Mitchell, and A. H. Heuer, "β→α Transformation in Polycrystalline SiC: IV, A Comparison of Conventionally Sintered, Hot-Pressed, Reaction-Sintered, and Chemically Vapor-Deposited Samples," J. Am. Ceram. Soc., **64** [2] 100-105 (1981).

2-6. FIGURE CAPTIONS

Fig. 2-1 Flow chart of processing procedures of SiC with Al, B, and C additions (referred to as ABC-SiC). Mechanical properties and oxidation behavior are discussed in Chapters 3 and 4, respectively.

Fig. 2-2 Densities of silicon carbides hot pressed at 1700°C and 1900°C with various amounts of Al, together with 0.6wt%B and 2wt%C additives. The theoretical density of SiC is 3.21 g/cm^3.

Fig. 2-3 (a) X-ray diffraction spectra of the starting β-SiC powder and of silicon carbides hot pressed for 1 hour at 1700°C, 1780°C, 1900°C, and 1950°C, respectively. Fig. 2-3b plots the volume fraction of the 4H phase in ABC-SiC processed for 1 hour as a function of temperature. By comparison, the material with 1 wt% Al contains negligible α phase after hot pressing at 1900°C for 1 hour.

Fig. 2-4 SEM micrographs of polished surfaces of a SiC containing 6 wt% Al (with 3 μm nominal size), 0.6 wt% B, and 2 wt% C: (a) normal to the hot pressing direction and (b) a cross-section which is parallel to the hot pressing direction. The gray background is SiC, while the darker and brighter regions are the secondary phases.

Fig. 2-5 SEM micrographs of a polished cross-section (parallel to the hot pressing direction) of a SiC containing 6 wt% Al (with 10 μm nominal size), 0.6 wt% B, and 2 wt% C. Note the secondary phase regions are larger than those in Fig. 2-4b.

Fig. 2-6 SEM micrographs of (a) the green compact and of silicon carbides, with 3 wt% Al-0.6 wt% B-2 wt% C additions, hot pressed under various conditions: (b) 1700°C/1h, (b) 1780°C/1h, and (c) 1900°C/4h (heavily etched in a molten salt mixture at 500°C for 8 hours).

Fig. 2-7 Formation of grain interlocks (schematics) in the microstructure when plate-shaped grains intersect edge to edge (a) and edge to the basal plane (b).

Fig. 2-8 SEM micrograph showing grain "imprints" on a the broad face of a plate-shaped grain. The specimen was etched in a molten salt mixture at 500°C for 8 hours. A Schematic illustration on the formation of the imprints is shown in Fig. 2-7b.

Fig. 2-9 (a) Optical and (b) SEM micrographs of an etched surface of ABC-SiC hot pressed at 1900°C for 1 h.

Fig. 2-10 TEM micrograph of ABC-SiC processed at 1780°C for 1h, showing a dual-phase plate-shaped grain (a). Selected area diffraction patterns show the bottom of the grain being 3C-SiC (b), the top being 4H-SiC (c), and the middle being mixture structures containing microtwins and stacking faults (d) (Courtesy of W. J. MoberlyChan).

Fig. 2-11 High resolution TEM micrograph showing lattice images of two neighboring SiC grains and an amorphous grain boundary film of ~ 1 nm thick (Courtesy of W. J. MoberlyChan).

Fig. 2-12 Auger electron spectra acquired of an intergranular fracture surface (a), and of the same area after ion sputtering away less than one nanometer of material from the surface (b). Al and O segregated in the amorphous grain boundary film (Courtesy of W. J. MoberlyChan).

Fig. 2-13 SEM fractograph showing triple junction materials. Each stripe of material represents a triple "point" among the imaged plate-shaped grain and two other grains on the opposite face of the fractured specimen.

Fig. 2-14 HR-TEM image of a crystalline triple point phase. This triple-point material shows a crystal orientation relationship with the bottom SiC grain (Courtesy of W. J. MoberlyChan).

Fig. 2-15 SEM micrograph (a) and wavelength dispersive X-ray maps of Al (b), Si (c), and O (d) of a polished specimen with 6wt%Al-0.6wt%B-2wt%C additives.

Fig. 2-16 AES spectra acquired of a SiC grain (a) and of secondary phases (b and c). (Courtesy of W. J. MoberlyChan)

Fig. 2-17 Scenario of sintering and microstructural development in ABC-SiC.

Fig. 2-18 SEM micrograph of a fracture surface of a porous SiC hot pressed at 2000°C for 1 hour. The starting submicron β-SiC powder was doped with 0.3 wt% Al, 0.6 wt% B, and 1.5 wt% C. Formation of the plate-shaped grains prior to densification resulted in a porous material.

CHAPTER 3

MECHANICAL PROPERTIES

3-1. INTRODUCTION

3-1.1. Toughened Ceramics and Fracture-Toughness Evaluation in Ceramics

The viability of advanced structural ceramics rests on their ability to withstand stresses without catastrophic failure, which in turn, rely on their toughness properties and flaw distributions. Earlier efforts (up to about 1965) were directed at improving the strength through improvement of processing method,[1] aiming at the elimination of large flaws in the material. Detection of very small flaws in a structural component, however, is very difficult if not impossible, and processing to keep flaws consistently small can be even more difficult. The high cost of making "perfect" ("flaw-free") ceramics imposes a limit in practice. Furthermore, service damage and slow crack growth during service are also concerns that raise the reliability issue for materials with low fracture toughness, even though the material may be carefully made "flaw free". Considering the realities of processing, crack detection, and service damage, people have realized that damage tolerance is a more realistic goal for reliable materials than flaw elimination. Numerous efforts have been made to produce tougher ceramics. For example, yttria stabilized zirconia (YSZ)[2] and *in situ* toughened silicon nitride[3,4] are developed with much higher toughness than conventional ceramic materials. More recently, considerable attention has been paid to improve the toughness of silicon carbide materials.[5-9]

The search for more damage tolerant ceramics has led to the identification and development of several toughening mechanisms in brittle materials. They include fiber reinforcement, whisker / platelet reinforcement, grain bridging and pullout, brittle or ductile particulate dispersion, transformation toughening, and microcracking. These mechanisms have all been successful to some degree in a variety of materials. A comparison of the various toughening mechanisms, maximum toughnesses, typical materials, and limitations are summarized in Table 3-1.

Table 3-1. Examples of Toughening Mechanisms in Ceramic Materials (after ref. [1])

Mechanism	Highest Toughness ($MPa\sqrt{m}$)	Example Materials	Limitations
Fibers	~40	CAS/SiC LAS/SiC Al_2O_3/SiC SiC/SiC C/SiC	Processing difficulty, cost, anisotropic properties
Transformation	~20	ZrO_2 HfO_2	Transformation temp.
Metal dispersion	15 - 25	Al_2O_3/Al WC/Co Al_2O_3/Ni	Chemical compatibility, oxidation
Whiskers/platelets	~15	Si_3N_4/SiC Al_2O_3/SiC Si_3N_4/ Si_3N_4	Hazard with whiskers, cost
Microcracking	~10	Al_2O_3/ZrO_2 Si_3N_4/SiC	Strength
Grain bridging	~10	Si_3N_4	Creep

It is noted that there is currently no "standard" test technique to evaluate fracture mechanics parameters on brittle materials (in contrast, E 399 is the standard for metals[10]). Various test techniques have been used to measure the fracture toughness of ceramics. They include the following method: pre-cracked double cantilever beam (DCB),[11] double torsion (DT),[12] single edge notched beam (SENB),[13] Chevron-notched beam,[14] single edge pre-cracked beam (SEPB),[15] controlled surface flaw,[16] indentation-strength measurement,[17] and indentation-crack size measurement.[18] It is important to pay attention to the assumptions, problems, and unknown factors involved in making fracture toughness measurements and the reproducibility from one technique to another. The measured toughness values from various techniques can vary by a factor of 2 for the same material.[14,19] Therefore, caution has to be taken when comparing toughness values in the literature especially when using fracture mechanics data on brittle materials. Generally speaking, the DCB and DT methods are the most credible measurements, but they require larger specimens, extensive machining, and sophisticated equipment to control and monitor crack growth. The SENB method typically overestimates the toughness as it treats the notch as a pre-crack. The indentation-crack size measurement offers an unique simplicity and economy in test procedure, but at a little cost in accuracy. As the latter technique is most commonly used to evaluate the toughness of the *in situ* toughened SiC materials in the literature, it is briefly reviewed here.

A Vicker's diamond indenter is loaded on a polished surface, causing irreversible inelastic deformation. At a critical load, radial cracks pop-in on tensile median planes.

With increased load, radial cracks propagate downward. Upon unloading, a residual stress field arises from accommodation of the impression of the deformation zone against the constraining elastic matrix. This field is tensile at the surface, and is responsible for extending the radial cracks at and near the surface. Ultimately, the radial cracks become half-penny shaped.[28] For sufficiently well-developed half-penny cracks, the driving force can be characterized by a residual stress intensity factor in the following form:[18]

$$K_{res} = \chi P / C^{3/2} = \xi (E / H)^{1/2} (P / C^{3/2}) \qquad (3\text{-}1)$$

where ξ is a geometric constant, E/H is the Young's modulus-to-hardness ratio of the material, χ is a constant which is the product of ξ and $(E/H)^{1/2}$, P is the indentation load, and C is the half- length of the radial cracks on the surface.

Assuming that the crack system is subject to conditions of mechanical equilibrium, the radial cracks remain stable at $K_{res} = K_C$. By measuring the crack size on a polished surface, one obtains the toughness of a material through equation (3-1), where the constant ξ is obtained by empirical calibration. The value of $\xi = 0.016 \pm 0.004$, calibrated by Lawn and co-workers[18] from a number of brittle materials with known toughness values (determined by more conventional measurements using DCB or DT specimens), has been widely used in literature.

The validity of Eq. (3-1) requires that the cracks are well-developed (to satisfy the "center-loading" assumption). Another assumption also used is that the volume of the

impression is accommodated by inelastic deformation of the nearby material, which requires the crack patterns to remain geometrically well behaved (no chipping).[18] Therefore, the indentation load is restricted to a range: at the upper limit to avoid chipping of material from the sides of the impression; at the lower limit to ensure large scale cracks compared to the dimension of the impression ($C \geq 2a$, where C is the half-length of the crack, and a is half-diagonal of the impression). Chipping partially releases the residual stress field, causing the measurement to yield an artificially high value of toughness. On the other hand, post indentation subcritical crack growth causes a lower value of toughness. The accuracy of this method to evaluate fracture toughness is suggested to be better than 30 to 40%, provided that the materials are "well behaved" in their indentation response.[18]

The indentation-crack size measurement is most valuable in toughness evaluation on a comparative basis, where a given material is subjected to optimization of some processing variables. In this study, this technique may be suitable for the "screening" of processing parameters of the *in situ* toughened SiC, but it is not suitable for the SiC platelet / SiC composites discussed in Chapter 5. The chipping problem in the composites is severe at high indentation loads, whereas at low loads the indentation crack interacts with only a small number of the reinforcing platelets. Therefore, the controlled surface flaw method was used to evaluate both the monolithic and the composite materials in this work (see detail in experimental procedures). The indentation cracks extended during subsequent bending so that they interact with more reinforcing platelets in the composites.

All measurements were made in direct comparison with a commercial SiC[i] to ensure the test results. The toughness properties of selected materials, under optimal processing conditions, were also evaluated in a collaborative study[ii] using cyclic fatigue pre-cracked disk-shaped compact-tension DC(T) specimens.

3-1.2. R-Curve Behavior

The toughening mechanisms in ceramic materials all depend on a process zone, or sometimes called crack shielding zone, either in front of the crack tip (such as microcracking) or behind it (such as the bridging mechanisms). These toughening mechanisms provide increasing crack growth resistance with crack extension, namely the R-curve behavior. Experimental work on Si_3N_4 [20,21] and coarse-grained Al_2O_3 [22] ceramics indicates that the R-curve behavior derives principally from the development of a zone of bridging grains behind the crack tip which acts to retard further crack extension. The ABC-SiC, described in chapter 2 of this study, was designed and fabricated to achieve the highest contribution from grain bridging by obtaining a microstructure comprised of high-aspect-ratio plate-shaped grains with weak grain boundaries.

Traditional R-curve measurements are made on specimens with long through-specimen-thickness pre-cracks. However, some of the most important mechanical properties, such as strength and damage tolerance, are determined in the domain of short cracks, i.e., cracks comparable with the scale of the microstructure.[24] The shape of the R-

[i] Hexoloy SA, Carborundum, Niagara Falls, NY. This material had an equiaxed microstructure of mean grain size ≈ 5 μm, with a density of 97%.
[ii] This work was performed by C. J. Gilbert in Prof. R. O. Ritchie's group at LBNL.

curve, especially in the short crack region, is also very important; stable crack growth can only occur when the elevation in material fracture resistance with respect to crack length (the slope of the R-curve) exceeds the elevation in the applied stress intensity with crack length for a given loading condition. Indentation cracks provide a means for evaluating toughness properties in the short-crack region. Toughness properties are assessable in the crack size range from tens of microns to several hundred microns.[24] Practically, the strength of indented beams are measured as a function of the indentation load, from which the R-curve is evaluated. Materials with single-valued toughness are characterized by a classical $\sigma \propto P^{-1/3}$ relation;[23] departure from this relation indicates the existence of an R-curve behavior. A weaker dependence of the strength on the indentation load, and hence on initial flaw size, means a pronounced R-curve.

In this study, indentation-strength tests were used to determine the flaw-tolerance and R-curve characteristics of the ABC-SiC hot pressed at 1900°C. The method to deconvolute R-curves from indentation-strength (I-S) data was first developed by Lawn and co-workers.[24] They evaluated the R-curve behaviors of a number of alumina materials with various grain sizes. Later Padture *et al.*[6] reported an R-curve for a SiC with 20 vol% of YAG (Al_2O_3-Y_2O_3) additives, showing enhanced long-crack toughness, but diminished short-crack toughness. In the ABC-SiC, the R-curve evaluated from the I-S data analysis were compared to that directly measured from pre-cracked DC(T) specimens.

3-2. EXPERIMENTAL PROCEDURES

3-2.1. Strength and Fracture Statistics

The ABC-SiC materials were prepared by hot pressing with 3 wt% Al, 0.6 wt% B, and 2 wt% C. Detailed descriptions of the materials can be found in Chapter 2. Beams of 3 x 3 x 28 mm were sectioned from the SiC billets processed at various conditions. The tensile surfaces of the bend bars were polished to a 1 μm diamond finish, and the tensile edges were beveled on a 6 μm diamond wheel to reduce edge flaws. The flexure strength was tested on a four-point bending jig with an outer span of 25.4 mm, an inner span of 9.5 mm, and at a crosshead speed of 0.05 mm/min. The strength was determined from the relation:

$$\sigma = \frac{3Pa}{bh^2} \tag{3-2}$$

where σ is the four-point bend strength, P is the load at fracture, a is one-half of the distance between the outer and inner spans, b is width of the beam, and h is the beam height. For each processing condition, the bend strength was averaged over 5 tests. To evaluate their statistical distributions of strengths, twenty measurements each were made on the ABC-SiC hot pressed at 1900°C and the commercial Hexoloy SA. Data were fit to a two-parameter Weibull distribution, and the Weibull modulus, m, and scaling factor, σ_0, were determined for both materials.

3-2.2. Fracture Toughness

The fracture toughness was measured using the controlled surface flaw method. The polished tensile surfaces of bend bars were indented using a Knoop indenter at loads between 98 to 137 N. The indentation crack was made parallel to the hot pressing direction and perpendicular to the long axis of the beam. The indented beams were tested under the same conditions as measuring the modulus of rupture. During bending, the crack experienced the sum of the applied and the residual stress intensities. The residual stresses dominated the initial fracture process, causing stable crack growth even in materials that have no R-curve behaviors.[25,26] The initial half-penny shaped indentation crack developed into a semi-elliptical shape at instability. The ratio of short axis to the long axis of the critical crack was found consistently to be ~0.65 (see Fig. 3-1). The fracture toughness was determined from the relation:[15]

$$K_C = Y\sigma\sqrt{a} \qquad (3\text{-}3)$$

where σ is the fracture stress, a is the crack depth at instability measured on the fracture surface using a scanning electron microscope (SEM), and Y is a geometric constant (which is 1.5. see discussions below). For an ideal half-penny shaped crack, the geometric constant is $2/\sqrt{\pi}$. Two correction factors should be considered here, namely the free surface correction and the crack geometry correction. For an elliptical surface crack, the stress intensity was obtained from:[15,27]

$$K_1 = \frac{\sigma M(\pi a)^{1/2}}{\Phi}\left(\frac{a^2}{c^2}\cos^2\phi + \sin^2\phi\right)^{1/4} \qquad (3\text{-}4)$$

where M is the free surface correction factor, a is the minor half-axis of the ellipse, c is the major half-axis of the ellipse, and ϕ is the polar angle from the major half-axis. The term Φ is a complete elliptic integral of the second kind and its maximum value of $\pi/2$ is reached when a/c = 1.[iii] For an ellipse with an a/c ratio of 0.65 for the critical cracks as shown in Fig. 3-1, Φ was determined to be 1.32 (which is 18% smaller than $\pi/2$). Taking the free surface correction factor as 1.12, we found $Y = (2 / \sqrt{\pi}) \times (1 + 0.18) \times 1.12 = 1.5$. As the residual stress field from indentation had significantly decayed after stable crack growth, the residual stress was ignored here. The fracture toughness values were averaged over 4 measurements. A commercial Hexoloy SiC was also evaluated under identical testing conditions for comparison.

3-2.3. Crack Growth Resistance-Curve (R-Curve) Measurements

The R-curve of the ABC-SiC hot pressed at 1900°C was deconvoluted from the strength-indentation load relation. Indentation cracks were produced on the polished tensile surfaces with a Vickers hardness tester, using indentation loads between 3 N and 200 N. Three indents, introduced at the same load, were placed ~2 mm apart from each

[iii] The term Φ is given by

$$\Phi = \int_0^{\pi/2}\left[\mathrm{Sin}^2\phi + \frac{a^2}{c^2}\cos^2\phi\right]^{1/2} d\phi$$

other on the tensile surface of each beam within the inner span. The measured strength at each indentation load was averaged over 3 to 4 tests.

Through collaboration, The R-curve was also directly measured using pre-cracked disk-shaped compact-tension DC(T) specimens.[28] Detailed experimental procedures can be found in Ref. [28].

3-2.4. Fractography and Crack Profiles

Scanning electron microscopy was used to examine the fracture surfaces, and the crack profiles on indented specimens (the cracks extended after post-indentation bending). In addition, indentation crack patterns were imaged under an optical microscope.

3-3. RESULTS AND DISCUSSIONS

3-3.1. The Effects of Processing Conditions and Microstructures on Mechanical Properties

Fig. 3-1a is a low magnification SEM fractograph of an ABC-SiC, hot pressed at 1700°C for 1 hour, showing a well defined initially semi-circular indentation crack front and a semi-elliptical crack front at instability. During bending of the indented beams, the residual stresses contribute to the fracture process, causing stable crack growth even in materials that have no R-curve behavior.[25,26] Near the top surface the crack grew from C_o to C_m, while in the depth direction the crack extended from a_o to a_m. Similar results were observed in the commercial Hexoloy SiC (Fig. 3-1b). The ellipticity (a_m/c_m) of the critical

crack front at instability was found consistently to be ~ 0.65. This value of ellipticity, together with the measured fracture stress of the indented specimens and the crack depth, were used in the calculation of fracture toughness (Eq. 3-3).

Figures 3-2a and 3-2b show the fracture toughness (measured from bend tests with a controlled surface flaw) and four-point bend strength of the ABC-SiC ceramics hot pressed for 1 hour at temperatures between 1700°C and 1950°C. Since fracture toughness values are sensitive to the particular testing methodology,[14,19] similar measurements were made on a Hexoloy SiC for comparison. When the sintering temperature increased from 1700°C to 1900°C, the fracture toughness increased from 4.3 to 9.1 $MPa{\cdot}m^{1/2}$. Note that the latter value is over 3 times that of Hexoloy SiC. These toughness values were consistent with more precise measurements using fatigue pre-cracked DC(T) specimens, where the ABC-SiC hot pressed at 1900°C for 1 hour exhibited a steady-state fracture toughness of K_c =9.1 $MPa{\cdot}m^{1/2}$. [28,29] The fracture toughness of Hexoloy SiC was determined to be 2.5 $MPa{\cdot}m^{1/2}$ using pre-cracked DC(T) specimens (see Fig. 3-10). The measured fracture toughness values from the two techniques are clearly quite consistent. The fracture toughness in excess of 9 $MPa{\cdot}m^{1/2}$ for the ABC-SiC is believed to be the highest of any monolithic SiC material reported to date. Table 3-2 summarizes key literature data on mechanical properties of various SiC ceramics.

Table 3-2. Mechanical Properties of Various SiC Ceramics

Author	Additions	Proc. Cond.	MOR (MPa)	K_C ($MPam^{1/2}$)	K_C test Method
This study	3Al-0.6B-2C	HP1900°C/4h	650	9.4	Controlled Flaw
	3Al-0.6B-2C	HP1900°C/1h	660	9.1	Controlled Flaw
				9.1	DC (T)
	3Al-0.6B-2C	HP1840°C/1h	760	8.9	Controlled Flaw
Hexoloy	B-C		410	2.8	Controlled Flaw
				2.5	DC (T)
P.F.Becher[29]	Al_2O_3			3.5 - 4.0	DCB
	B-C			2.5 - 3.0	DCB
N.P.Padture[6,30]	20 Vol% Al_2O_3+Y_2O_3	1900°C/30' + 2000°C/3h	350	~8* (~4)	Indentation
K.Suzuki[7]	2-15 Al_2O_3	1950°C/15h	~600	5.7	Chevron Notch
M.A.Mulla[8]	Al_2O_3	2050°C/30'	600	~6	Straight Notch
S. S. Shinozaki[31]	5 wt% Al_2O_3	1950°C/5h + HIP1900°C/2h	592	4.7	SEPB
	5 wt% Al_2O_3	1950°C/5h + HIP1900°C/2h	650	5.3	SEPB
C.H.Kim[5,32]	16 wt% Al_2O_3+Y_2O_3	HP1800°C/30'		4.2	Indentation
	10 wt% Al_2O_3+Y_2O_3	2000°C/5h		8.3	Indentation
K. Y. Chia[19] (Hexoloy-SX)	Y-Al compound	Sinter + HIP	800	~6	Chevron Notch

* The toughness was determined to be approximately twice that of the Hexoloy SiC, which was assumed to be 4 $MPam^{1/2}$. [30]

The toughness of a material can be evaluated directly from the strength of indented specimens.[iv] Such strength degradation datum with indentation cracks is also a useful parameter to characterize a material's response to typical surface flaws, especially in cases where the ceramic surface is subjected to incidental sharp-particle contact events.[16] Fig. 3-3 illustrates the flaw tolerance of selected ABC-SiC ceramics versus the commercial Hexoloy SiC. The flaws were produced by Knoop indentation with the loads (from 98 N to 137 N) indicated in the plot. Significant improvement in flaw tolerance was evident for the *in situ* toughened ABC-SiC materials. For example the ABC-SiC, hot pressed at 1900°C for 4 hour, exhibited an indentation-strength of nearly 400 MPa with a Knoop indentation at a load of 137 N on the tensile surface, showing an 60% retention of its strength. On the other hand, the Hexoloy SiC with a Knoop indentation at a lower load (98 N) showed a bend strength of only 110 MPa, corresponding to 27% of its strength.

As the hot pressing temperature was raised from 1700°C to 1840°C, the average bend strength increased (Figure 3-2b). Upon processing at temperatures above 1900°C,

---

[iv] Chantikul et al.[17] developed the indentation-strength method to measure the fracture toughness of brittle materials. After calibration, the toughness of a material was determined by

$$K_C = 0.59(E/H)^{1/8}(\sigma P^{1/3})^{3/4} \qquad (3\text{-}5)$$

where E/H is the modulus to hardness ratio, σ is the fracture strength of the indented specimen, and P is the Vickers indentation load. Extending this theorem to the application of Knoop indentation, the present author obtained an expression for SiC materials:[33]

$$K_C = 0.77(\sigma P^{1/3})^{3/4} \qquad (3\text{-}6)$$

where P is the Knoop indentation load.

It should be pointed out that both expressions (3-5) and (3-6) are valid only for materials with no rising R-curve behavior.

however, the bend strength decreased, primarily because of larger pre-existing flaws induced by excessive grain growth and secondly due to a decrease in toughness. Figure 3-4 examines the effect of sintering time on fracture toughness and bend strength, where the ABC-SiC ceramics were hot pressed and held at 1900°C for times ranging from 15 minutes to 4 hours. As the soaking time increased, the fracture toughness increased while the strength slightly decreased. The increased scatter in measured toughness was mostly the result of the increase in difficulty in measuring the size of the critical crack in the coarser microstructures.

The fracture toughness and bend strength are plotted versus the square root of grain length in Figure 3-5a. This plot indicates that some degree of grain growth was beneficial for both toughness and strength. Upon increasing the grain length from ~1 μm to ~9 μm, the fracture toughness increased by more than a factor of 2, while some improvement in strength was also observed as the grain length increased from ~1 μm to ~5 μm. From elementary fracture mechanics, it is known that strength is dictated by the material's toughness and flaw distribution. The flaw size generally scales with the grain size. The much improved toughness with grain growth over-compensated the effect of larger flaws and resulted in an increase in strength. The two highest strengths in this study were obtained by hot pressing at 1840°C/1h and 1900°C/15 minutes, respectively. These processing conditions produced the optimal grain sizes for strength, as the materials exhibited good toughness and relatively small flaws. When the grains are too big, flaw size became a dominant factor, and as a consequence the strength decreased with further grain

growth. For example, the materials showed lower strength by hot pressing either fro 1 hour at temperatures above 1900°C or for a longer time at 1900°C (see Figures 3-2b and 3-4). In Figure 3-5b the fracture toughness and bend strength are plotted versus the aspect ratios of the plate-like grains. The fracture toughness increased from 4.3 to 9.5 $MPa{\cdot}m^{1/2}$ when the aspect ratio increased from ~3 to ~9. The strength, however, was not sensitive to the aspect ratio (Fig. 3-5b).

It is noted that the mechanical properties of the ABC-SiC are not functions of the grain width. When the grain length increased from ~3 μm to ~9 μm, accompanying a significant increase in toughness, the grain thickness remained basically unchanged (see Table 2-4). As will be discussed later in section 3-3.5, toughening in the ABC-SiC is attributed to frictional grain bridging. This mechanism provides an increase in toughness (in terms of energy) that scales with the pullout length (see equation 3-11). Under interfacial property limiting conditions, the pullout length is proportional to the diameter of long fibers or rod-like grains. For example, the fracture toughness of Si_3N_4 scales with the square-root of the grain diameters.[29] With a plate-like geometry, the pullout length would scale with the plate thickness. Observations, however, showed that the toughness of the ABC-SiC were not proportional to the grain width (toughness significently varied while the grain width remained basicly unchanged), indicating that some characteristics of the microstructure (such as the grain interlocks), other than the interfacial strength, limited the pullout length. This issue will be further discussed later in fractographic analysis.

To conclude this section, the physical and mechanical properties of the ABC-SiC hot pressed at 1900°C for 1 hour are summarized in Table 3-3. The material exhibits a microstructure comprising of highly elongated grains with mainly the 4H crystal structure. It has a Vickers hardness of 24 GPa, a 4-point bend strength of 660 MPa with a Weibull modulus of 18.6, and a fracture toughness of 9.1 $Mam^{1/2}$. A material processed under similar conditions is used for the characterization of R-curve behavior.

Table 3-3. Processing Conditions and Properties of an *in situ* Toughened ABC-SiC

Sintering additives	3wt%Al-0.6wt%B-2wt%C
Hot pressing conditions	1900°C / 1h
Density	3.18 g/cm^3
Crystal structure	75% (4H) + 25% (3C)
Grain size (cross sectional)	
Length	5.5+/- 2.4 μm
Width	0.7 +/- 0.2 μm
Apparent aspect ratio	7.6 +/- 2.3
Hardness (Vickers, 500 g load)	24.0 +/- 1.7 GPa
Four-point bend strength	660 +/- 20 MPa
Fracture toughness	
Four-point bending with controlled-surface flaw	9.1 +/- 0.4 $MPa{\cdot}m^{1/2}$
DC(T) with fatigue pre-crack	9.1 $MPa{\cdot}m^{1/2}$
Weibull Modulus (20 beams)	18.6

3-3.2. R-Curve Behavior

Indentation fracture strength, σ_m, versus the indentation load, P, is plotted in Fig. 3-6 for both the ABC-SiC and the Hexoloy SA. For the Hexoloy SiC, data followed a typical $\sigma_m \propto P^{-1/3}$ response, indicating a single-valued toughness, or no rising R-curve behavior.[23,24] By comparison, for the ABC-SiC the degradation in strength with respect to the indentation load had a slope much lower than -1/3. More specifically, the ABC-SiC exhibited pronounced flaw tolerance, with comparatively enhanced long-crack strength. For example, with Vickers indentation cracks produced at a load P = 78N, the retained strength of the ABC-SiC was ~4 times that of the Hexoloy. The bend strength from polished beams of the ABC-SiC was 1.6 times that of the Hexoloy (shown arbitrarily at a load P = 1.1 N in Fig. 3-6a).

These σ_m versus P measurements were subsequently used to deconvolute the R-curve, in accordance with an indentation-strength K-field analysis.[24] During post-indentation bending, the crack experiences a total stress intensity, K_t, which is sum of the residual stress intensity, K_{res}, and the applied stress intensity, K_a, as follows:[24,26]

$$K_t = K_{res} + K_a = \frac{\chi P}{C^{3/2}} + Y\sigma C^{1/2}, \qquad (3\text{-}7)$$

where χ and Y are residual-contact and crack-geometry coefficients, P is the indentation load, σ the applied stress, and C the surface crack size.

Fig. 3-7 schematically illustrates the relationships between K_t, K_{res}, K_a, as well as the material crack resistance, K_R. The residual stress intensity, K_{res}, decreases with $C^{-3/2}$, and the intersection of the K_{res} field with the R-curve defines the initial indentation crack size, C_0. During post-indentation bending, the total stress intensity K_t drives the crack to grow in a stable manner until fracture instability occurs at the applied stress $\sigma = \sigma_m$ and final crack length, C_m, which satisfies the following balance and tangency conditions, respectively:[24]

$$K_t(C) = K_R(C) \tag{3-8a}$$

$$\frac{\partial K_t(C)}{\partial C} = \frac{\partial K_R(C)}{\partial C} \tag{3-8b}$$

Accordingly, the R-curve can be determined by solving Eqs. (3-8a) and (3-8b) simultaneously for the conditions at each data point in Fig. 3-6a, provided that the coefficients χ and Y are known. In other words, the R-curve is determined as the envelope of tangency conditions for the family of $K_t(C)$ curves.[6,24]

First, however, the coefficients χ and Y must be appropriately calibrated as follows. These parameters were determined using the Hexoloy (since the fracture toughness is single-valued and well-documented) and then applied to the ABC-SiC.[v] For a

[v] The coefficient χ is the product of a geometric constant and the square root of the modulus-to-hardness ratio (see Eq. 3-1), which were believed to be the same for the ABC-SiC and the Hexoloy.

material with single-valued toughness, like Hexoloy SA, the following relations follow from Eqs. (3-7) and (3-8):

$$\sigma_m P^{1/3} = \frac{3}{4}\frac{K_c}{Y}\left(\frac{K_c}{4\chi}\right)^{1/3} \tag{3-9a}$$

$$C_m P^{-2/3} = \left(\frac{4\chi}{K_c}\right)^{2/3} \tag{3-9b}$$

Because K_c was not a function of C for the Hexoloy, the parameters $\sigma_m P^{1/3}$ and $C_m P^{-2/3}$ were found to be invariant (Fig. 3-8). Solving Eqs. (3-9a) and (3-9b) simultaneously for the Hexoloy data, and taking the toughness of Hexoloy as $K_c \sim 2.75$ $MPam^{1/2}$,* yielded values for χ and Y as $\chi = 0.084$ and $Y = 0.93$. Note that this estimate of χ is in excellent agreement with the values between 0.080 to 0.087 (see Table 3-4) as calculated for Hexoloy SiC by measuring the initial indentation crack size after each indentation load, P, and using the well-established relation,[18]

$$K_c = \frac{\chi P}{(C_0)^{3/2}}. \tag{3-10}$$

Again, K_c for Hexoloy was taken as 2.75 $MPam^{1/2}$.

In the ideal case of a half-penny, semi-circular crack, the geometric coefficient $Y = 2/\sqrt{\pi} \sim 1.13$. The radial cracks, however, tend to form a semi-elliptical rather than a semi-

* The fracture toughness of Hexoloy SA SiC has been reported in the range from 2.1 $MPam^{1/2}$ to 4.6 $MPam^{1/2}$, depending on the particular measurement method, in the literature.[6,19] The value of 2.75 $MPam^{1/2}$ was reported in Ref. [34] using Chevron-notched specimens. We have measured 2.5 $MPam^{1/2}$ using pre-cracked DC(T) specimens and 2.8 $MPam^{1/2}$ using the controlled surface flaw method.[35]

circular shape during stable crack growth (see Fig. 3-1 as examples). In fact, as determined by fractographic analysis, the crack front was found consistently to have a

Table 3-4. Coefficient χ calculated from Eq. 3-10 for the Hexoloy SA SiC at Various Indentation Loads

Indentation load, P (N)	4.9	9.8	19.6	39.2	78.4
Initial crack size, C_0 (μm)	28	45	70	115	173
Critical crack size, C_m (μm)	75	114	170	286	439
Coefficient, $\chi = K_c C_0^{3/2}/P$	0.083	0.085	0.082	0.087	0.080

shape factor of a/c ~ 0.65 (where a is the crack depth) at the onset of instability. Therefore the crack geometric constant Y is expected to be lower than 1.13. The calibrated value of Y = 0.93 was consistent with physical reality, and was used in subsequent calculations.

Using the values for χ and Y quoted above, a family of $K_t(C)$ curves were constructed for the ABC-SiC and the Hexoloy from the data in Fig. 3-6, and the R-curves were thus constructed (Fig. 3-9). The data points in Fig. 3-9 were generated with a relationship developed by Hsueh and Becher as follows:[36]

$$C_m = \left(\frac{\chi}{Y}\right)^{1/2}\left(\frac{\partial \sigma_m}{\partial P}\right)^{-1/2} \qquad (3\text{-}11)$$

where the slope $\partial\sigma_m/\partial P$ was found from Fig. 3-6b. This approach yielded the same result as the tangency envelope approach. Notice that the R-curve for the ABC-SiC rises rapidly and reaches a very high steady-state toughness, in contrast to the single valued toughness for the Hexoloy.

Fig. 3-10 compares the R-curve deconvoluted from the indentation-strength measurements with that directly measured from the fatigue-precracked DC(T) specimen. The horizontal axis here is the crack extension for DC(T) specimens, or the crack depth for the indented bend beam specimens. The R-curve results compare well for cracks (or crack extension) greater than ~120 μm. For crack sizes or initial crack extensions less than ~120 μm, however, a significant discrepancy existed, with the DC(T) measurements yielding higher values of material resistance. This discrepancy was mainly caused by the difference in the initial flaw size. As pointed out by Lawn,[25] the extension of short (on the order of one bridge spacing), semi-circular flaws were strongly influenced by the discrete tensile residual stresses arising from thermal expansion and elastic anisotropy. The effect of this field depressed the toughness in the small crack regime. For longer cracks exceeding several bridge spacings, the influence of the local tensile residual stresses approached zero.

In 4H-SiC the residual stress among grains from thermal expansion and elastic anisotropy was estimated to be ~480 MPa (see Eq. 3-15 and discussion later). Because of this discrete, fluctuating residual stress field which varied from grain-to-grain, a crack which was on the order of the bridge spacing experiences not only a closing force from

bridging, but also an opening force from local tensile residual stress. The local tensile field reduced the measured toughness to below levels measured in long cracks. This led to a macroscopically steep R-curve for short cracks when the crack size was less than several bridge spacings. In the ABC-SiC such an effect disappeared after ~120 μm of crack extension (Fig. 3-10). On the other hand, the fatigue precrack might have residual bridging which caused the initial toughness to be high from measurements on DC(T) specimens, although caution was taken to cycle the specimens for a long time at the threshold stress intensity to wear-out the pre-existing bridging elements.[28]

3-3.3. Fracture Statistics

The improved flaw tolerance of the ABC-SiC appeared to have reduced the distribution in fracture strength relative to the Hexoloy SA (Fig. 3-11). The Weibull modulus, m, was determined to be 18.6, and the scale factor, σ_0, to be 658 MPa for the ABC-SiC. For the Hexoloy, in comparison, m was 5.8 and σ_0 was 400 MPa. Both the enhanced flaw tolerance and high Weibull modulus are consistent with the pronounced rising R-curve behavior. It is encouraging to note that although the microstructure of the ABC-SiC is significantly more coarse (length of the plate-shaped grains) than that of the Hexoloy, both the Weibull modulus and the fracture strength have improved simultaneously. This is not always the case in toughened ceramics. In grain-bridging ceramics, such as alumina, an enhanced long-crack toughness from coarser microstructures is normally accompanied by a sacrifice in fracture strength.[25,37]

3-3.4. Fractography and Crack Profiles

Fig. 3-12 shows optical micrographs of Vickers indentation crack patterns in Hexoloy SiC, and two ABC-SiC materials processed at 1700°C and 1900°C, respectively. Since the indentation crack sizes were not measured to quantify the toughness values in this study, no efforts were made to prevent slow crack growth. Qualitatively, though, the indentation cracks in the Hexoloy were straight and long (Fig. 3-12a); the cracks were shorter in the ABC-SiC with a fine microstructure (Fig. 3-12b, hot pressed at 1700°C). These observations are consistent with the fracture toughness values measured from the controlled surface flow method (The fracture toughness of the fine grained ABC-SiC is higher than that of the Hexoloy, Fig. 3-2). The ABC-SiC with plate-shaped grains (1900°C/4h) were much tougher, on which the indentation cracks were produced at a much higher load and the cracks exhibited zigzagged paths (Fig. 3-12c).

Observations of crack-microstructure interaction were made of the extended radial cracks of Vickers indentations after bend tests. Comparisons of crack-microstructure interactions in an ABC-SiC with plate-shaped grains and the reference material are shown in Fig. 3-13. Extensive crack deflection at the grain boundaries and many grain bridging sites were evident in the ABC-SiC. By contrast, the crack in the reference SiC was straight and transgranular, with no indication of crack-wake bridging.

A long plate-shaped grain (indicated by an arrow) is shown in Fig. 3-13a that has been fractured and is being pulled out, a behavior analogous to that of a long fiber in

composites. At larger crack openings, the grains that are nearly perpendicular to the main crack have better opportunity to be fully pulled out (Fig. 3-14a). For the grains that are oriented at an angle to the main crack, it is possible that after some sliding the grains become locked up with the matrix. They experience increasing bending force and eventually fracture (Fig. 3-14b and c). In some cases the strong pullout resistance causes the surrounding matrix to fracture. Pullout of clusters of grains, as well as single ones, are also frequently observed; an example is shown in Fig. 3-14c. Contacting facets (steps), which frequently occur on the main crack, provide high frictional stress when these facets slide over each other (Fig. 3-14d).

Figures 3-15a through 3-15c show fractographs of the ABC-SiC ceramics hot pressed at various temperatures. After processing at relatively low temperatures (1700°C and 1780°C), the fracture mode was predominantly intergranular. Upon hot pressing at 1900°C, limited transgranular fractured facets occurred; however, intergranular fracture still dominated, with the majority of the plate-like grains exhibiting evidence of pullout. In comparison, the fracture surface of Hexoloy SiC exhibited complete transgranular fracture (Fig. 3-15d), consistent with the very low fracture toughness of this material.

The complex, interlocking nature of the microstructure with plate-shaped grains (see Fig. 2-6d) in the ABC-SiC limited the grain pullout length. Fig. 3-16 shows a fracture surface of the material hot pressed at 1900°C for 4 hours, where grains *a* and *b* formed an interlock. Grain *b* fractured at the interlock, and left strips of triple junction materials, as

indicated by arrows, on the broad surface of grain *a*. As an aside, it is expected that this interlocked structure may inhibit grain boundary sliding at elevated temperatures, thereby improving the creep resistance; such issues, however, are beyond the scope of this study.

Debonding at the grain boundaries in the ABC-SiC materials was presumably the result of the weak amorphous thin film at the boundaries. The crystalline phases at the grain triple junctions might also assist to deflect cracks around the grain boundaries because of their higher CTE (coefficient of thermal expansion) compared to that of SiC. Loss of the amorphous grain boundary film and/or the triple junction materials would make the grain boundaries stronger and would result in a lesser degree of grain pullout. Fig. 3-17 compares the fracture surfaces of three materials: a) hot pressed at 1900°C, b) hot pressed at 1950°C, and c) hot pressed at 1900°C and then annealed at 2000°C. After processing at 1900°C, the material exhibited dominantly intergranular fracture and showed extensive grain pullout. Upon hot pressing at 1950°C, the material displayed larger fraction of transgranular fracture. The specimen annealed at 2000°C showed complete transgranular failure. As discussed in Chapter 2, the ABC-SiC was made through a liquid-phase sintering mechanism. Sintering or annealing at too high temperatures might result in a loss of the liquid phase, which would be expected to leave pores at the triple junctions and eliminate the grain boundary film.

3-3.5 Toughening Mechanisms

The much improved toughness and strength properties of the ABC-SiC under optimal processing conditions were dictated by its unique microstructure, consisting of high-aspect-ratio plate-shaped grains with an amorphous thin film at grain boundaries. As indicated by both fracture surface and crack profile studies, cracks in the ABC-SiC processed at temperatures ≤ 1900°C generally followed along the grain boundaries. With very fine grains (for example, after hot pressing at 1700°C), toughening from grain bridging and pullout was minimal. After hot pressing at higher temperatures (*e.g.*, at 1900°C), growth of the plate-like grains with increased aspect ratio highly enhanced the effect of crack bridging, which provided the *in situ* toughened ABC-SiC significantly rising R-curve behavior and a record-high plateau toughness (Fig. 3-10). The grain bridging and pullout mechanism has been treated extensively in the literature (see refs. [22,29] as examples). Fig. 3-18 shows a schematic diagram of a crack with a number of grains pulling out. Generally, toughening derives from the closing traction in the crack wake across opposing crack faces, either via intact grains spanning the crack surfaces (Fig. 3-13a) or via frictional contact at sliding facets (Fig. 3-14d).

The closing traction can be represented by the grain bridging function, p(u), where u is the crack opening displacement.[29] Based on energy balance arguments, the energy increase, ΔG, can be calculated by integrating the bridging function over the bridging zone:[28,29]

$$\Delta G = f\int_0^{u_f} p(u)du \qquad (3\text{-}12)$$

where f is the area fraction of the bridging grains and u_f is the critical crack opening at the end of the bridging zone, which equals to the pullout length, l_{po} (see Fig. 3-18).

The bridging stress declines with increase in crack opening, and can be most simply described as[29]

$$p(u) = \mu\sigma_N(1-\tfrac{u}{u_f}) \qquad (3\text{-}13)$$

where μ is the coefficient of friction between sliding SiC grains, and σ_N the normal stress exerted by one grain on another. Inserting the expression (3-13) into equation (3-12) and integrating yield the increase in toughness

$$\Delta G = \tfrac{1}{2} f\mu\sigma_N l_{po} \qquad (3\text{-}14)$$

From crack profile and fracture surface observations, l_{po}, is taken as 2 μm, and a reasonable value for the coefficient of friction, μ, as 0.6. The normal stress, σ_N, can have two sources: a) thermal expansion and elastic modulus anisotropy, and b) the increasing bending force during pullout of grains that incline to the main crack. As a rough approximation, we estimate only the thermal stress here from a knowledge of the crystallographic dependence of the thermal expansion coefficient, α, and the elastic modulus, E. The residual stress induced by the thermoelastic misfit can be estimated as:[28]

$$\sigma_N = -\frac{\Delta(\alpha E)\Delta T}{2(1-\nu^2)} \qquad (3\text{-}15)$$

For the 4H-SiC structure, $\Delta(\alpha E) \cong 0.5$ MPa/°C at 25.[38] Setting ΔT as the temperature difference between the processing temperature, 1900°C, and the testing temperature, 25°C, and poisson's ratio, $\nu \cong 0.2$,[39,40] σ_N is estimated to be 480 MPa.

The fracture toughness of the ABC-SiC (processed at 1900°C) rises over the bridging zone from ~ 2.7 to 9.1 MPam$^{1/2}$, which corresponds to an energy increase, $\Delta G = K_c^2 / E - K_0^2 / E \approx 180$ J/m^2, assuming E = 420 GPa. Inserting values of l_{po} = 2 μm, μ = 0.6, σ_N = 480 Mpa, and ΔG = 180 J/m^2, equation (3-14) gives the area fraction f = 0.62. This is a reasonable value compared to the fracture surfaces (Figures 3-15c and 3-17a), where the majority of grains participated in pullout.

Other toughening mechanisms, such as elastic grain bridging and crack deflection, may also play a role. For example, elastic bridging by the debonded grains, located immediately behind the crack tip, contributes to the overall toughness of the material. The energy increase from elastic bridging can be estimated from[28]

$$\Delta G_{EB} = f \frac{\sigma_F^2}{2E} l_{db} \qquad (3\text{-}16)$$

where σ_F is the fracture stress of single crystal SiC grains, and l_{db} the debond length. If the debond length is taken as 2 μm, Young's modulus as 420 GPa, and the strength of a grain bridge as 2 GPa, then even if every grain on the fracture surface participates in the bridging process, ΔG_{EB} is ~9 J/m^2, which is much smaller than the contribution from frictional pullout.[28] Crack deflection is associated with production of the bridging ligaments, but it cannot directly account for the rising R-curve behavior.

3-4 CONCLUSIONS

The mechanical properties of the ABC-SiC processed at various conditions have been evaluated through direct comparison to a commercial Hexoloy SiC. The microstructural origins of the improved fracture toughness / R-curve behavior and the improved strength of the *in situ* toughened ABC-SiC materials are studied. Based on this work, the following conclusions can be made:

1. The ABC-SiC materials made under optimal processing conditions exhibited fracture toughness and flexure strength in excess of 9 MPam$^{1/2}$ and 650 MPa, respectively. This fracture toughness value, over 3 times that of the commercial Hexoloy SiC, is the highest reported to date for any monolithic SiC materials. The best toughness of 9.4 MPam$^{1/2}$ (averaged value) was achieved by hot pressing at 1900°C for 4 hours (with a strength of 650 MPa); the best strength of 760 MPa (averaged value) was obtained by processing at 1840°C for 1 hour (with a toughness of 8.9 MPam$^{1/2}$). The Weibull modulus of a high toughness ABC-SiC was determined to be 18.6 in comparison to 5.6 for the Hexoloy SiC.

2. The much improved toughness and strength of the ABC-SiC were attributed to an unique microstructure that comprised of interlocking high-aspect-ratio plate-shaped grains. Toughening in the ABC-SiC was mainly attributed to grain bridging and pullout by the plate-shaped grains, which led to a significant rising R-curve behavior. The pullout length was possibly limited by the grain interlocks. In contrast, the commercial Hexoloy SiC fractured transgranularly at a toughness, K_c, below 3 $MPam^{1/2}$ with no rising R-curve behavior.

3. The intergranular failure in the ABC-SiC, hot pressed at temperatures $\leq$ 1900°C, was associated with the thin amorphous film at grain boundaries. When processed at higher temperatures (either by hot pressing or by an subsequent annealing), the materials showed transgranular fracture, indicating a possibility of losing the grain boundary phase at these temperatures.

3-5. REFERENCES

[1]L. C. De Jonghe, MSE130 lecture notes, University of California at Berkeley, (1996).

[2]R. Garvie, R. Hannink, and R. Pascoe, "Ceramic Steel?", Nature, **258**, 703 (1975).

[3]M. J. Hoffmann and G. Petzow, "Microstructural Design of Si_3N_4 Based Ceramics," in Silicon Nitride Ceramics, ed. I. W. Chen, P. F. Becher, M. Mitomo, G. Petzow, and T. S. Yen, MRS Symposium Proc., Vol. 287, pp.3-14, (1993).

[4]P. F. Becher, S. L. Hwang, and C. H. Hsueh, "Using Microstructure to Attack the Brittle Nature of Silicon Nitride Ceramics," MRS Bulletin, **20** [2] 23-27 (1995).

[5]S. K. Lee and C. H. Kim, "Effects of α-SiC versus β-SiC Starting Powders on Microstructure and Fracture Toughness of SiC Sintered with Al_2O_3-Y_2O_3 Additives," J. Am. Ceram. Soc., 77 [6] 1655-58 (1994).

[6]N. P. Padture and B. R. Lawn, "Toughness Properties of a Silicon Carbide with an *in situ* Induced Heterogeneous Grain Structure," J. Am. Ceram. Soc., 77 [10] 2518-22 (1994).

[7]K. Suzuki, "Pressureless-Sintered Silicon Carbide with Addition of Aluminum Oxide," in Silicon Carbide Ceramics--2. Edited by S. Somiya and Y. Inomata, Elsvier Applied Science, NY, NY, pp.162-82, (1991).

[8]M. A. Mulla and V. D. Krstic, "Mechanical Properties of β-SiC Pressureless Sintered with Al_2O_3 Additions," Acta Metall. Mater., **42** [1] 303-08 (1994).

[9]S. S. Shinozaki, "Unique Microstructural Development in SiC Materials with High Fracture Toughness," MRS Bulletin, **20** [2] 42-5 (1995).

[10]E 399 - 83, "Standard Test Method for Plane-Strain Fracture Toughness of Metallic Materials," Annual Book of ASTM Standard, Sec. 3, Vol. 03.01, (1989).

[11]W. L. Fourney and T. Kobayashi, "Influence of Loading System on Crack Propagation and Arrest Behavior in a Double-Cantilever Beam Specimen," pp. 47-59, in Fracture Mechanics Applied to Brittle Materials, ASTM STP 678. Ed. S. W. Freiman, American Society for Testing and Materials, Philadelphia, PA, (1979).

[12]B. J. Pletka, E. R. Fuller, Jr., and B. G. Koepke,, "An Evaluation of Double Torsion Testing--Experimental," pp.19-37, in Fracture Mechanics Applied to Brittle Materials, ASTM STP 678. Ed. S. W. Freiman, American Society for Testing and Materials, Philadelphia, PA, (1979).

[13]G. K. Bansel and W. H. Duckworth, "Fracture Surface Energy Measurements by the Notch-Beam Technique," pp.38-46, in Fracture Mechanics Applied to Brittle Materials, ASTM STP 678. Ed. S. W. Freiman, American Society for Testing and Materials, Philadelphia, PA, (1979).

[14]I. Merkel and U. Messerschmidt, "Fracture Toughness of Sintered SiC Ceramics: a Comparison between Different Methods," Mat. Sci. and Eng., A151, 131-135 (1992).

[15]T Nose and T. Fujii, "Evaluation of Fracture Toughness for Ceramic Materials by a Single-Edge-Precracked-Beam Method," J. Am. Ceram. Soc., **71** [5] 328-33 (1988).

[16]J. J. Petovic and M. G. Mendiratta, "Fracture from Controlled Surface Flaw," pp. 83-102, in Fracture Mechanics Applied to Brittle Materials, ASTM STP 678. Ed. S. W. Freiman, American Society for Testing and Materials, Philadelphia, PA, (1979).

[17]P. Chantikul, G. R. Anstis, B. R. Lawn, and D. B. Marshall, "A Critical Evaluation of Indentation Techniques for Measuring Fracture Toughness: II, Strength Method," J. Am. Ceram. Soc., **64** [9] 539-43 (1981).

[18]G. R. Anstis, P. Chantikul, B. R. Lawn, and D. B. Marshall, "A Critical Evaluation of Indentation Techniques for Measuring Fracture Toughness: I, Direct Crack Measurements," J. Am. Ceram. Soc., **64** [9] 533-38 (1981).

[19]K. Y. Chia and S. K. Lau, "High Toughness Silicon Carbide," Ceram. Eng. Sci. Proc., **12** [9-10] 1845-1861 (1991).

[20]C. W. Li, D. J. Lee, and S. C. Lui, "R-Curve Behavior and Strength for *In-Situ* Reinforced Silicon Nitrides with Different Microstructures," J. Am. Ceram. Soc., **75** [7] 1777-85 (1992).

[21]C. W. Li and J. Yamanis, "Super Toughness Silicon Nitride with R-Curve Behavior," Ceram. Eng. Sci. Proc., **10** [7-8] 632-645 (1989).

[22]G. Vekinis, M. F. Ashby, and P. W. R. Beaumont, "R-Curve Behavior of Al_2O_3 Ceramics," Acta Metall. Mater., **38** [6] 1151-1162 (1990).

[23]D. B. Marshall, B. R. Lawn, and P. Chantikul, "Residual Stress Effects in Sharp-Contact Cracking: II, Strength Degradation," J. Mater. Sci., **14** [9] 2225-35 (1979).

[24]L. M. Braun, S. J. Bennison, and B. R. Lawn, "Objective Evaluation of Short-Crack Toughness Curves Using Indentation Flaws: Case Study on Alumina-Based Ceramics," J. Am. Ceram. Soc., **75** [11] 3049-57 (1992).

[25]B. R. Lawn, Fracture of Brittle Solids -- Second Edition. Cambridge University Press, Cambridge, U. K., (1993).

[26]D. B. Marshall, "Controlled Flaws in Ceramics: A Comparison of Knoop and Vickers Indentation," J. Am. Ceram. Soc., **66** [2] 127-31 (1983).

[27]P. C. Paris and G. C. Sih, "Stress Analysis of Cracks," pp. 30-81, in Fracture Toughness Testing and Its Applications, ASTM STP 381. American Society for Testing and Materials, Philadelphia, PA, (1965).

[28]C. J. Gilbert, J. J. Cao, W. J. MoberlyChan, L. C. De Jonghe, and R. O. Ritchie, "Cyclic Fatigue And Resistance-Curve Behavior Of An *In Situ* Toughened Silicon Carbide With Al-B-C Additions," Acta Metallurgica et Materialia, in press, (1996).

[29]P. F. Becher, "Microstructural Design of Toughened Ceramics," J. Am. Ceram. Soc., **74** [2] 255-69 (1991).

[30]N. P. Padture, "*In Situ*-Toughened Silicon Carbide," J. Am. Ceram. Soc., **77** [2] 519-23 (1994).

[31]S. S. Shinozaki, J. Hangas, K.R. Carduner, M. J. Rokosz, K. Suzuki, and N. Shinohara, "Correlation Between Microstructure and Mechanical Properties in Silicon Carbide with Alumina Addition," J. Mater. Res., **8** [7] 1635-43 (1993).

[32]D. H. Kim and C. H. Kim, "Toughening Behavior of Silicon Carbide with Additions of Yttria and Alumina," J. Am. Ceram. Soc., **73** [5] 1431-34 (1990).

[33]J. J. Cao, "Fracture toughness Measurement from Bend Strength of Beams with Knoop Indentations," unpublished report, (1995).

[34]G. V. Srinivasan, S. K. Lau, and R. S. Storm, "High Temperature Hexoloy™ SX Silicon Carbide, Final Report," $ORNL_{91}$-SG341/1, (1991).

[35]J. J. Cao, W. J. MoberlyChan, L. C. De Jonghe, C. J. Gilbert, and R. O. Ritchie, "*In Situ* Toughened Silicon Carbide With Al-B-C Additions," J. Am. Ceram. Soc., **79** [2] 461-69 (1996).

[36]C. H. Hsueh and P. F.Becher, "Dtermination of the R-curve from the Strength-Indentation Load Relation," J. Am. Ceram. Soc., **78** [8] 2237-39 (1995).

[37]D. Kovar and M. J. Readey, "Role of Grain Size in Strength Variability of Alumina," J. Am. Ceram. Soc., 77 [7] 1928-38 (1994).

[38]Z. Li and R. C. Bradt, in Silicon Carbide'87, Ceramic Transactions, Vol. 2, pp. 313. Ed. J. D. Cawley and C. E. Semler, The American Ceramic Society, Westerville, Ohio, (1987).

[39]Morton Advanced Materials, "CVD Silicon Carbide," Technical Bulletin #107, (1994).

[40]K.Yamada and M. Mohri, "Properties and Applications of Silicon Carbide Ceramics," in Silicon Carbide Ceramics--1, Edited by S. Somiya and Y. Inomata, Elsvier Applied Science, NY, NY, pp.13-44, (1991).

3-6. FIGURE CAPTIONS

Fig. 3-1 Low magnification SEM fractographs showing cracks induced by Knoop indentation in an ABC-SiC processed at 1700°C/1h (a) and in Hexoloy SiC (b). During bending, the crack propagated in a stable manner and the critical crack front became elliptical with an ellipticity of ~ 0.65. The crack depth, a_m, at instability was used to calculate fracture toughness in equation (3-3).

Fig. 3-2 Fracture toughness (a) and four-point bend strength (b) of the ABC-SiC materials hot pressed between 1700°C and 1950°C. Data for Hexoloy SiC, measured under identical conditions, are included for comparison.

Fig. 3-3 Comparison of flaw tolerance among Hexoloy SiC and selected ABC-SiC materials. The flaws were induced by Knoop indentation on the tension surfaces of the bend bars. The indentation loads and the hot pressing conditions are indicted here.

Fig. 3-4 Fracture toughness, K_c, and four-point bend strength, σ_F, as a function of soaking time during hot-pressing at 1900°C.

Fig. 3-5 Fracture toughness, K_c, and four-point bend strength, σ_F, as a function of the square root of grain length (a) and as a function of apparent grain aspect ratio (b) in hot pressed silicon carbides.

Fig. 3-6 Strength-indentation load relations for Hexoloy-SiC and the ABC-SiC plotted in logarithm scales (a) and in linear scales (b), respectively. Note that for Hexoloy SiC data followed a typical $\sigma_m \propto P^{-1/3}$ response, indicating a single-valued toughness, whereas the ABC-SiC shows strongly enhance flaw-tolerance, indicating a pronounced R-curve behavior.

Fig. 3-7 A schematic diagram showing stress intensity factors of the indentation residual stress field, K_{res}, the applied bending stress field, K_a, and the total stress field, $K_{res} + K_a$, as well as the material crack resistance, K_R. Point I at the intersection of K_{res} and K_R represents the initial indentation crack size, C_0. Point T represents crack extension to C_m at the onset of instability. The $K_{res} + K_a$ curve is tangential with the K_R curve at point T.

Fig. 3-8 Plots of parameters $\sigma_m P^{1/3}$ (a) and $C_m P^{-2/3}$ (b) versus the indentation load P. The horizontal lines for Hexoloy SiC are used to calibrate the coefficients χ and Y in equations (3-6a) and (3-6b).

Fig. 3-9 R-curve construction for the ABC-SiC and for Hexoloy SiC. The thinner solid curves are plots of the total stress intensities, K_t, versus crack size in Eq. (3-4) using the strength of indented specimens at each indentation load, P, from Fig. 3-6a. The R-curve is an envelop of tangency to the family of K_t curves. The data points here are determined after Ref. [35].

Fig. 3-10 Comparison of the R-curves deconvoluted from the indentation-strength measurements with that directly measured from precracked DC(T) specimens. Note that the very high plateau (steady-state) fracture toughness of ~9 $MPam^{1/2}$ fro the ABC-SiC in comparison to a single-valued toughness blow 3 $MPam^{1/2}$ for the Hexoloy SiC. The horizontal axis here is the crack extension in the DC(T) specimens, or the crack depth in the indented beam specimens. (Courtesy of C. J. Gilbert for the DC(T) data)

Fig. 3-11 Weibull distributions of flexure strength of the ABC-SiC (processed at 1900°C) and the commercial Hexoloy SiC. Note that the ABC-SiC simultaneously exhibits much better Weibull modulus and mean strength.

Fig. 3-12 Optical micrographs illustrating the radial crack patterns from Vickers indentation in Hexoloy SiC (a), an ABC-SiC hot pressed at 1700°C for 1 hour (b), and an

ABC-SiC hot pressed 1900°C for 4 hours (c). The indentation loads are 39.6 N for (a) and (b), and 98 N for (c).

Fig. 3-13 SEM micrographs of crack paths in (a) an *in situ* toughened ABC-SiC (1900/4h), and (b) Hexoloy SiC. Note the numerous grain-bridging sites in (a) in contrast to the straight and transgranular path in (b). The horizontal arrow shows direction of crack growth.

Fig. 14 SEM micrographs showing that grains were pulled out (a), a grain fractured after some sliding (b), a group of grains were pulled out (c), and contacting facets provided additional sliding friction (d).

Fig. 3-15 SEM fractographs of the ABC-SiC ceramics hot pressed under various conditions: (a) 1700°C/1h, (b) 1780°C/1h, (c) 1900°C/1h, and (d) Hexoloy SiC. These ABC-SiC materials failed intergranularly, whereas the Hexoloy SiC fractured transgranularly.

Fig. 3-16 SEM fractograph shows that grain *b* fractured at the interlock with grain *a*, leaving "triple-point" materials as indicated by arrows on the flat surface of grain *a*.

Fig. 3-17 SEM fracture surfaces of 3 silicon carbides processed under various conditions: (a) hot pressed at 1900°C/1h, (b) hot pressed at 1950°C/1h, and (c) hot pressed at 1900°C/1h and then annealed at 2000°C/3h.

Fig. 3-18 A schematic diagram of a crack with a number of grains pulling out (after Ref. [21]).

CHAPTER 4

OXIDATION BEHAVIOR

4.1. INTRODUCTION

Since advanced SiC materials are projected to mainly be used in high temperature applications, oxidation resistance is of great importance. The oxidation behavior of silicon carbide has been extensively studied for many years, with continuing research activities.[1-10] The generally excellent oxidation resistance of SiC is the result of the formation of a protective silica layer on the surface. The oxidation reaction takes place at the SiC / SiO_2 interface, while the growth rate of the oxide scale is generally believed to be limited by diffusion of oxygen through the oxide.[6, 11, 12]

As has been discussed in the previous chapters, the additions of sintering aids are necessary to densify SiC. Sintering additives, if incorporated into the oxide scale, can change the oxygen diffusivity and thus affect the oxidation resistance. For example, the addition of B reduces the viscosity of the resulting glass, and thus increases the oxygen diffusivity, which in turn raises the oxidation rate. The oxidation behavior of SiC, influenced by impurities and sintering additives, is not well understood in spite of the extensive studies. Large variations on oxidation kinetics exist in the literature.[5,13] A more striking phenomenon is the frequently observed bubbles in the oxide scale of polycrystalline SiC, whereas the origin of bubble formation is still a subject of argument.[2,4,6,10]

Most oxidation studies are performed on SiC single crystals,[4,11,12] CVD SiCs,[7-10] and conventional low-fracture-toughness SiCs with low concentrations of additives.[2-6] On the other hand, current focus of research activities on SiC as a structural material has been directed to the development of tougher, more flaw-tolerant materials, which commonly have higher concentrations of sintering aids.[14-20] For example, under carefully controlled sintering atmospheres, the additions of 10 to 26 wt% Al_2O_3 plus Y_2O_3 (YAG) [14-16] to β-SiC powders have resulted in microstructures containing plate-shaped SiC grains, which provide fracture toughness twice that of the conventional SiC such as Hexoloy. The ABC-SiC materials, described in Chapters 2 and 3, exhibited a fracture toughness over 3 times and strength 1.6 times those of Hexoloy SiC. The oxidation behavior of these *in situ* toughened SiC materials has not been reported in the literature.

The purpose of this chapter is to investigate the oxidation behavior of an ABC-SiC and a hot pressed SiC with 10 wt% YAG, and to compare with that of the commercial Hexoloy SiC containing B and C additives. The influence of sintering aids on bubble formation and the thickness of the oxide scales are examined using scanning electron microscopy (SEM). In order to improve the oxidation resistance of the ABC-SiC, a two-step processing technique was explored. By heat treatment of the green compact at an intermediate temperature, for a prolonged time (typically several tens hours), prior to densification, it has been known to homogenize a number of ceramics both chemically and microstructurally.[21,22] During the homogenization heat treatment, solid sintering aids re-distribute by surface diffusion, which has a lower activation energy than other mass

transport mechanisms. Meanwhile, breaking down of agglomerates and interparticle necking in the powder compact lead to an uniform distribution of pores, and subsequently a uniform microstructure. Homogenization of the sintering aids during the heat treatment is the primary concern in this study.

4-2. EXPERIMENTAL PROCEDURES

4-2.1. Materials

Brief descriptions of the experimental materials are listed in Table 4-1. Sample A (Hexoloy SiC) is used as a reference material. Sample B[i] is doped with 10 wt% YAG (6 wt% Al_2O_3[ii] + 4 wt% Y_2O_3[iii]) and hot pressed at 1950°C for 4 hours. Sample C is an ABC-SiC hot pressed with 3 wt% Al-0.6 wt% B-2 wt% C additions, at 1900°C for 1 hour (detailed descriptions of this material can be found in Chapters 2 and 3). The two-step processed sample D is the same as sample C except an additional pre-heat treatment at 1200°C for 42 hours prior to hot pressing. All samples were ground and polished to a 1 μm finish before the oxidation experiments.

4-2.2. Oxidation Experiments and Analysis

Oxidation was performed in air, at 1400°C, for 20 hours, in a box furnace equipped with $MoSi_2$ heating elements. All samples were loaded in an alumina boat which

---

[i] Courtesy of M. Sixta.
[ii] AKP-53, Sumitomo Chemicals, Tokyo, Japan.
[iii] Grade C, H. C. Starck, Germany.

was covered with alumina plates. Heating and cooling rates were controlled at 10°C /min. The oxide scales were examined and their thickness was measured by SEM. Energy dispersive spectroscopy (EDS) was performed to obtain the compositional information of the oxide scales.

Table 4-1 Description of the Experimental SiC Materials and Oxidation Results

Material	Sintering Additives (wt%)	Hot Pressing Conditions	Oxide Scale Thickness (μm)
A (Hexoloy SiC)	B-C	Sintered	1.6
B (YAG-SiC)	$6Al_2O_3$-4 Y_2O_3	1950°C / 4h	17 - 28
C (ABC-SiC)	3 Al-0.6B-2C	1900°C / 1h	5.0
D (2-step processed ABC-SiC)	3 Al-0.6B-2C	1200°C / 42h +1900°C / 1h	2.6

4-3. RESULTS AND DISCUSSIONS

Figures 4-1 and 4-2 show low magnification micrographs of the top and cross-sectional views of the oxidized surfaces, respectively. The thickness of the oxide scales, measured with an SEM at higher magnifications, are listed in Table 4-1. The morphologies and thickness of the oxide scales are remarkably different with various sintering additives. At low magnifications (< 100x), sample A shows an uniform and thin oxide layer, consistent with the well-known fact that conventional SiC with B and C additives has excellent oxidation resistance. Sample B, with 10 wt% YAG additives, exhibits extremely severe oxidation, having numerous bubbles of sizes up to millimeters in diameter. The high toughness ABC-SiC (sample C) exhibits moderate oxidation. The oxidation resistance of

the two-step processed ABC-SiC is nearly as good as that of the reference material. The various sintering additives are presumably incorporated into the oxide scale, and thus affect the permeability of oxygen. The oxidation rate of SiC is generally believed to be controlled by inward diffusion of oxygen through the oxide layer.[6,11,12]

The addition of YAG into SiC (sample B) accelerates oxidation, forming a thick and rough oxide layer (Figures 4-1b and 4-2b). The oxide scale is nearly 20 times that of the reference material. Bubbles ranging from a few microns to millimeters in diameter were observed (Fig. 4-1b). The oxide layer of this sample appeared to have been liquid at the oxidation temperature. Bubbles were formed by the escape of gaseous oxidation products. Cracking occurred, most likely during cooling, at the SiO_2 / SiC interface as shown in Fig. 4-2b. Thus, the oxide scale in YAG-SiC did not provide a protective layer to prevent further oxidation. As a consequence, the SiC materials with substantial amounts of YAG additives might not suitable for high temperature applications in oxidizing atmospheres.

The high toughness ABC-SiC (sample B) exhibited moderate oxidation resistance. The thickness of the oxide scale was ~3 times that of the reference material; bubbles up to ~10 μm in size were observed (Figures 4-1c and 4-2c). Formation of these bubbles were found to correlate to the secondary phase inclusions, which had been identified mainly as $Al_8B_4C_7$ and Al_4O_4C (see Chapter 2). Fig. 4-3 shows micrographs of the same area before and after oxidation (the sample shown in Fig. 4-3b was oxidized at 1300°C for 2 hours).

The darker regions in Fig. 4-3a indicate secondary phases, while Fig. 4-3b shows that bubble formation corresponds to the secondary phase regions. Compared with the regularly hot pressed material (sample C), the two-step processed ABC-SiC (sample D) exhibited better oxidation resistance, showing an uniform and thin oxide scale.

As have been discussed in Chapter 2, the bulk secondary phase regions related to the Al additive in the regularly hot pressed ABC-SiC. The green compact of sample D, having the same additives as in sample C, was pre-heat treated at 1200°C for 42 hours prior to hot pressing at 1900°C for 1 hour. This two-step processing technique was believed to be effective to reduce or eliminate bulk secondary phases. At elevated temperatures, the Al melt has an equilibrium vapor pressure near its surface. Considering mass transport of Al through a vapor phase from the surface of the Al melt to an ambient where Al is absent, the flux of Al can be described by the Hertz-Langmir equation:[23]

$$J_{Al} = \frac{P}{\sqrt{2\pi MRT}} \qquad (5\text{-}1)$$

where P is the equilibrium vapor pressure of Al at a particular temperature T, M is its molecular weight, and R is the gas constant. Quantitative assessment of the evaporation process was not conducted because the oxygen content in the green compact might affect the evaporation. During the prolonged heat treatment, surface diffusion might also contribute to homogenization.

If all the Al uniformly "coats" the surfaces of the fine SiC powders (with an

assumed surface area of 25 m^2/g), then the 3 wt% Al would provide a coating of thickness h = 4.7 (angstroms) based on the relation:

$$25 \times 10^4 (cm^2/g) \times 94.4\ (g) \times h \times 10^{-8}\ (cm) \times 2.7\ (g/cm^3) = 3\ (g) \qquad (5\text{-}2)$$

This rough estimate shows that the Al can possibly be uniformly distributed as a couple of absorbed monolayers on the SiC particles.

Fig. 4-4 shows SEM micrographs of the oxidized surfaces at a higher magnification than Fig. 4-1. Bubbles were observed in the oxide scale of the reference material (Fig. 4-4a), consistent with the observations made earlier by Mieskowski *et al.* in polycrystalline SiC.[4] Singhal[2] attributed bubble formation to CO evolution at the SiC / SiO_2 interface. Mieskowski *et al.*[4] hypothesized that bubbles resulted from the preferential oxidation of the abundant C inclusions in polycrystalline SiC. Based on oxidation studies on CVD SiC with excess C and thermodynamic calculations, however, Fergus *et al.*[10] indicated that the C inclusion could not be responsible for bubble formation, instead bubbling could be the result of volatilization of a boron hydroxide. Li *et al.*[6] believed that bubble formation in polycrystalline SiC was due to the presence of B. Boron was easily oxidized and B_2O_3 reacted with SiO_2 to formed a low-melting-point eutectic phase, which diffused towards the outer surface of the scale and assisted the formation of bubbles. In the Al-B-C doped materials (samples C and D), graphite inclusions were not detected by transmission electron microscopy (TEM) and Auger electron spectroscopy (AES) studies,[24] and therefore graphite could not be responsible for bubble formation in the

ABC-SiC. The bubbles formed in the regularly hot pressed sample C related to the Al-containing secondary inclusions as shown in Fig. 4-3. Bubbles were rarely observed in the two-step-processed ABC-SiC (sample D). The bright inclusions in the oxide scale of this material were much finer (the existence of these inclusions indicated a need of further refining the two-step processing schedules).

Fig. 4-5 shows examples of EDS spectra performed on the oxide scales (excluding the bubbles or inclusions). The Al / Si atomic ratio in the oxide scale of sample C was 12 / 88, whereas in sample D it was 8 / 92, in contrast to the ~4 / 96 ratio in the initial powder compact. Aluminum was present in the oxide at higher concentrations than the bulk ABC-SiC, indicating that Al preferentially incorporated into the oxide. Some Al might have been lost (escaped from the powder compact) during the homogenization heat treatment of sample D, explaining the low Al content in the oxide scale of sample D than that in sample C. Singhal and Lange[25] reported that increasing Al_2O_3 additives in hot pressed SiC increased the oxidation rate. They suggested the formation of an impure Al-rich silicate liquid in the oxide surface at the oxidation temperature (1370°C in their experiment). The low Al content in the oxide scale of sample D is therefore responsible for its reduced thickness compared to that of sample C.

The features in the oxide scales (Fig. 4-4) suggest (partial) crystallization of the SiO_2. Morphologies of the crystalline phases varied in different materials. The nature of the oxides (crystalline or glass) would influence the oxidation rate, as the oxygen diffusivity varies in different phases. However, further study on this issue is left as a

subject of future work.

4-4. SUMMARY AND CONCLUSIONS

The oxidation behavior of an ABC-SiC and a hot pressed SiC with Al_2O_3-Y_2O_3 (YAG) additives were studied in comparison with a commercial SiC. Based on this work, the following conclusions can be made:

1. The oxidation resistance of SiC is very sensitive to the sintering additives. The thickness of the oxide scales differed by a factor of nearly 20 in the tested materials. Furthermore, the sintering additives had strong effect on the smoothness (roughness) and morphologies of the oxide scales. Thus, in the course of developing high toughness SiC ceramics, the influence of sintering additives on oxidation behavior must be considered.

2. The two-step processed ABC-SiC exhibited superior oxidation resistance compared to the regularly hot pressed material. The former showed a more uniform and thinner oxide scale. In the regular processed ABC-SiC, bubble formation was found to correlate to the secondary phase inclusions. The two-step processing technique homogenized the sintering additives, and therefore minimized bubble formation.

3. The addition of YAG to SiC severely degraded the oxidation resistance, causing large surface bubbles and cracking in the oxide / SiC interface. Thus, the YAG-added SiC, though possibly achieving improved fracture toughness at room temperature, might not be suitable for services in oxidizing atmospheres at elevated temperatures.

4-5. REFERENCES

[1]G. Ervin, "Oxidation Behavior of Silicon Carbide," J. Am. Ceram. Soc., **41** [9] 347-52 (1958).

[2]S. C. Singhal, "Oxidation Kinetics of Hot-Pressed Silicon Carbide," J. Mater. Sci., 11, 1246-53, (1976).

[3]J. A. Costello and R. E. Tressler, "Oxidation Kinetics of Hot-Pressed and Sintered α-SiC," J. Am. Ceram. Soc., **64** [6] 327-31 (1981).

[4]D. M. Mieskowski, T. E. Mitchell, and A. H. Heuer, "Bubble Formation in Oxide Scales on SiC," J. Am. Ceram. Soc., **67** [1] C17-C18 (1984).

[5]J. A. Costello and R. E. Tressler, "Oxidation Kinetics of Silicon Carbide Crystals and Ceramics: I, In Dry Oxygen," J. Am. Ceram. Soc., **69** [9] 674-81 (1986).

[6]J. Li, P. Eveno, and A. M. Huntz, "Oxidation of SiC," Werkstoffe und Korrosion, 41, 716-725, (1990).

[7]J. W. Fergus and W. L. Worrell, "The Oxidation of Chemically Vapor Deposited Silicon Carbide," Corrosion and Corrosive Degradation of Ceramics, Eds R. E. Tressler and M. McNallan, Ceramic Transactions, Vol. 10, 41-51 (1990).

[8]R. Berjon, J. Rodriguez, and F. Sibieude, "AES Study of the SiO2/SiC Interface in the Oxidation of CVD β-SiC," Surface Science, 271, 237-243 (1992).

[9]T. Narushima, T. Goto, Y. Yokoyama, M. Takeuchi, Y. Iguchi, and T. Hirai, "Active-to-Passive Transition and Bubble Formation for High-Temperature Oxidation of Chemically Vapor-Deposited Silicon Carbide in CO-CO_2 Atmosphere," J. Am. Ceram. Soc., 77 [4] 1079-82 (1994).

[10]J. W. Fergus and W. L. Worrell, "Effect of Carbon and Boron on the High-Temperature Oxidation of Silicon Carbide," J. Am. Ceram. Soc., **78** [7] 1961-64 (1995).

[11]Z. Zheng, R. E. Tressler, and K. E. Spear, "Oxidation of Single-Crystal Silicon Carbide, Part I," J. Electrochem. Soc., **137** [3] 854-858 (1990).

[12]Z. Zheng, R. E. Tressler, and K. E. Spear, "Oxidation of Single-Crystal Silicon Carbide, Part II," J. Electrochem. Soc., **137** [9] 2812-2816 (1990).

[13]Y. W. Kim, M. Mitomo, and H. Hirotsuru, "Grain Growth and Fracture Toughness of Fine-Grained Silicon Carbide Ceramics," J. Am. Ceram. Soc., **78** [11] 3145-48 (1995).

[14]S. K. Lee and C. H. Kim, "Effects of α-SiC versus β-SiC Starting Powders on Microstructure and Fracture Toughness of SiC Sintered with Al_2O_3-Y_2O_3 Additives," J. Am. Ceram. Soc., 77 [6] 1655-58 (1994).

[15]N. P. Padture, "*In Situ*-Toughened Silicon Carbide," J. Am. Ceram. Soc., 77 [2] 519-23 (1994).

[16]N. P. Padture and B. R. Lawn, "Toughness Properties of a Silicon Carbide with an in Situ Induced Heterogeneous Grain Structure," J. Am. Ceram. Soc., 77 [10] 2518-22 (1994).

[17]S. S. Shinozaki, "Unique Microstructural Development in SiC Materials with High Fracture Toughness," MRS Bulletin, **20** [2] 42-5 (1995).

[18]M. A. Mulla and V. D. Krstic, "Mechanical Properties of β-SiC Pressureless Sintered with Al_2O_3 Additions," Acta Metall. Mater., **42** [1] 303-08 (1994).

[19]J. J. Cao, W. J. MoberlyChan, L. C. De Jonghe, C. J. Gilbert, and R. O. Ritchie, "In Situ Toughened Silicon Carbide With Al-B-C Additions," J. Am. Ceram. Soc., **79** [2] 461-69 (1996).

[20]C. J. Gilbert, J. J. Cao, W. J. MoberlyChan, L. C. De Jonghe, and R. O. Ritchie, "Cyclic Fatigue And Resistance-Curve Behavior Of An *In Situ* Toughened Silicon Carbide With Al-B-C Additions," Acta Metallurgica et Materialia, in press, (1996).

[21]M. Y. Chu, L. C. De Jonghe, M. K. F. Lin, and F. J. T. Lin, "Precoarsening to Improve Microstructure and Sintering of Powder Compacts," J. Am. Ceram. Soc., **74** [11] 2902-11 (1991).

[22]T. Ohji and L. C. De Jonghe, "Presintering Heat Treatment, densification, and Mechanical Properties of Silicon Carbide," J. Am. Ceram. Soc., 77 [6] 1685-87 (1994).

[23]F. W. Sears and G. L. Salinger, Thermodynamics, Kinetic Theory, and Statistical Thermodynamics (3rd Ed.), Addison Wesley, (1975).

[24]W. J. MoberlyChan, "The β-3C to α-4H Phase Transformation and Microstructural Development in SiC Hot Pressed with Al, B and C Additives," to be published.

[25]S. C. Singhal and F. F. Lange, "Effect of Alumina Content on the Oxidation of Hot Pressed Silicon Carbide," J. Am. Ceram. Soc., **58** [9-10] 433-35 (1975).

4-6. FIGURE CAPTIONS

Fig. 4-1 SEM micrographs showing the morphologies of the oxidized surfaces of SiCs with various sintering additives. Micrographs (a) through (d) are for samples A through D, respectively.

Fig. 4-2 SEM Cross-sectional views of oxidized SiC materials with various sintering additives. Images (a) through (d) are for samples A through D, respectively.

Fig. 4-3 SEM micrographs of the same area of the polished and oxidized surfaces of the ABC-SiC (sample C): a polished surface (a) and the oxidized surface (b). Bubble formation correlated to the secondary inclusions.

Fig. 4-4 SEM top views of oxidized SiC materials: Hexoloy SiC (a), ABC-SiC (b) and a two-step processed ABC-SiC (c).

Fig. 4-5 EDS spectra of the oxide scales on sample C (a) and sample D (b).

PART III. OXIDE-COATED SiC PLATELET / SiC COMPOSITES

CHAPTER 5

PROCESSING, MICROSTRUCTURES, and MECHANICAL PROPERTIES OF OXIDE-COATED SiC PLATELETS / SiC COMPOSITES

5-1. INTRODUCTION

The dispersion of second-phase particles can improve the fracture toughness of ceramics. However, the choice of toughening phases in a SiC matrix is limited by the severe sintering conditions. High temperature stability and chemical compatibility of the reinforcement with SiC are necessary requirements. The incorporation of TiB_2 [1] and TiC [2,3] particulates in SiC matrix raises the fracture toughness to ~ 6 $MPam^{1/2}$. The thermal expansion coefficient mismatch between TiB_2 or TiC and the matrix SiC generates a compressive hoop stress and a tensile radial stress around the particles, causing crack deflection and an increment in fracture toughness. At elevated temperatures, however, the internal stresses are relieved and the toughness degrades.[4] Moreover, many projected applications for advanced ceramics involve thermal cycling. The composites with high CTE mismatch may subject to subcritical fatigue crack growth and eventually catastrophic failure even without bearing external loads.

SiC platelets have been shown to be effective reinforcements in alumina,[5,6] aluminum nitride,[7] and mullite.[8] The apparent chemical compatibility of α-SiC platelets makes them an ideal reinforcing phase in a SiC matrix. A high aspect ratio of the platelets can potentially provide significant toughening.[9] Without a protective barrier, however, the

reinforcement of SiC platelets in a SiC matrix is likely to be negated by exaggerated growth the platelets and strong bonding between the matrix and the platelets. Therefore, fabrication of useful SiC platelet / SiC composites requires a means of protection to the platelets. Production of an interfacial phase can protect the integrity of the platelets during sintering and hopefully also achieve a weak bonding between the platelets and the matrix, thereby promoting crack deflection and/or platelet bridging and pullout. The isolation of the platelets from the matrix can be accomplished by the encapsulation of the platelets with an appropriate oxide. A layer of silica, for example, is readily introduced by oxidation of the platelets in air. Yttria, alumina, or titania coatings from aqueous solutions onto a number of ceramic substrates have been demonstrated by De Jonghe and co-workers.[5,10-13] A preliminary use of alumina-coated SiC platelets in a β-SiC matrix has shown promising mechanical properties, yielding in some instances a fracture toughness of over 7 $MPam^{1/2}$.[14]

The objective of this work aimed at fabrication of oxide-encapsulated SiC platelets reinforced SiC composites with no or minor CTE mismatch. SiC platelets were encapsulated with alumina, yttria, and silica. The relative effects of these coatings in the composites were evaluated. Efforts were made to achieve coupled-toughening from platelets reinforcement and *in situ* toughening in the matrix.

5-2. EXPERIMENTAL PROCEDURES

5-2.1. Encapsulation of SiC Platelets in Oxides

The SiC platelets,[i] with a predominantly 4H crystal structure, have diameters ranging from 3 to 30 microns (average 10 microns), and thickness ranging from 0.5 to 3 microns. Three types of oxide encapsulation were used in this study.

5-2.1a Production of a Silica Layer on SiC Platelets

SiC platelets were oxidized in air at 1300°C for 3 hours to form a layer of silica. The oxidation kinetics was known to follow parabolic kinetics,[15-17] from which the thickness of the silica layer was estimated to be about 100 nm.

5-2.1b Encapsulation with Alumina

Kapolnek and De Jonghe[11] and Mitchell and De Jonghe[5] obtained heterogeneous precipitation of hydrated basic aluminum sulfate on powder surfaces using urea decomposition in aqueous solutions of salts. The SiC platelets used in this study were coated with this alumina precursor extending the procedures described in Ref. [5, 14] as follows.

A small amount of polymeric dispersant[ii] was dissolved at room temperature in distilled water. SiC platelets were then added. An aqueous solution of hydrated aluminum

---

[i] Third Millennium Technologies, Inc., Grade -400 mesh.
[ii] PVP K30, GAF Chemical Corporation.

sulfate[iii] and urea[iv] was mixed with the suspended platelets in a flat-bottom distilling flask. The slurry contained 0.1 M hydrated aluminum sulfate, 0.2 M urea, 10 g/L platelets, and 0.75 g/L PVP K30. The mixture was vigorously stirred using a mechanical stirrer, and slowly heated to 92°C and held for 24 hours. The platelets were coated with a hydrated basic aluminum sulfate by heterogeneous precipitation. The coated platelets were then annealed in an inert gas at 880°C for 6 hours, which converted the coatings to crystalline alumina.

5-2.1c Encapsulation with Yttria

The hydrolysis of yttrium salts by urea decomposition was first used to synthesize monodispersed particles of yttrium hydroxycarbonate.[18] Garg and De Jonghe[10] extended this method to encapsulate powders and whiskers of silicon nitride with a yttria precursor. This method had also been used to coat alumina fibers.[12] In the present work, SiC platelets were coated in the same manner with the following modifications to the processing parameters.

A suspension contained 0.1 M yttrium nitrate,[v] 0.75 M urea, 10 g/L SiC platelets, and 0.75 g/L PVP K30 was slowly heated on a heating mantel, capped with a water-cooled reflux condenser, to a final temperature of 65°C and held for 20 hours. Magnetic stirring was maintained to prevent the platelets from settling or agglomerating. After the reaction run, the suspension was allowed to settle, and the supernatant was discarded. The

[iii] crystals, Fisher Scientific.
[iv] Mallinckrodt
[v] NOAH Tech. Co., TA.

coated platelets were re-sedimented in water to remove any free precipitates, rinsed twice in acetone, and air dried at room temperature. The coated platelets were then calcined at 650°C for 12 hours to convert the coating to crystalline yttria.

5-2.2. Production of Oxide-Encapsulated SiC Platelet / SiC Composites

The β-SiC powders with 3 wt% Al, 0.6 wt% B, and 2 wt% C sintering additives for the matrix were prepared as described in chapter 2. Appropriate quantities of α-SiC platelets with the various types of encapsulations were mixed with the β-SiC powder mixture, cold compacted into 38 mm diameter discs at a uniaxial pressure of 35 MPa, and then hot pressed at various temperatures. Fig. 5-1 shows a schematic processing route.

5-2.3. Mechanical Testing

Bend bars of the composites were prepared in the same manner as described in chapter 3. Strength was again evaluated in 4-point bend tests and the fracture toughness by the controlled surface flaw method.

5-3. RESULTS AND DISCUSSION

5-3.1. Encapsulation of SiC Platelets

Successful coating requires careful control of the processing parameters, including the reaction temperature (reaction kinetics), concentrations of the salts and urea, and surface area of the platelets. Controlled heterogeneous precipitation on the platelet surface

is necessary and homogeneous precipitation has to be avoided. In principle, the coating processes of alumina and yttria precursors are quite similar. The microstructural development of the coating of alumina precursor can be found in Ref. [5]; here we only discuss the coating process of yttria. Upon heating in an aqueous solution, urea decomposes according to the reaction:[19]

$$(NH_2)_2CO + H_2O \rightarrow 2\ NH_3 + CO_2 \qquad (5\text{-}1)$$

The product ammonia acts as a base slowly and uniformly added to the solution, and therefore causes the pH of the system to progressively increase.[19] Yttrium hydroxycarbonate (YBC) forms by the hydrolysis of yttrium nitrate in a urea-containing aqueous solution.[18] The pH decreases upon formation of yttrium hydroxycarbonate. Measurements indicate that the pH of the suspension drops initially due to the ionization of yttrium nitrate. Subsequently, the pH rises as a result of continued urea decomposition. After ~2 hours, the pH stabilizes at approximately 5.5, due to the rate balance between urea decomposition and precipitation of the yttria precursor, until the coating run is terminated after 20 hours (Fig. 5-2). The constant pH should correspond to a yttrium hydroxycarbonate concentration between the homogeneous nucleation and the heterogeneous nucleation limits, as traditionally shown on a LaMer diagram.[20] Therefore, nuclei can form heterogeneously either on the surface of the platelets or on existing precipitates. Simultaneously, the already existing precipitates grow. Since the concentration never reaches the homogeneous nucleation limit, free precipitation in the solution is minimized. The morphology of the obtained coating is consistent with such a

mechanism. Experimental observation shows that the coating initially appears as discrete particles on the surface of the SiC platelets. These precipitates grow, meanwhile the population of the precipitates increases with time. Eventually the coating covers the entire surfaces.

Figure 5-3a and 5-3b exhibit SEM micrographs of the uncoated and yttria-coated SiC platelets, respectively. This calcined yttria coating completely covers the platelets. X-ray diffraction determines that the coating has been converted to crystalline yttria after calcination at 650°C for 12 hours. The heating rate and the soaking temperature of the calcination process have to be carefully controlled to avoid extensive cracking of the deposit. Annealing at excessive temperatures (e.g., 900°C) induces film cracking (Fig. 5-3c). From the cracked coating, we may estimate the thickness of the yttria film to be approximately 0.25 μm.

Fig. 5-4 shows an SEM micrograph of alumina coated platelets after calcination. The coating presents a good coverage on the platelets and has a thickness of 1 to 2 μm. Experiments also show that etching the platelets with HF, prior to the application of alumina coating, does not significantly affect the morphology nor the thickness of the alumina coating under identical coating conditions.

5-3.2. Coated SiC Platelets in a Fine-Grained SiC Matrix

SiC composites were hot pressed to nearly full density at 1700°C for 1 hour. The polished surfaces of the composites were examined by optical and scanning electron microscopy. Fig. 5-5 shows two polished perpendicular surfaces of a composite with alumina-coated platelets. The bright areas are the alumina coatings that continuously surround the platelets. During hot pressing, the platelets had rotated and preferentially aligned in a plane perpendicular to the hot pressing direction. Similar observation on preferential orientation of platelets was reported in an alumina-matrix composite.[21]

The current sintering additives of a combination of Al, B, and C effectively promoted densification of the composites. This processing temperature of 1700°C was very low for SiC matrix composites. Previous work showed that particulate TiC and TiB_2 reinforced SiC materials were hot pressed at temperatures upwards 2100°C.[1-3] Densification of a composite with a large volume fraction of reinforcement phase could be hindered by the percolation of the second phase. The oxide coating prevented the platelets from physically contacting each other. In addition, creep of the oxide coating during hot pressing eased sliding of the platelets relative to each other. The low processing temperature also suppressed the $\beta \rightarrow \alpha$ phase transformation in the matrix and ensured a fine-grained microstructure. Transmission electron microscopy revealed all β-phase, mostly equiaxed grains ranging from submicron to 2 microns in the matrix.[22]

The measured fracture toughness results are listed in Table 5-1. The coatings are essential in these composites. The alumina-coated platelets reinforced SiC composite shows a 50% increase in the fracture toughness over that of the monolithic material. Note that the toughness of the composite is twice that of the commercial Hexoloy SiC. On fractographs, the alumina-coated platelets were noticed to interact with the crack, resulting in more tortuous fracture surfaces. In a composite with uncoated platelets, however, the crack breaks through most of the uncoated platelets, resulting in a minimal increase in toughness over that of the monolithic SiC (Table 5-1). A thin layer of silica, introduced by oxidation, also does not produce effective separation between the matrix and platelets, with only a limited increase in toughness. Two possible reasons can be cited. First, the oxidation product has been considered as a mechanically strong protective layer,[15-17] thereby suggesting the bonding between silica and silicon carbide is very strong. Strong interfacial bonding is known to be disadvantageous in ceramic composites. Second, there is a possibility that the silica layer is completely reduced by sintering additives during hot pressing.

The composite with yttria-coated platelets shows very limited increase in toughness over that of the monolithic SiC (see Table 5-1). The bonding strength between SiC and yttria is not known. Moreover, the morphology of the yttria coating changed to isolated islands during sintering; the yttria coating does not fully separate the platelets from contacting the matrix (Fig. 5-6). Therefore, the platelets may have been partially sintered together with the matrix.

The strengths of the composites are lower than the monolithic materials (Table 5-1). The addition of platelets may have induced larger internal flaws.

Table 5-1. Comparison of Mechanical Properties of Monolithic Silicon Carbides and Oxide-Encapsulated SiC_P / SiC Composites

Materials	Hot Pressing Temperatures[i]	Bend Strength (MPa)	Fracture Toughness (MPa$\sqrt{m}$)
Commercial Hexoloy SiC	sintered	400 ± 40	2.9 ± 0.1
Monolithic ABC-SiC	1700°C	600 ± 90	4.2 ± 0.1
"	1780°C	630 ± 100	5.9 ± 0.3
"	1840°C	770 ± 50	8.9 ± 0.5
"	1900°C	660 ± 20	9.1 ± 0.5
Composite with Al_2O_3-coated platelets	1700°C	470 ± 10	6.3 ± 0.8
"	1780°C	390 ± 10	7.7 ± 1.0
"	1840°C		7.9 ± 0.2
"	1900°C	380 ± 10	8.1 ± 0.8
Composite with uncoated platelets	1700°C	440 ± 30	4.8 ± 0.3
Composite with Y_2O_3-coated platelets*	1700°C	400 ± 30	4.7 ± 0.4
Composite with oxidized platelets**	1700°C	530 ± 60	4.4 ± 0.2

[i] All materials were hot pressed for ~1 hour except the Hexoloy, which was free sintered at an unreported temperature.

* This composite contained 14 vol% of platelets. ** Contained 10 vol% of platelets. All the other composites contained 20 vol% of platelets.

5-3.3. Alumina-Coated SiC Platelets in a Self-Toughened Matrix

In an attempt to combine the toughening effects from platelet reinforcement and matrix-grain-bridging, alumina-coated SiC platelets / SiC composites were processed at temperatures ranging from 1700°C to 1900°C. When the hot pressing temperature was below ~1800°C, the composites exhibited higher toughness than the corresponding monolithic materials (Fig. 5-7). Fig. 5-8 shows fracture surfaces of a composite processed at 1780°C. The platelets provided sites for crack deflection and participated in pullout to a certain degree (Fig. 5-8a). At the same time, the matrix fractured intergranularly and the matrix-grains were pulled out (Fig. 5-8b). The overall toughness of the composite was a simple additive combination of the platelet reinforcement and matrix-grain-bridging in energy terms,[23,24] and could be described as

$$K_C = [E^c(J^0 + \Delta J^{gb} + \Delta J^{pr})]^{1/2} \qquad (5\text{-}2)$$

where E^c is the elastic modulus of the composite, J^0 is the energy consumption by lattice bond rupture, ΔJ^{gb} is the energy consumed by matrix grain bridging, and ΔJ^{pr} is the energy by platelet reinforcement.

From the expression (5-2), a better composite toughness was expected in a toughened matrix with highly elongated grains. The composites hot pressed at temperatures above ~ 1800°C, however, showed lower toughness than the corresponding monolithic materials. Three reasons could be envisioned. First, the presence of the

reinforcing platelets inhibited growth of the elongated grains in the matrix. Thus, grain-bridging in the matrix was less effective compared to the *in situ* toughened monolithic SiC under the same hot pressing conditions. Becher[23] showed that the added SiC whiskers in an Si_3N_4 composite worked as effective grain-growth inhibitors. Second, the high processing temperature influenced the stability of the alumina coating on the platelets. The higher the sintering temperature, the larger the alumina grain size in the coating. The large grain size would enhance grain boundary grooving and pin-hole formation. Thus the alumina coating might become isolated islands instead of a continuous barrier. We have observed in an yttria-coated SiC platelet / SiC composite that a uniform yttria-coating changed to discrete islands (Fig. 5-6). Finally, at temperatures > 1800°C, the alumina-coating might have been degraded due to a chemical reaction between alumina and SiC as was suggested by a thermodynamic calculation.[25]

5-4. CONCLUSIONS

Hot pressed SiC matrix composites containing oxide-encapsulated α-SiC platelets were prepared and investigated. The platelets were either encapsulated with hydrated aluminum sulfate or yttrium hydroxycarbonate (later calcined to form alumina or yttria) from aqueous solutions, or oxidized to form a silica layer. The coated platelets were then used to fabricate SiC composites. Encapsulation of SiC platelets with oxide coatings prevented direct contact of the platelets (platelet network), and eased densification of the composites. An alumina coating proved to be most effective to protect the integrity of the

SiC platelets, and to promote crack deflection, thereby resulting in an increase in fracture toughness. A composite with alumina-coated platelets in a fine-grained matrix exhibited a fracture toughness 50% higher than the monolithic material processed under the same conditions. Coupled toughening from matrix-grain-bridging and coated-platelets reinforcement resulted in a toughness of 8 $MPam^{1/2}$, representing a two and a half-fold increase in toughness over the commercial Hexoloy SiC. Tailoring the microstructure of the composite to promote coupled-toughening, however, was limited by the stability of the alumina-coating at the densification temperature of the composites. In fact, an *in situ* toughened monolithic SiC showed higher fracture toughness (> 9 $MPam^{1/2}$) and better strength than the composites.

5-5. REFERENCES

[1]Y. Ohya, M. J. Hoffmann, and G. Petzon, "Sintering of in-situ Synthesized SiC-TiB_2 Composites with Improved Fracture Toughness", J. Am. Ceram. Soc., **75** [9] 2479-83 (1992).

[2]G. Wei and P. Becher, "Improvements in Mechanical Properties in SiC by the Addition of TiC Particles", J. Am. Ceram. Soc., **67** [8] 571-74 (1984).

[3]M. Janney, "Microstructural Development and Mechanical Properties of SiC and of SiC-TiC Composites", Am. Ceram. Soc. Bull., **65** [2] 357-62 (1986).

[4]B. Lin, T. Yano and T. Iseki, "High - Temperature Toughening Mechanism in SiC / TiC Composites", J. Ceram. Soc. Japan, **100** [4] 509-513 (1992).

[5]T. D. Mitchell, Jr., L. C. De Jonghe, "Alumina-SiC Composites from Coated Powders", J. Am. Ceram. Soc., **78** [1] 199-204 (1995).

[6]Y. Chou and D. J. Green, "Silicon Carbide Platelet/Alumina Composites: 2, Mechanical Properties", J. Am. Ceram. Soc., **76** [6] 1452-58 (1993).

[7]N. Claussen, "Ceramic Platelet Composites", in Proceedings of the 11th RISO International Symposium on Metallurgy and Materials Science 1990, structural Ceramics Processing, Microstructure and Properties. Edited by J. J. Bentzen, J. B. Bilde-Sorensen, N. Christiansen, A. Horsewell, and B. Ralph. RISO National Laboratory, Roskidle, Denmark, (1990).

[8]C. Nischik, M. M. Seibold, N. A. Travitzky, and N. Claussen, "Effect of Processing on Mechanical Properties of Platelet-Reinforced Mullite Composites", J. Am. Ceram. Soc., **74** [10] 2464-68 (1991).

[9]K. T. Faber and A. G. Evans, "Crack Deflection Processes - 1. Theory", Acta Metall., **31** [4] 565-76 (1983).

[10]A. K. Garg and L. C. De Jonghe, "Microencapsulation of silicon nitride particles with yttria and yttria-alumina precursors", J. Mater. Res., **5** [1] 136-42 (1990).

[11]D. Kapolnek and L. C. De Jonghe, "Particulate Composites from Coated Powders," J. Europ. Ceram. Soc., 7, 1-7 (1991).

[12]J. P. Daniel and L. C. De Jonghe, "Coating of Ceramic Fibers with Yttria", A. Ceram. Soc. Ann. Meet., Indianapolis, April 1994, Paper No. SIII-105-94.

[13]M. Gopal, W. J. MoberlyChan, and L. C. De Jonghe, "Synthesis of Rutile and Anatase at Low Temperatures", ibid, Paper No. SVIIa-8-94.

[14]T. Mitchell, Jr., L. C. De Jonghe, W. J. MoberlyChan, and R. O. Ritchie, "Silicon Carbide Platelet/Silicon Carbide Composites", J. Am. Ceram. Soc., **78** [1] 97-103 (1995).

[15]Z. Zheng, R. E. Tressler, and K. E. Spear, "Oxidation of Single-Crystal Silicon Carbide, Part I," J. Electrochem. Soc., 137 [3] 854-858 (1990).

[16]Z. Zheng, R. E. Tressler, and K. E. Spear, "Oxidation of Single-Crystal Silicon Carbide, Part II," J. Electrochem. Soc., 137 [9] 2812-2816 (1990).

[17]J. Li, P. Eveno, and A. M. Huntz, "Oxidation of SiC", Werkstoffe and Korrosion. **41**, 716-25 (1990).

[18]M. Akinc and D. Sordelet, Adv. Ceram. Mater., **2** [3A] 232 (1987).

[19]J. E. Blendell, H. K. Bowen, and R. L. Coble, Am. Ceram. Soc. Bull., **63** [6] 797-802 (1984).

[20]V. K. LaMer and R. H. Dinegar, J. Am. Chem. Soc., **72** [11], 4847 (1950).

[21]Y. Chou and D. J. Green, "Silicon Carbide Platelet/Alumina Composites: I, Effect of Forming Technique on Platelet Orientation," J. Am. Ceram. Soc., **75** [12] 3346-52 (1992).

[22]J. J. Cao, W. J. MoberlyChan, L. C. De Jonghe, B. Dalgleish, and M. Y. Niu, "Processing and Characterization of SiC Platelet / SiC Composites," Advances in Ceramic-Matrix Composites II, Ceramic Transactions, Vol. 46, pp. 277-88, (1994).

[23]P. F. Becher, "Microstructural Design of Toughened Ceramics," J. Am. Ceram. Soc., **74** [2] 255-69 (1991).

[24]P. F. Becher, E. R. Fuller, and P. Angelini, "Matrix-Grain-Bridging Contributions to the Toughness of Whisker-Reinforced Ceramics," J. Am. Ceram. Soc., **74** [9] 2131-35 (1991).

[25]A. Gadalla, M. Elmasry, and P. Kongkachuichay, "High Temperature Reactions Within SiC-Al2O3 Composites," J. Mater. Res., 7 [9] 2585-92 (1992).

5-6. CAPTIONS

Fig. 5-1 The pH values of the solution in an yttria-precursor coating run.

Fig. 5-2 A schematic processing route for oxide-encapsulated SiC_p / SiC composites. SiC platelets were encapsulated in either alumina, yttria, or silica. The β-SiC powders were mixed with 3 wt% Al, 0.6 wt% B, and 2 wt% C. After mixing the coated platelets with the β-SiC powders, the composites were hot pressed at various temperatures.

Fig. 5-3 SEM micrographs of the uncoated (a) and yttria-coated (b) SiC platelets. Annealing the coated platelets at an excessive temperature (900°C) induced cracking in the coating (see insert).

Fig. 5-4 SEM micrograph of alumina-coated SiC platelets.

Fig. 5-5 SEM micrographs of polished surfaces of a SiC composite hot pressed at 1700°C: a) of a surface perpendicular to the hot pressing direction and b) of a surface parallel to the hot pressing direction. The composite is near fully dense. The alumina-coating provided a continuous barrier to protect the integrity of the platelets and a weak interphase.

Fig. 5-6 TEM micrograph of a SiC composite with yttria-coated platelets. Note that the yttria coating changed its morphology to discrete islands after hot pressing of the composite.

Fig. 5-7 Fracture toughness of monolithic ABC-SiC and alumina-coated SiC platelets reinforced SiC composites hot pressed at various temperatures. The toughness of a commercial Hexoloy SiC, measured under identical conditions, is also shown for comparison.

Fig. 5-8 Fractograph of an alumina-coated SiC platelet / SiC composite hot pressed at 1780°C for 1 hour. Crack deflection and some pullout occurred at the platelets (a) and intergranular fracture of the matrix grains provided matrix-grain-bridging (b).

PART IV. CONCLUSIONS

CHAPTER 6

CONCLUSIONS

Monolithic SiC ceramics with Al, B, and C additions (ABC-SiC) and oxide-encapsulated SiC platelet / SiC composites were prepared by hot pressing. The processing-microstructure-property relations were investigated with the aim of improving the fracture toughness. Sintering behavior, phase transformations, and microstructural development of the hot pressed SiC ceramics were analyzed using a number of characterization techniques. The mechanical properties of the ABC-SiC and the composites processed at various conditions were evaluated through direct comparison to a commercial SiC (Hexoloy SA). The improved fracture toughness / R-curve behavior and the improved strength of the *in situ* toughened ABC-SiC materials were correlated to the microstructural observations. Based on this work, the following conclusions can be made:

1. The combination of Al, B, and C sintering additives were very effective in densification of SiC and in promotion of the β-to-α phase transformation. With the additions of 3 wt% Al, 0.6 wt% B, and 2 wt% C, β-SiC was densified by hot pressing at 1700°C, which is about 300°C below the common sintering temperatures for SiC materials. Under such processing conditions, a β-phase fine-grained microstructure was obtained. By hot pressing at higher temperatures, the β-to-α (3C-to-4H) phase transformation took place, forming initially (β + α) dual phase plate-shaped grains. The α portion of the grain preferentially grew in the basal plane, and pulled the β part to grew with it. Growth of the

highly elongated grains inevitably produced grain interlocks. Thus a microstructure was obtained containing a 3-D interlocking network of high-aspect-ratio plate-shaped grains. An amorphous thin grain-boundary film (1 nm), and partially crystalline triple junctions were observed. Isolated bulk secondary phases, having similar sizes as the added Al powders, was identified mainly as $Al_8B_4C_7$.

2. The ABC-SiC materials, under optimal processing conditions, showed excellent flaw tolerance and a significant rising R-curve behavior with a steady-state fracture toughness in excess of 9 $MPam^{1/2}$. This fracture toughness value, over 3 times that of the commercial Hexoloy SiC, is believed to be the highest reported to date for any monolithic SiC materials. The Hexoloy SiC, in contrast, displayed a toughness below 3 $MPam^{1/2}$ with no rising R-curve behavior. The four-point bend strength of the high toughness ABC-SiC was 1.6 times that of the Hexoloy SiC, with a weibull modulus of 18.6 for the ABC-SiC in comparison to 5.6 for the Hexoloy SiC. The best fracture toughness of 9.4 $MPam^{1/2}$ (averaged value over 4 measurements) was achieved by hot pressing at 1900°C for 4 hours (with a strength of 650 MPa); the best average strength of 760 MPa (with the highest value being 840 MPa) was obtained by processing at 1840°C for 1 hour (with a toughness of 8.9 $MPam^{1/2}$).

3. The much improved toughness and strength of the ABC-SiC were attributed to its unique microstructure. The amorphous thin film at grain boundaries led to crack deflection, grain boundary debonding, and formation of bridging ligaments. Grain bridging and subsequent pullout of the high-aspect-ratio plate-shaped grains dissipated large

amounts of energy, providing an effective toughening mechanism in the ABC-SiC. In contrast, the commercial Hexoloy SiC fractured transgranularly, consistent with the low fracture toughness of this material with no rising R-curve behavior.

4. The oxidation behavior of an ABC-SiC and a hot pressed SiC with Al_2O_3-Y_2O_3 (YAG) additives were studied in comparison with the commercial Hexoloy SiC. The oxidation resistance of SiC ceramics was found to be very sensitive to the sintering additives. The Hexoloy SiC exhibited the best oxidation behavior, while the ABC-SiC showed much better oxidation resistance than the YAG-added SiC. The two-step processed ABC-SiC displayed a more uniform and thinner oxide scale than the regularly hot pressed material. In the regularly processed ABC-SiC, bubble formation was found to correlate to the secondary-phase inclusions. The two-step processing technique was believed to homogenize the sintering additives in the material, thus minimizing bubble formation. The addition of YAG to SiC severely degraded the oxidation resistance, causing large surface bubbles and cracking at the oxide / SiC interface.

5. Hot pressed SiC matrix composites containing oxide-encapsulated α-SiC platelets were prepared and investigated. The platelets were either encapsulated with hydrated aluminum sulfate or yttrium hydroxycarbonate (later calcined to form alumina or yttria) from aqueous solutions. Encapsulation of SiC platelets with oxide coatings prevented direct contact of the platelets (platelet network), and eased densification of the composites. An alumina coating proved to be most effective to protect the integrity of the SiC platelets, and to promote crack deflection, thereby resulting in an increase in fracture toughness. A

composite with a fine-grained matrix exhibited a fracture toughness 50% higher than the monolithic material processed under the same conditions. Coupled toughening from matrix-grain-bridging and coated-platelets reinforcement resulted in a toughness of 8 $MPam^{1/2}$, representing two and a half-fold increase in toughness over the commercial Hexoloy SiC. Tailoring the microstructure of the composite to promote coupled-toughening, however, was limited by the processing temperature of the composite at which the alumina coating was stable.

(a) 3C (β) - SiC

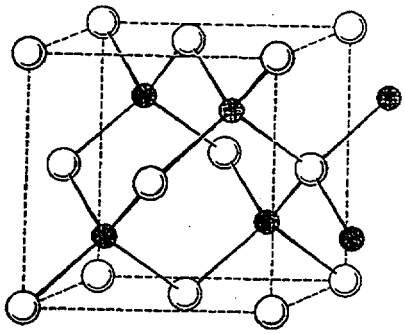

(b) 2H (α) - SiC

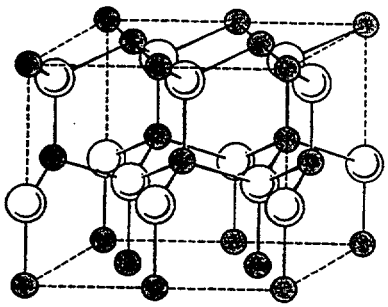

(c) 6H (α) - SiC

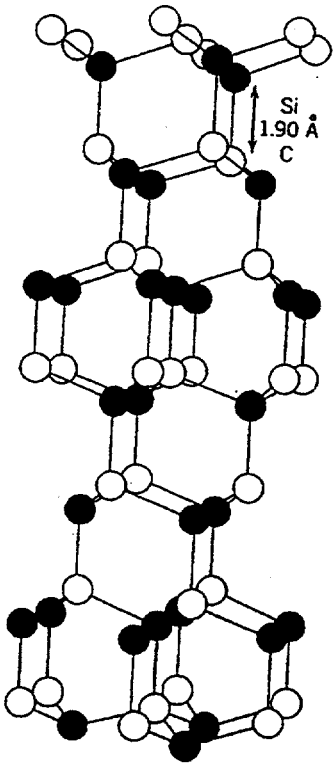

Fig. 1-1 Crystal structures of (a) 3C-, (b) 2H-, and (c) 6H-SiC.

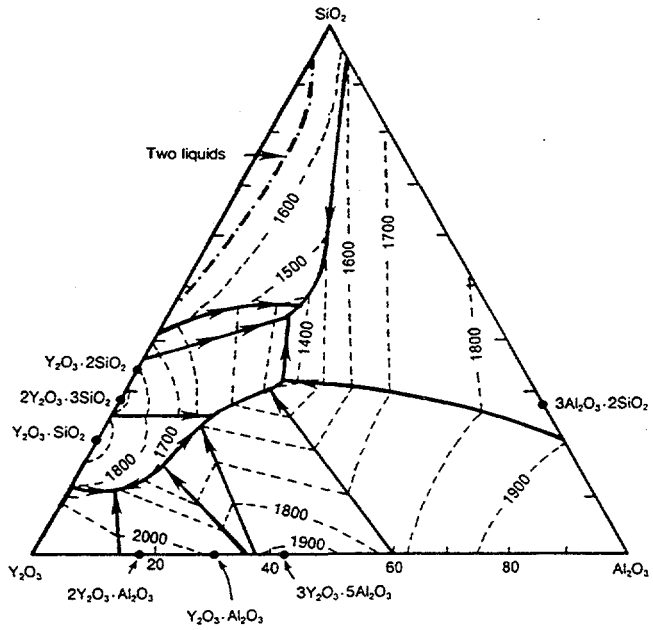

Fig. 1-2 Equilibrium phase diagram between Al_2O_3-Y_2O_3-SiO_2.

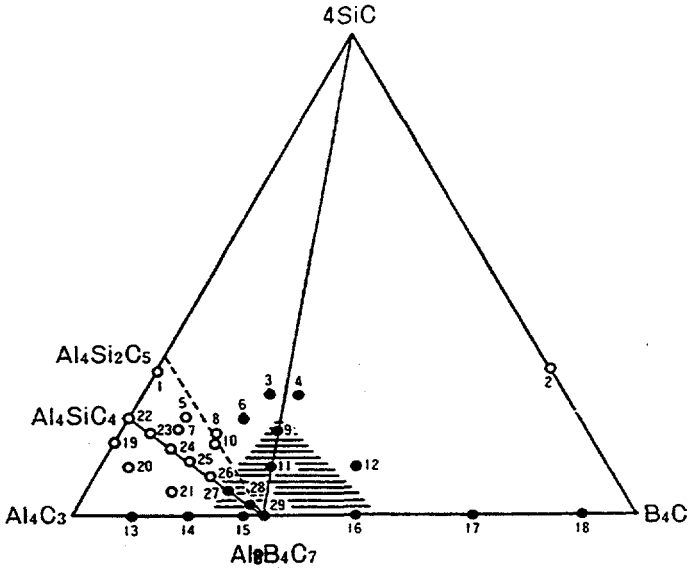

Fig. 1-3 Phase relationships for the SiC-B_4C-Al_4C_3 system at 1800 ℃. The shaded area is the region where a liquid was formed at 1800 ℃.

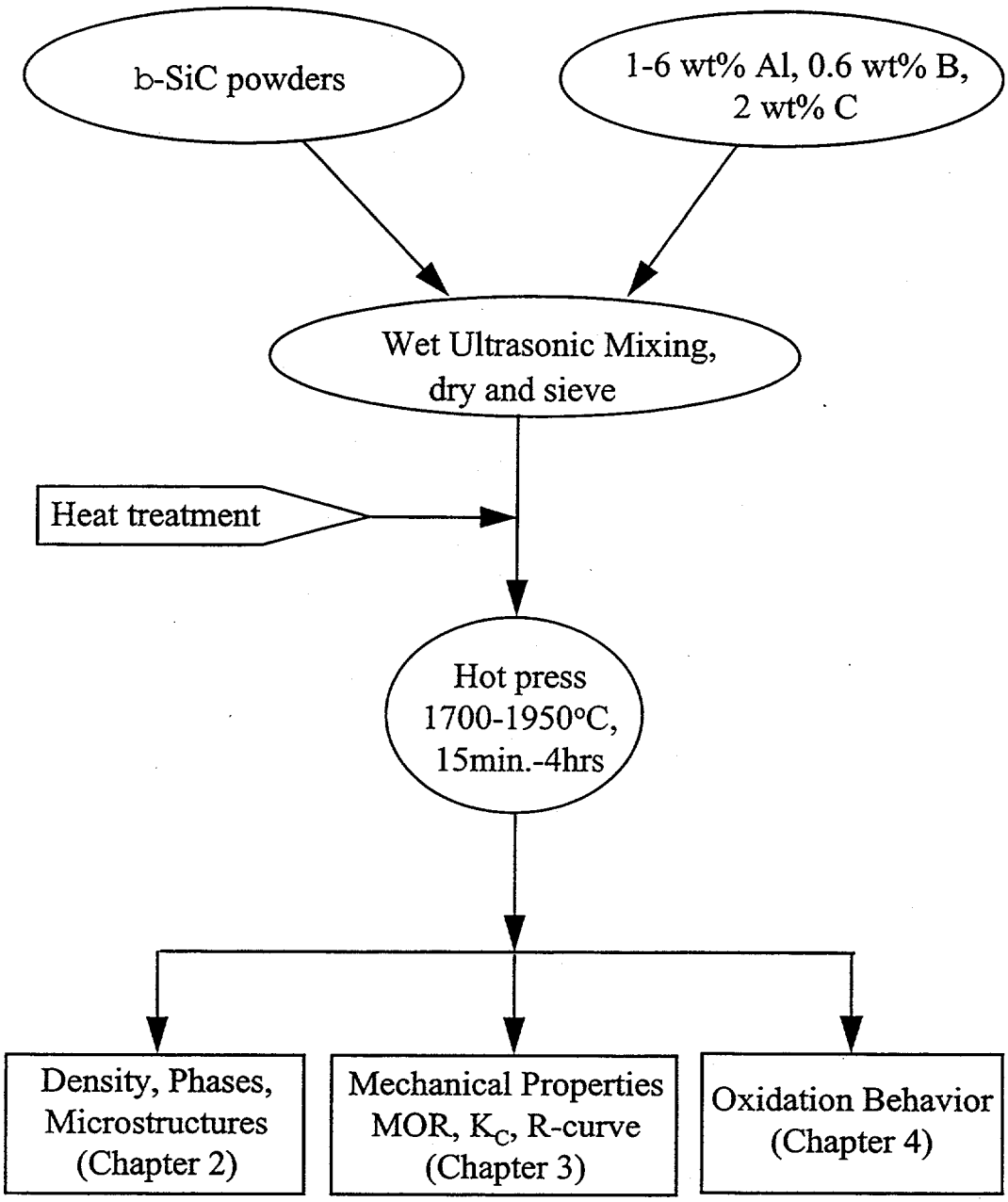

Fig. 2-1 Flow chart of processing procedures of SiC with Al, B, and C additions (referred to as ABC-SiC). Mechanical properties and oxidation behavior are discussed in chapters 3 and 4, respectively.

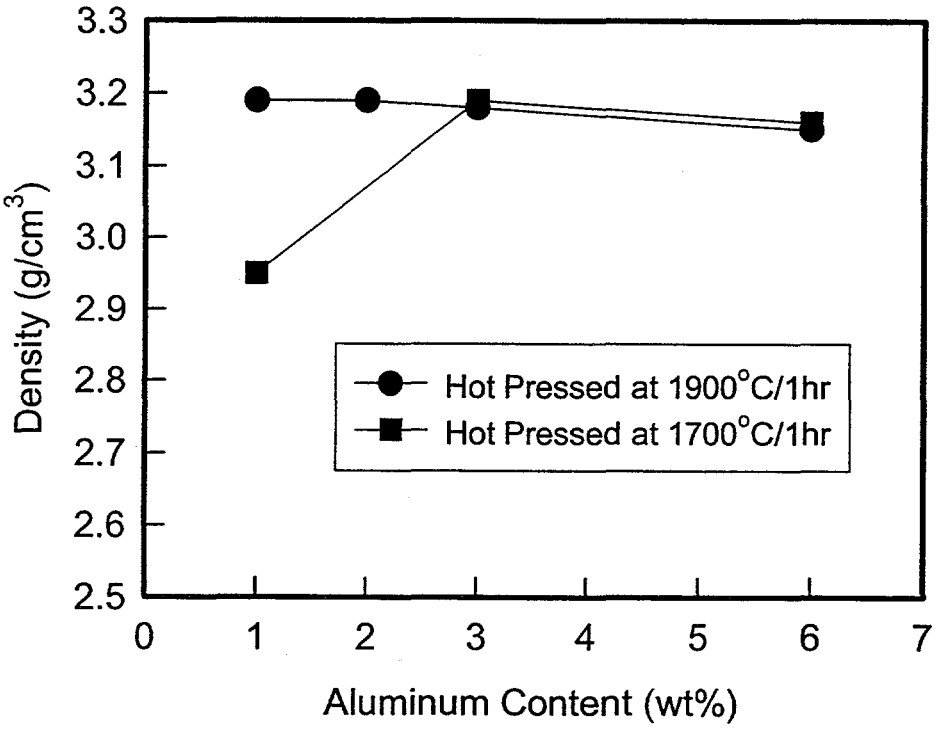

Fig. 2-2 Densities of silicon carbides hot pressed at 1700°C and 1900°C with various amounts of Al, together with 0.6wt%B and 2wt%C additives. The theoratical density of SiC is 3.21 g/cm^3.

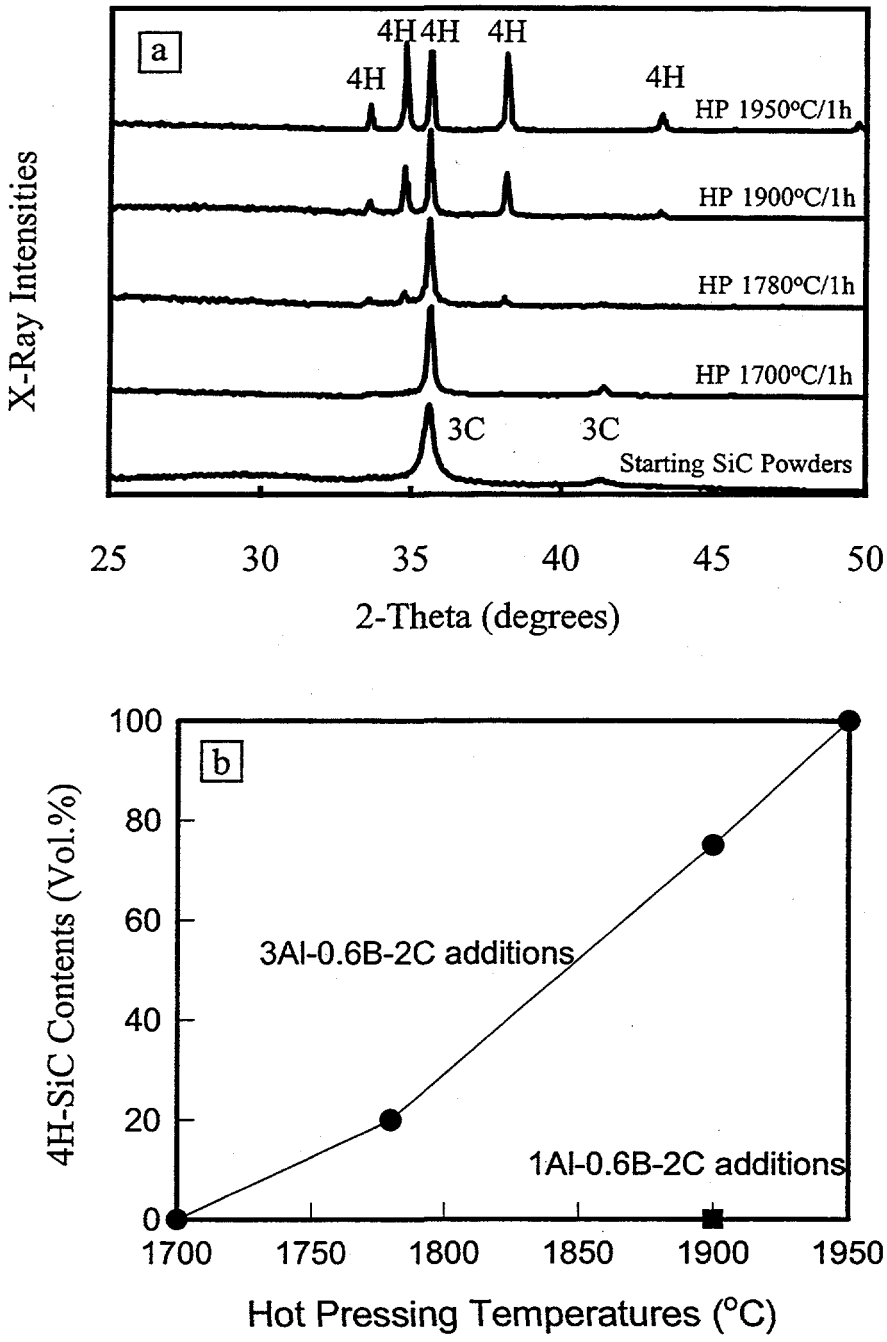

Fig. 2-3 X-ray diffraction spectra of the starting β-SiC powder and of the ABC-SiC materials hot pressed for 1 hour at 1700°C, 1780°C, 1900°C, and 1950°C, respectively (a). Fig. 2-3b plots the volume fraction of the 4H phase in ABC-SiC processed for 1 hour with 3 wt% Al-0.6 wt% B-2 wt% C as a function of temperature. The material with 1 wt% Al contains negligible α phase after hot pressing at 1900°C for 1 hour.

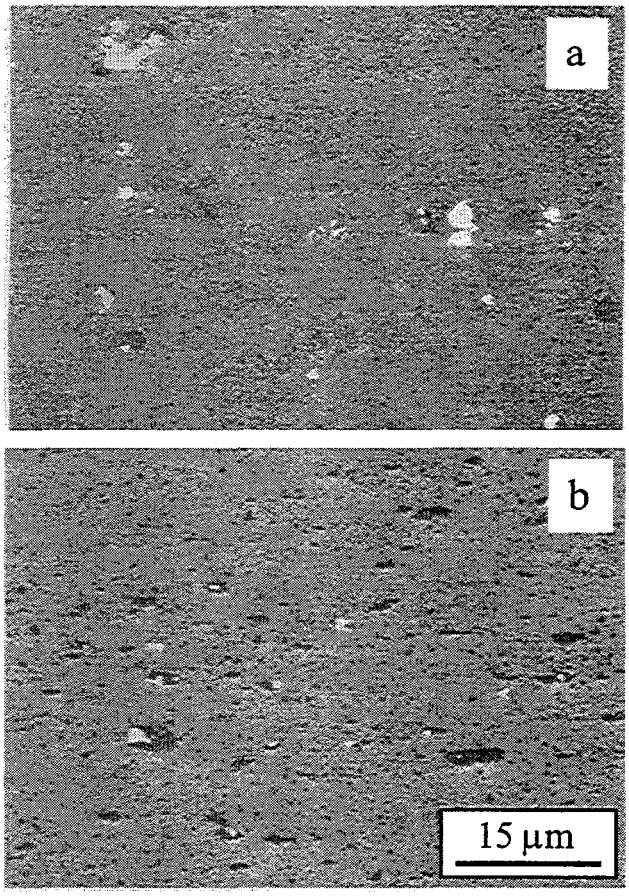

Fig. 2-4 SEM micrographs of polished surfaces of a SiC with 6 wt% Al (3 μm nominal size), 0.6 wt% B, and 2 wt% C: (a) normal to the hot pressing direction and (b) a cross-section which is parallel to the hot pressing direction. The gray background is SiC, while the darker and brighter regions are the secondary phases.

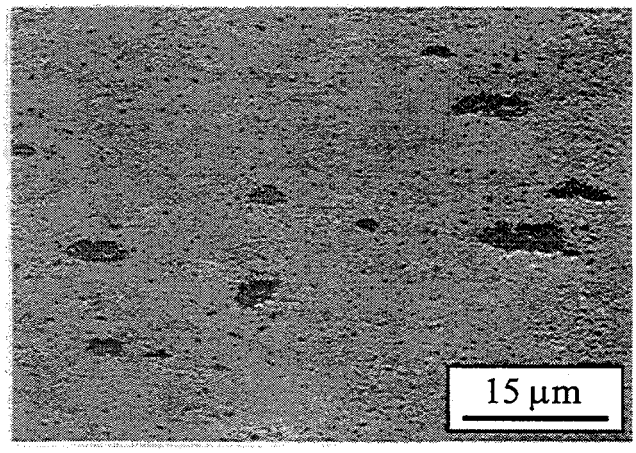

Fig. 2-5 SEM micrographs of a polished cross-section (parallel to the hot pressing direction) of a SiC with 6 wt% Al (10 μm nominal size), 0.6 wt% B, and 2 wt% C. Note that the secondary phase regions are larger than those in Fig. 2-4b.

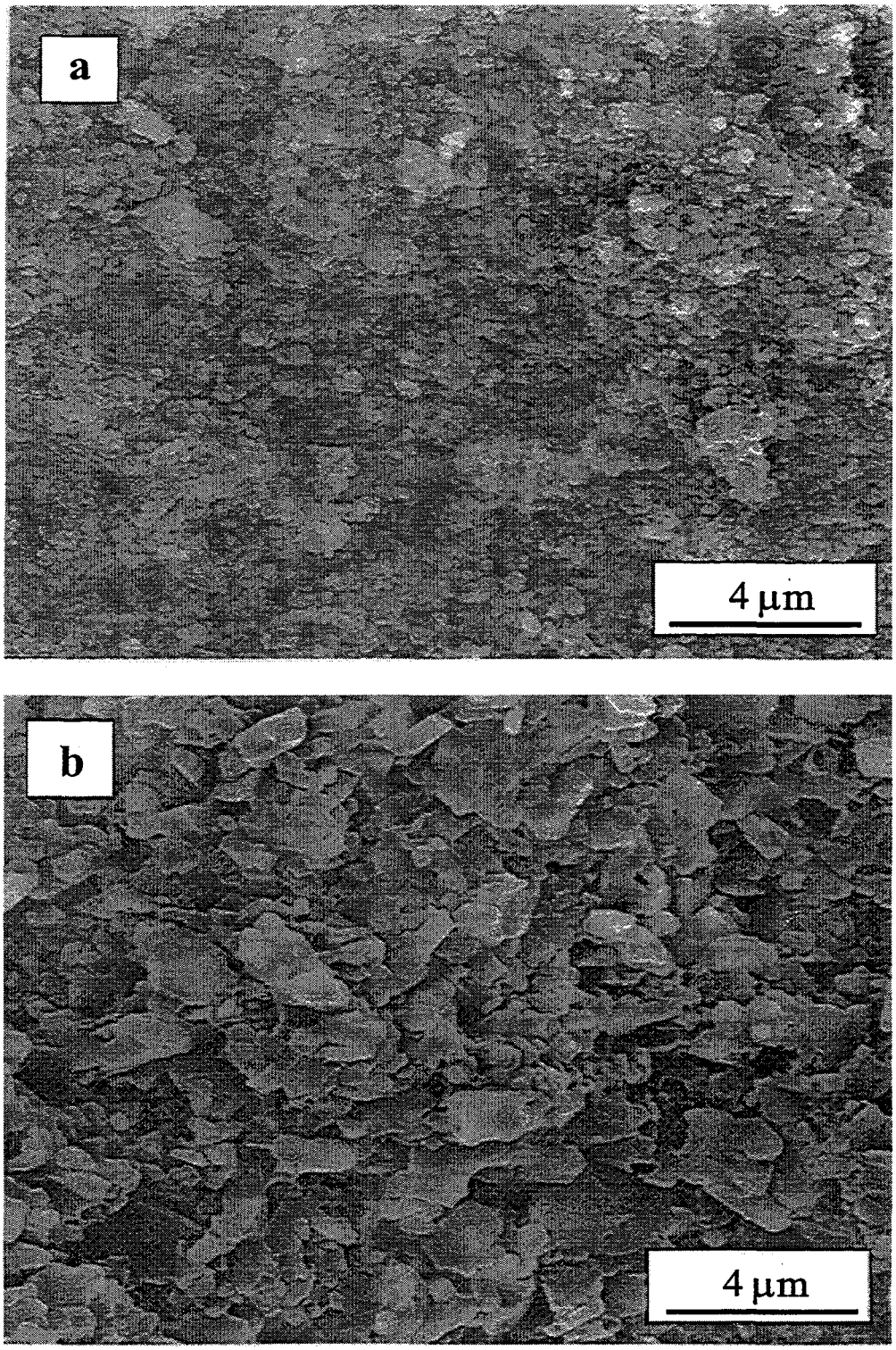

Fig. 2-6 SEM micrographs of (a) the green compact and of ABC-SiC hot pressed under various conditions: (b) 1700°C/1h, (b) 1780°C/1h, and (c) 1900°C/4h (etched in a molten salt mixture at 500°C for 8 hours).

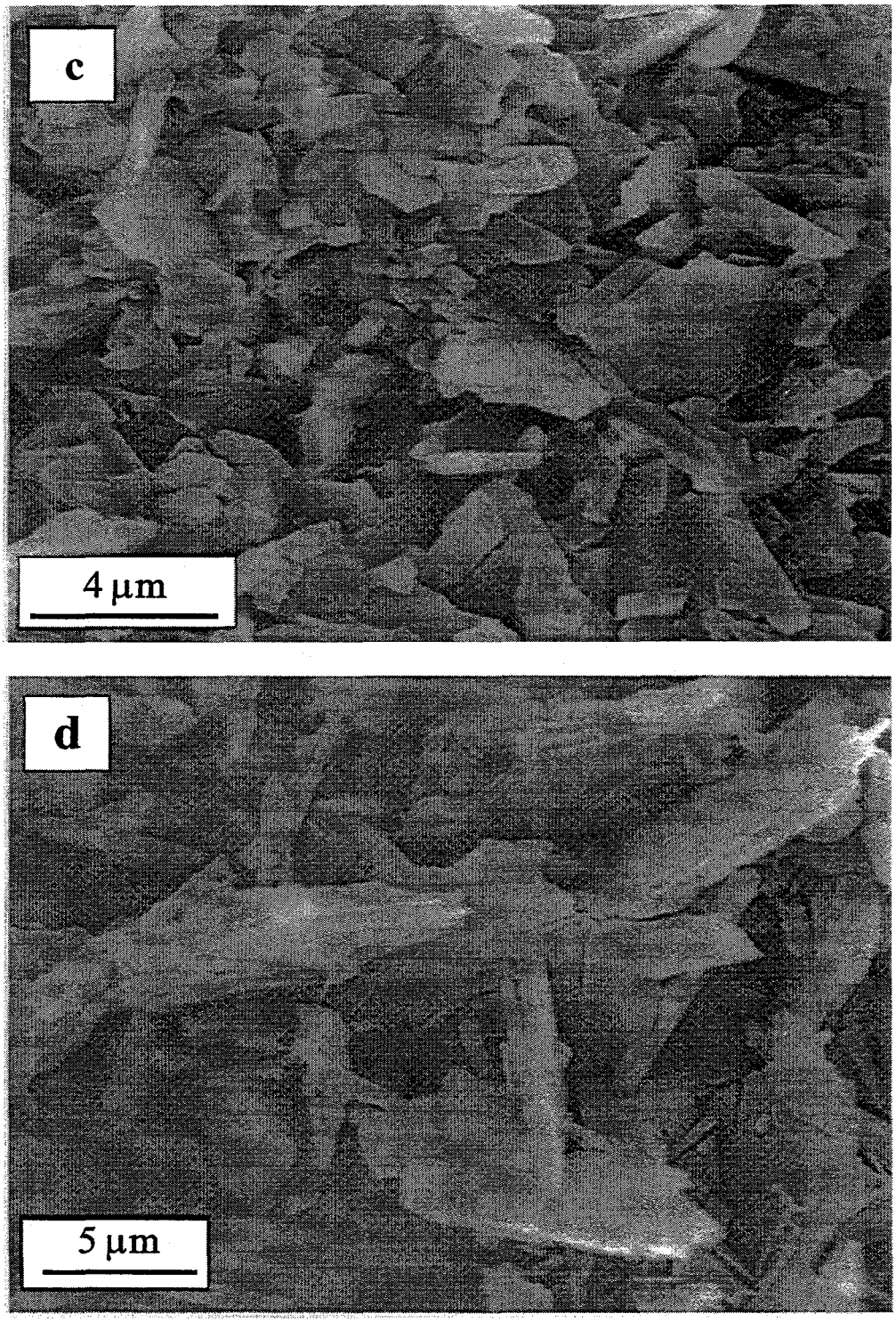

Fig. 2-6 SEM micrographs of (a) a green compact and of the ABC-SiC hot pressed at various conditions: (b) 1700°C/1h, (c) 1780°C/1h, and (d) 1900°C/4h (etched in a molten salt mixture at 500°C for 8 hours).

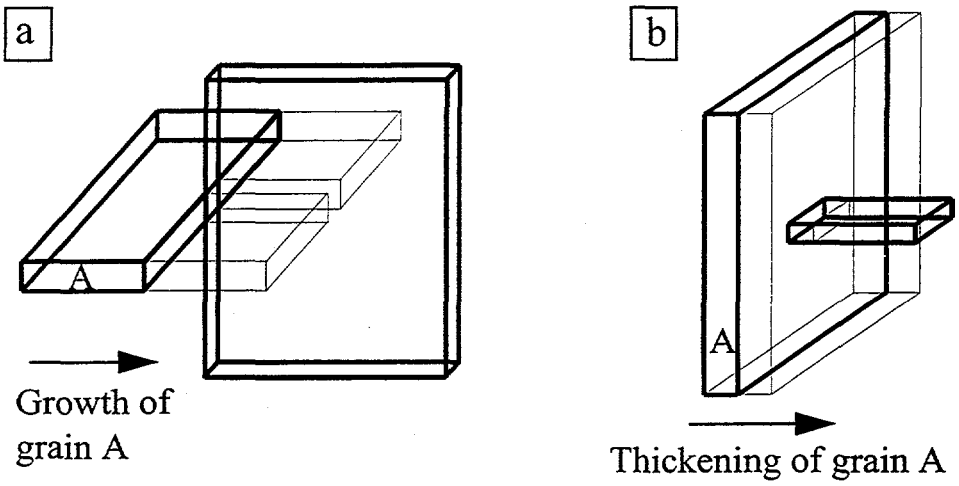

Fig. 2-7 Formation of grain interlocks (schematics) in the microstructure when plate-shaped grains intersect edge to edge (a), or edge to the basal plane (b).

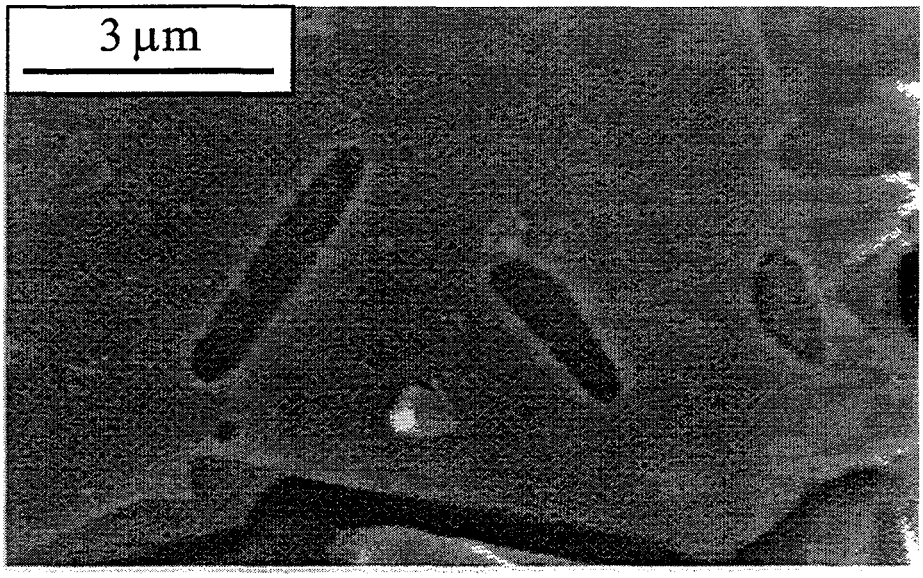

Fig. 2-8 SEM micrograph showing grain "imprints" on a the broad face of a plate-shaped grain. The specimen was etched in a molten salt mixture at 500°C for 8 hours. A Schematic illustration on the formation of the imprints is shown in Fig. 2-7b.

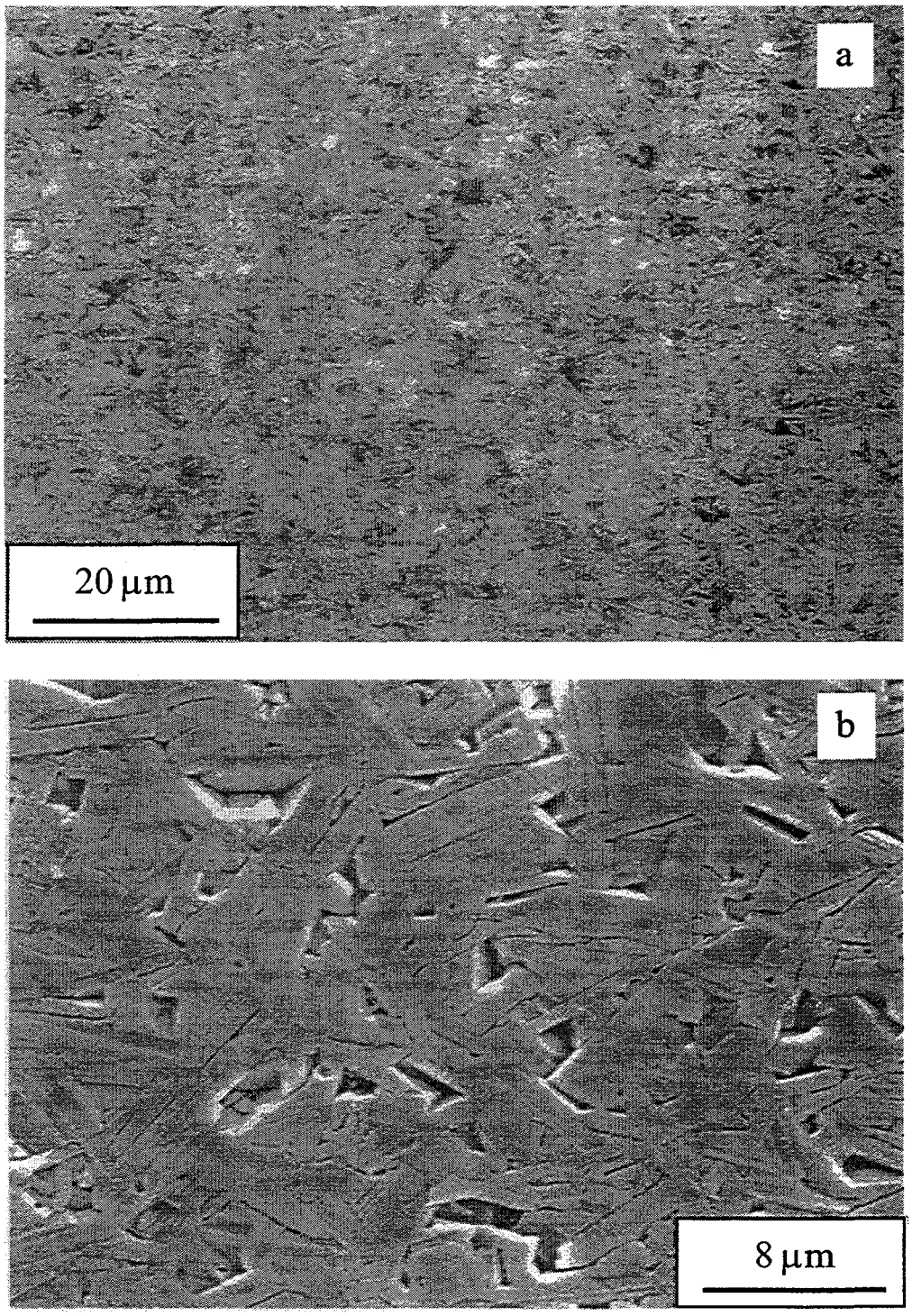

Fig. 2-9 (a) Optical and (b) SEM micrographs of an etched surface of the ABC-SiC hot pressed at 1900°C for 1 h.

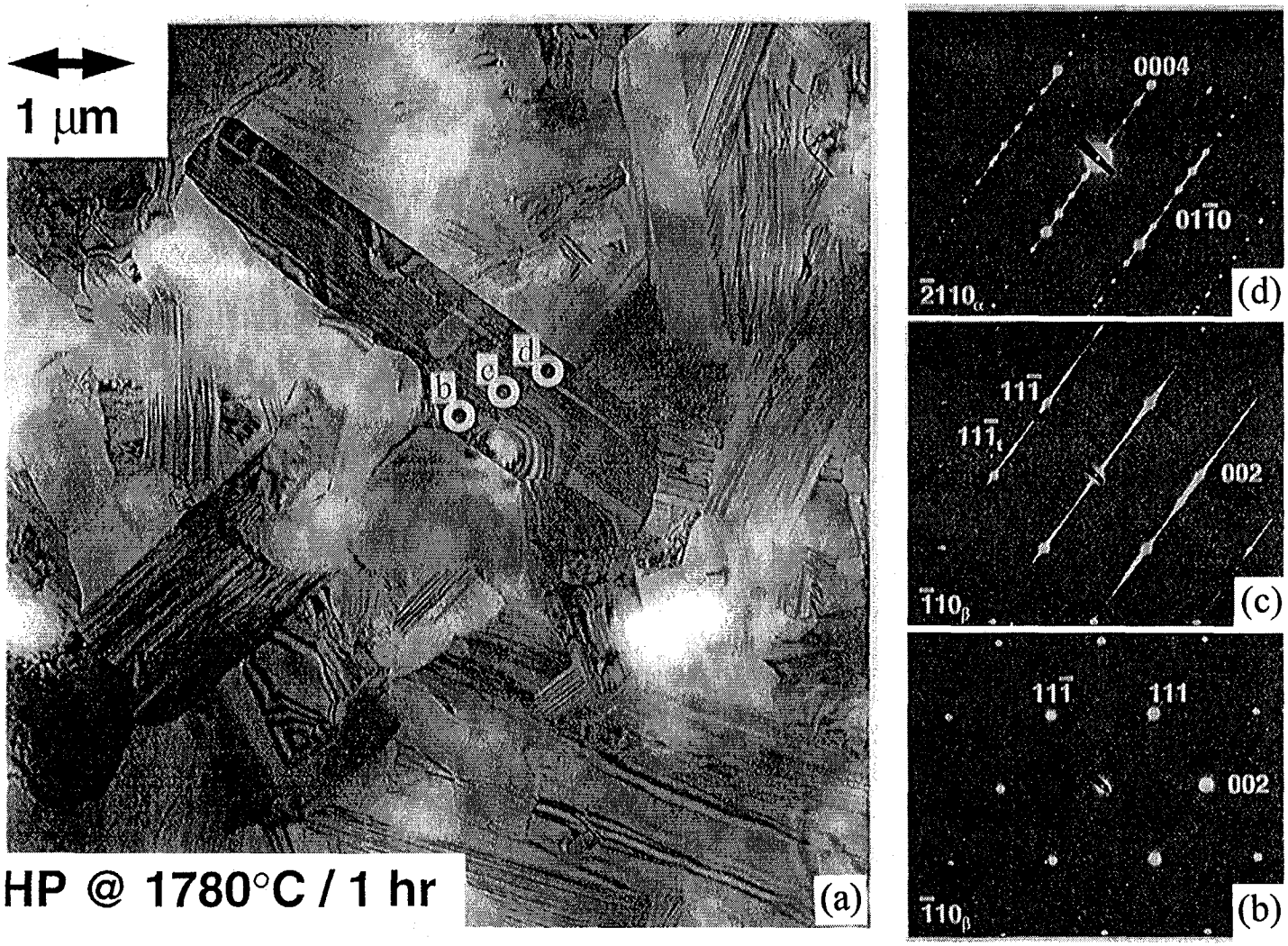

Fig. 2-10 TEM micrograph of ABC-SiC processed at 1780°C for 1h, showing a dual-phase plate-shaped grain (a). Selected area diffraction patterns show the bottom of the grain being 3C-SiC (b), the top being 4H-SiC (c), and the middle being mixture structures containing microtwins and stacking faults (d) (Courtesy of W. J. MoberlyChan).

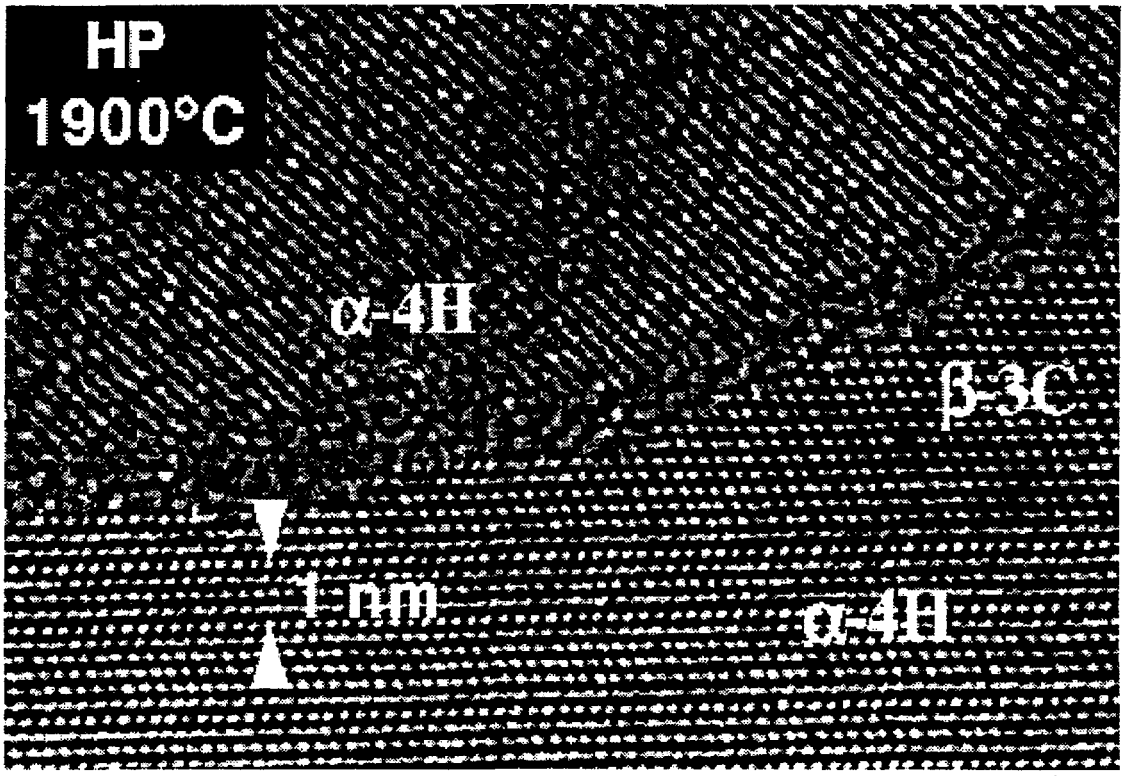

Fig. 2-11 High resolution TEM micrograph shows lattice images of two neighboring SiC grains, and an amorphous grain boundary film of less than one nanometer thick (Courtesy of W. J. MoberlyChan).

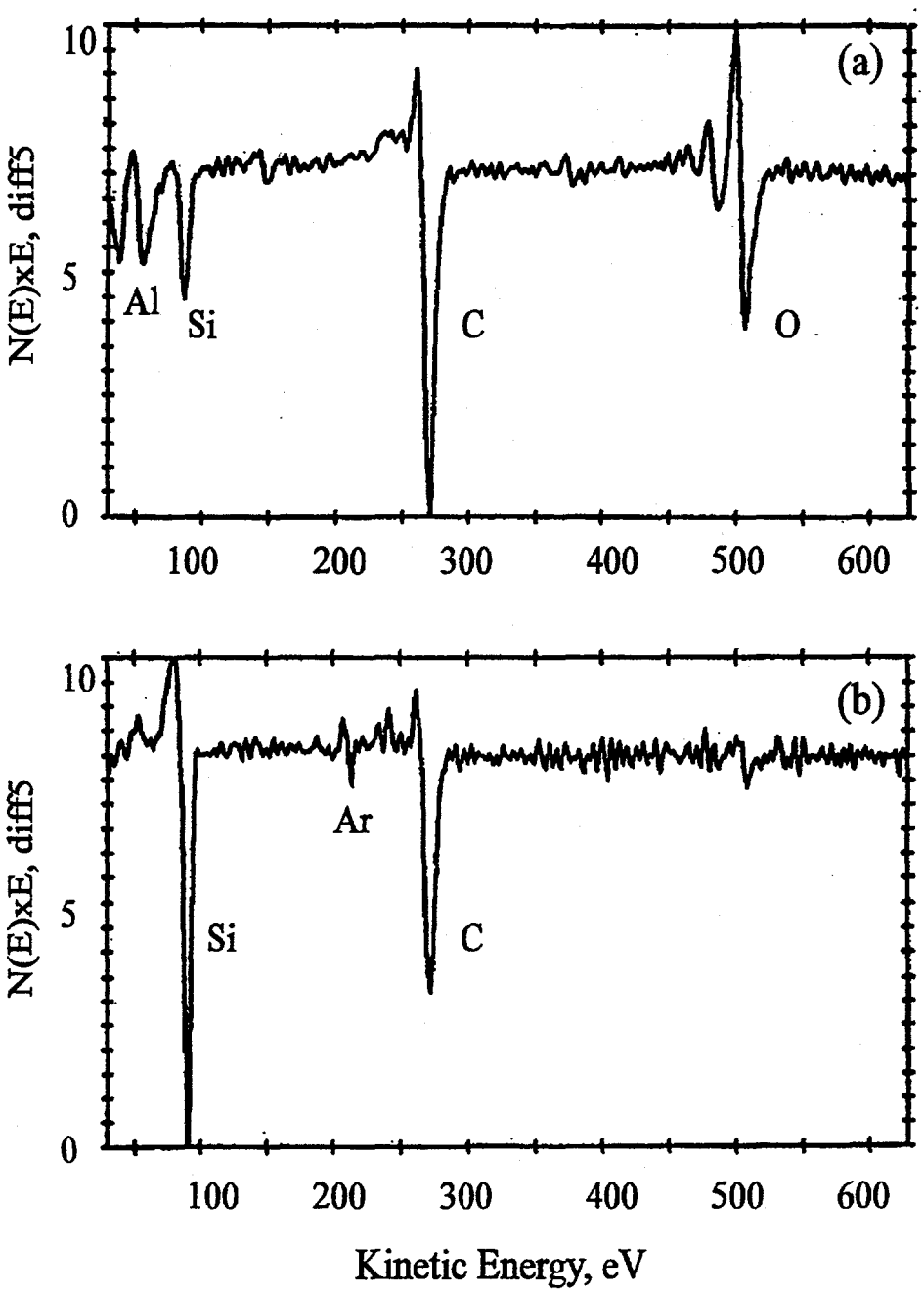

Fig. 2-12 Auger electron spectra acquired of an intergranular fracture surface (a), and of the same area after ion sputtering away less than one nanometer of material from the surface (b). Al and O segregated in the amorphous grain boundary film.

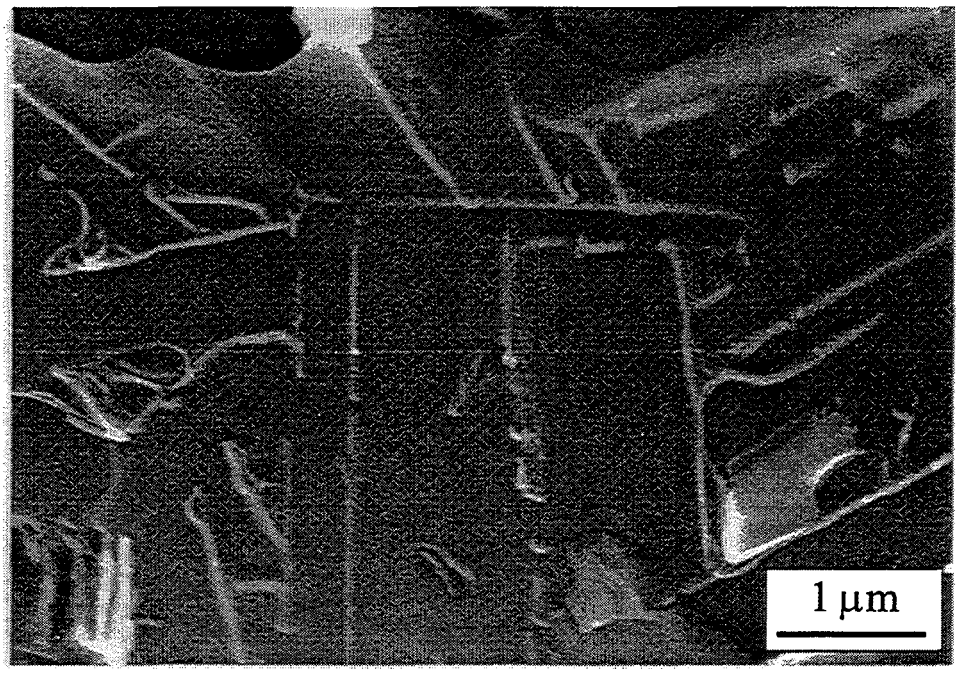

Fig. 2-13 SEM fractograph showing triple junction materials. Each stripe of material represents a triple "point" among the imaged plate-shaped grain and two other grains on the opposite face of the fractured specimen.

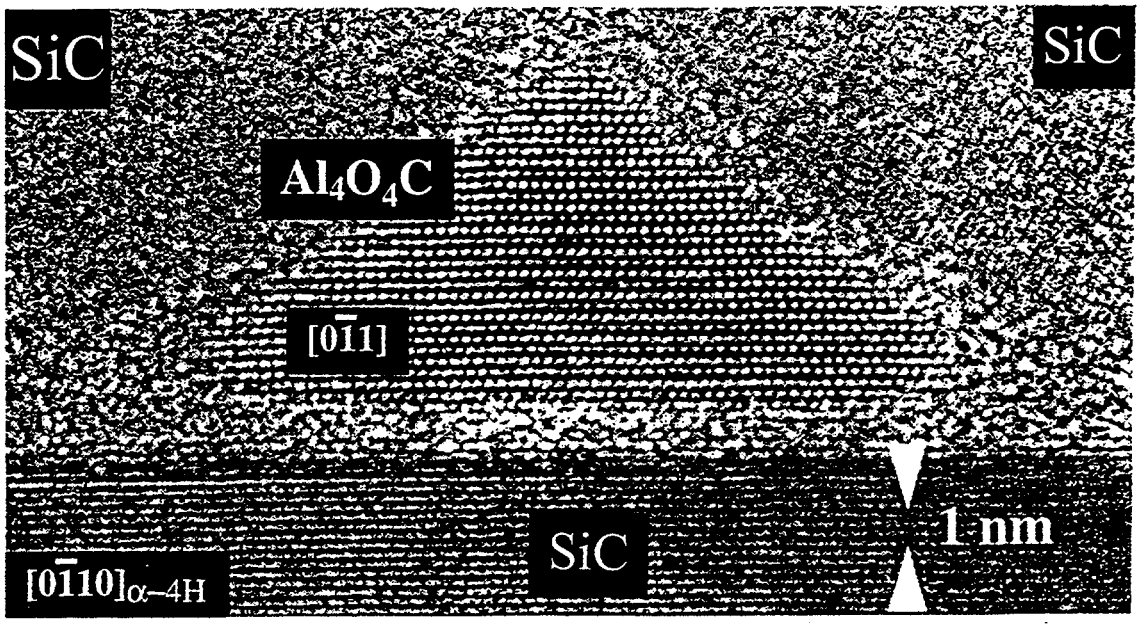

Fig. 2-14 HR-TEM image of a crystalline triple point phase. This triple-point material shows a crystal orientation relationship with the bottom SiC grain (Courtesy of W. J. MoberlyChan).

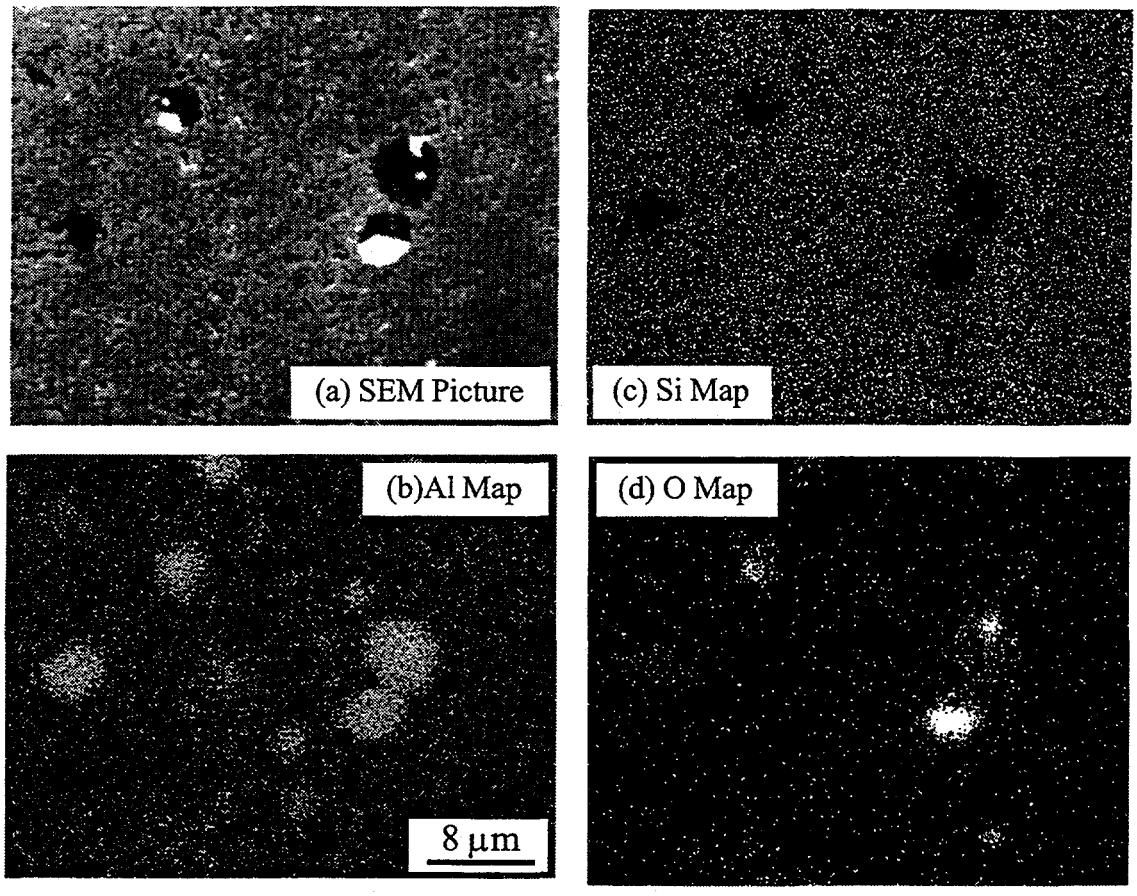

Fig. 2-15 SEM micrograph (a) and wavelength dispersive X-ray maps of Al (b), Si (c), and O (d) of a polished specimen with 6 wt% Al, 0.6 wt% B, and 2 wt% C sintering additives.

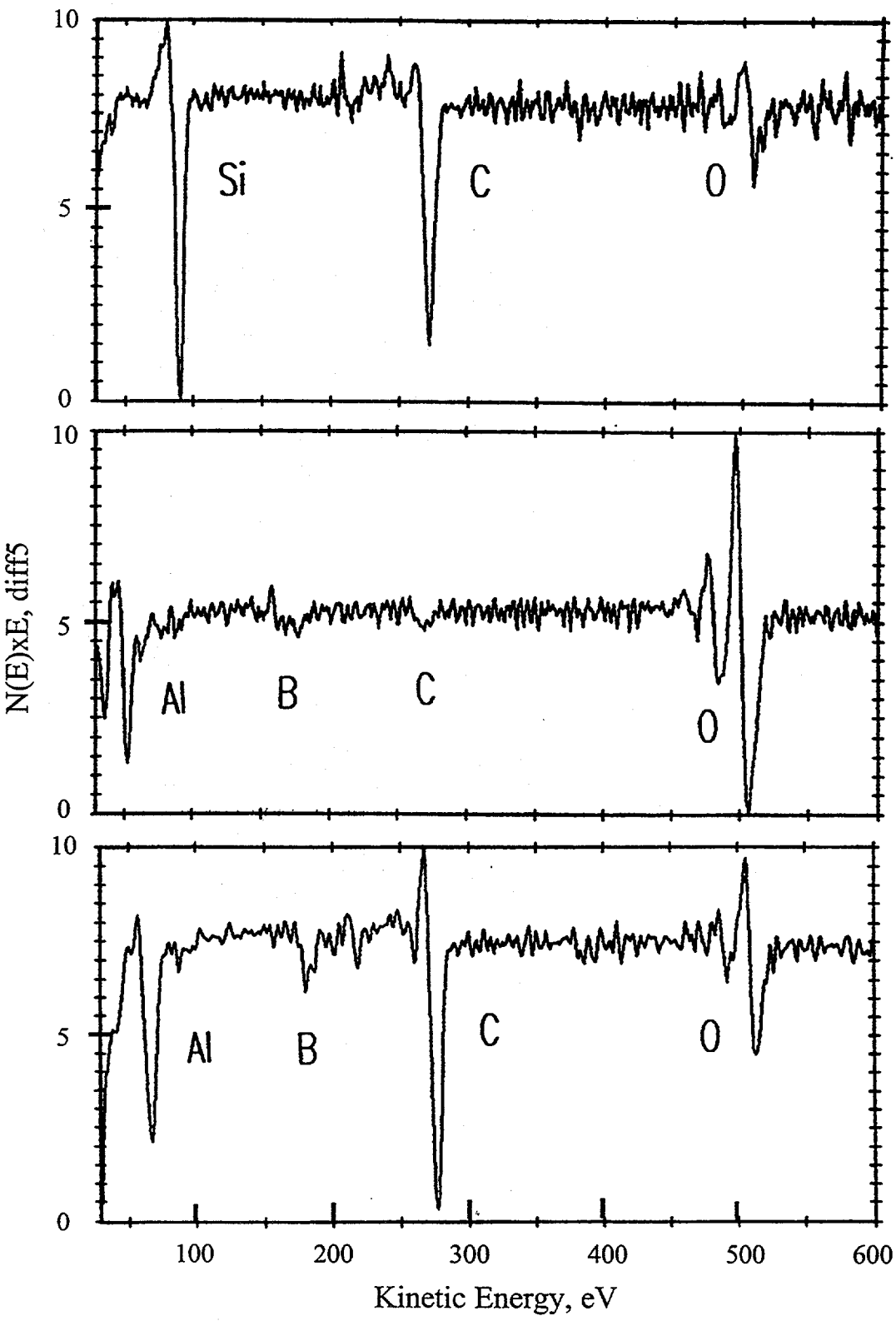

Fig. 2-16 AES spectrums acquired of a SiC grain (a) and of secondary phases (b and c). (Courtesy of W. J. MoberlyChan)

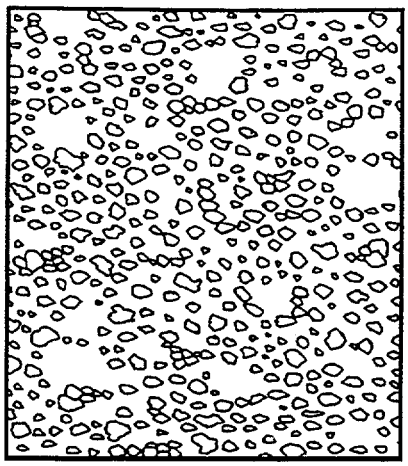

Green Compact

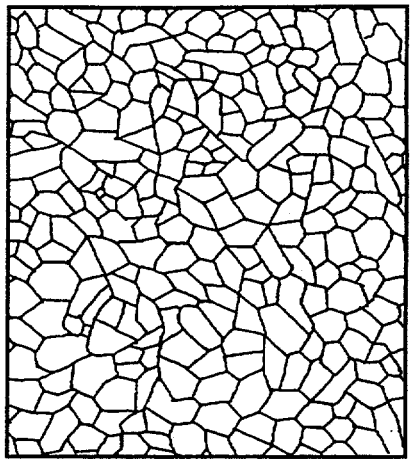

Stage I:
a) Liquid Formation
b) Particle Rearrangement
c) Densification

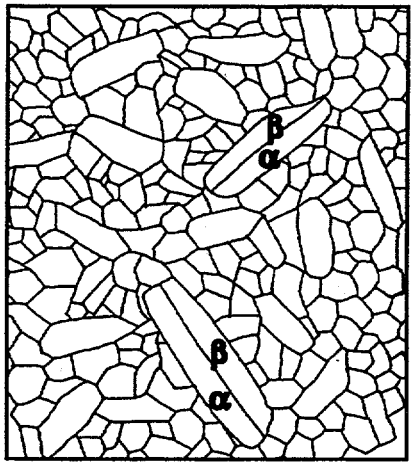

Stage II:
a) β-to-α Transformation
b) Formation of Plate-Shaped Grains

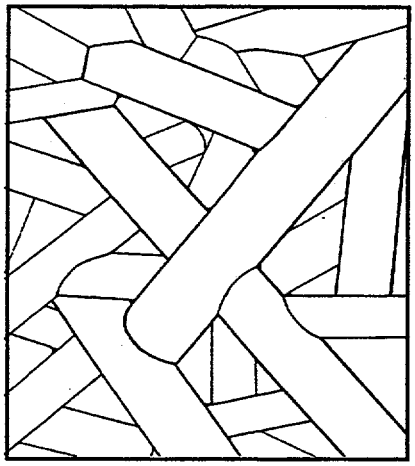

Final Microstructure:
Interlocked High-Aspect-Ratio Plate-Shaped Grains

Fig. 2-17 Scenario of sintering and microstructural development in ABC-SiC.

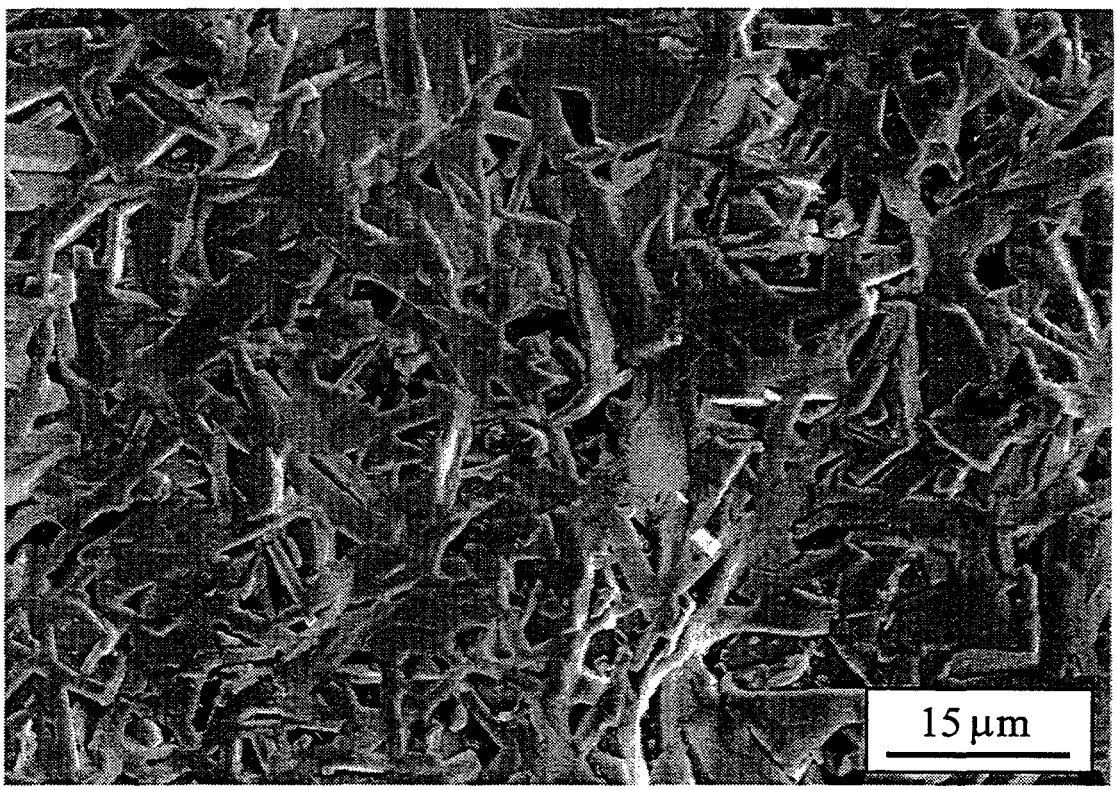

Fig. 2-18 SEM micrograph of a fracture surface of a porous SiC hot pressed at 2000°C for 1 hour. The starting submicron β-SiC powder was doped with 0.3 wt% Al, 0.6 wt% B, and 1.5 wt% C. Formation of the plate-shaped grains prior to densification resulted in a porous material.

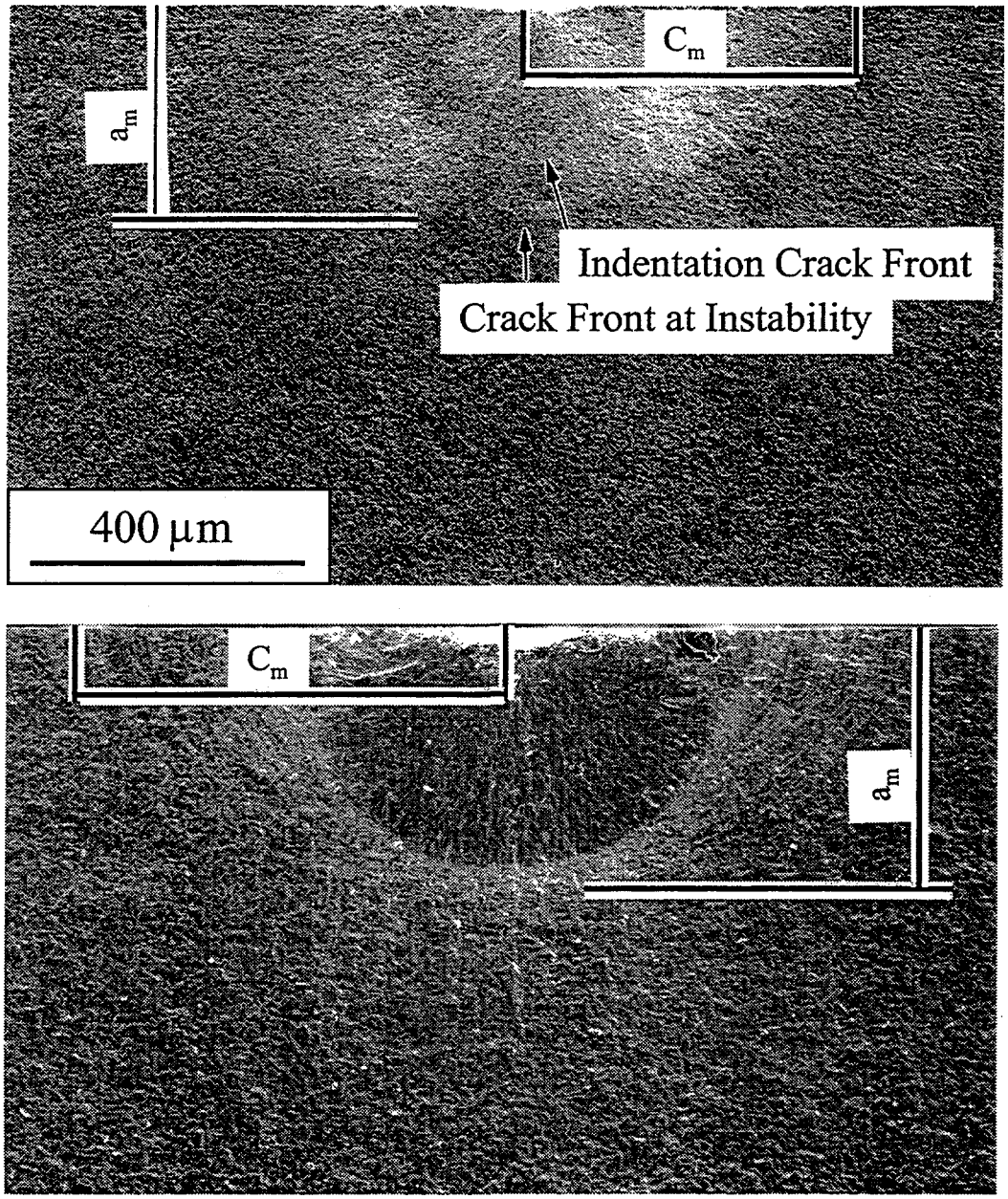

Fig. 3-1 SEM micrographs showing cracks induced by the Knoop indentation in an ABC-SiC processed at 1700°C/1h (a) and in Hexoloy SiC (b). During bending, the crack propagated in a stable manner and the critical crack front became elliptical with an ellipticity of ~ 0.65. The crack depth, a_m, at instability was used to calculate the fracture toughness in equation (3-2).

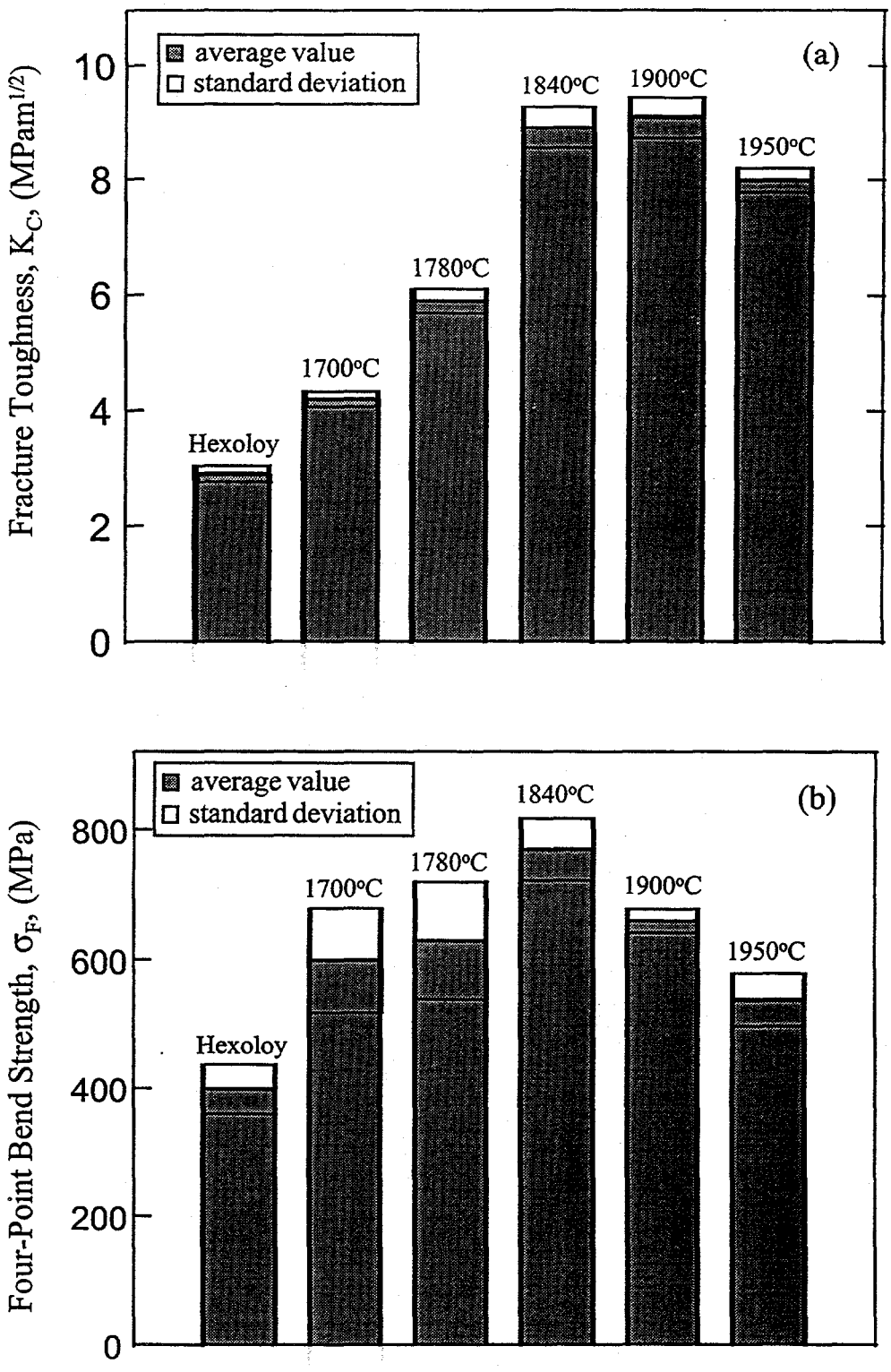

Fig. 3-2 Fracture toughness (a) and four-point bend strength (b) of the ABC-SiC materials hot pressed between 1700°C and 1950°C. Data for Hexoloy SiC, measured under identical conditions, are included for comparison.

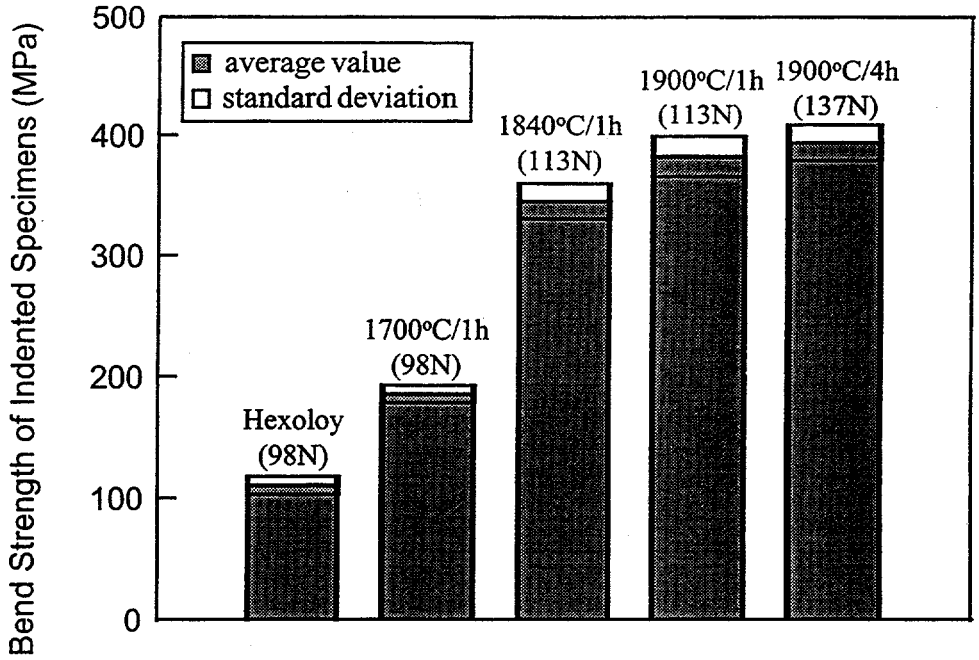

Fig. 3-3 Comparison of flaw tolerance among Hexoloy SiC and selected ABC-SiC materials. The flaws were induced by Knoop indentation on the tension surfaces of the bend bars. The indentation loads and the hot pressing conditions are indicted in the figure.

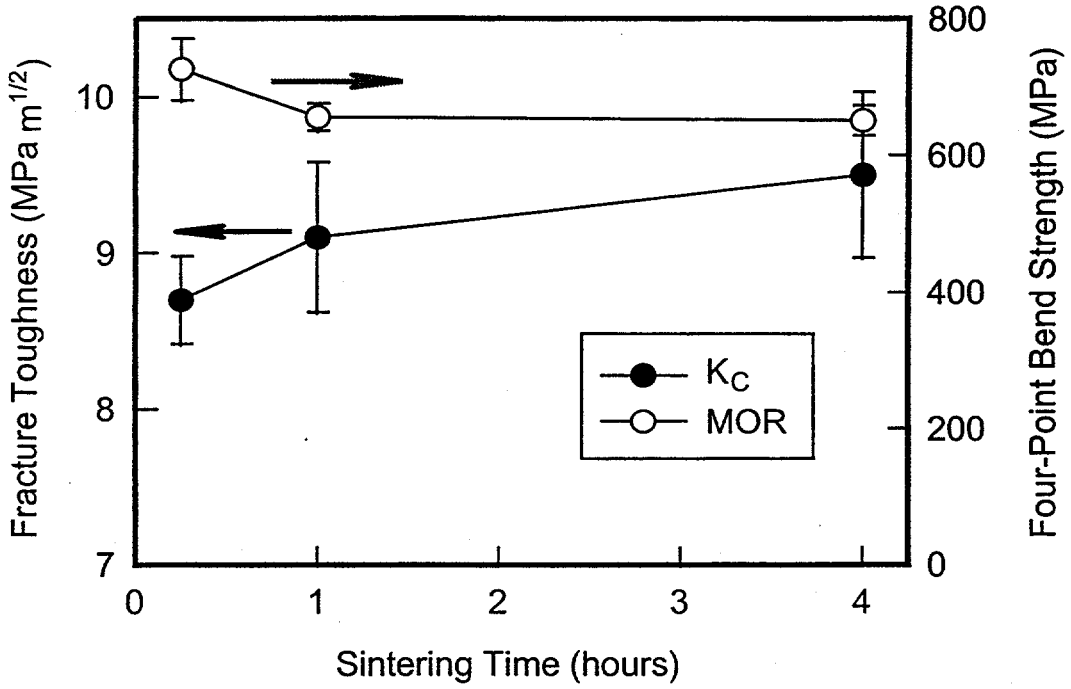

Fig. 3-4 Fracture toughness, K_c, and four-point bend strength, σ_F, as a function of hot-pressing time at 1900°C.

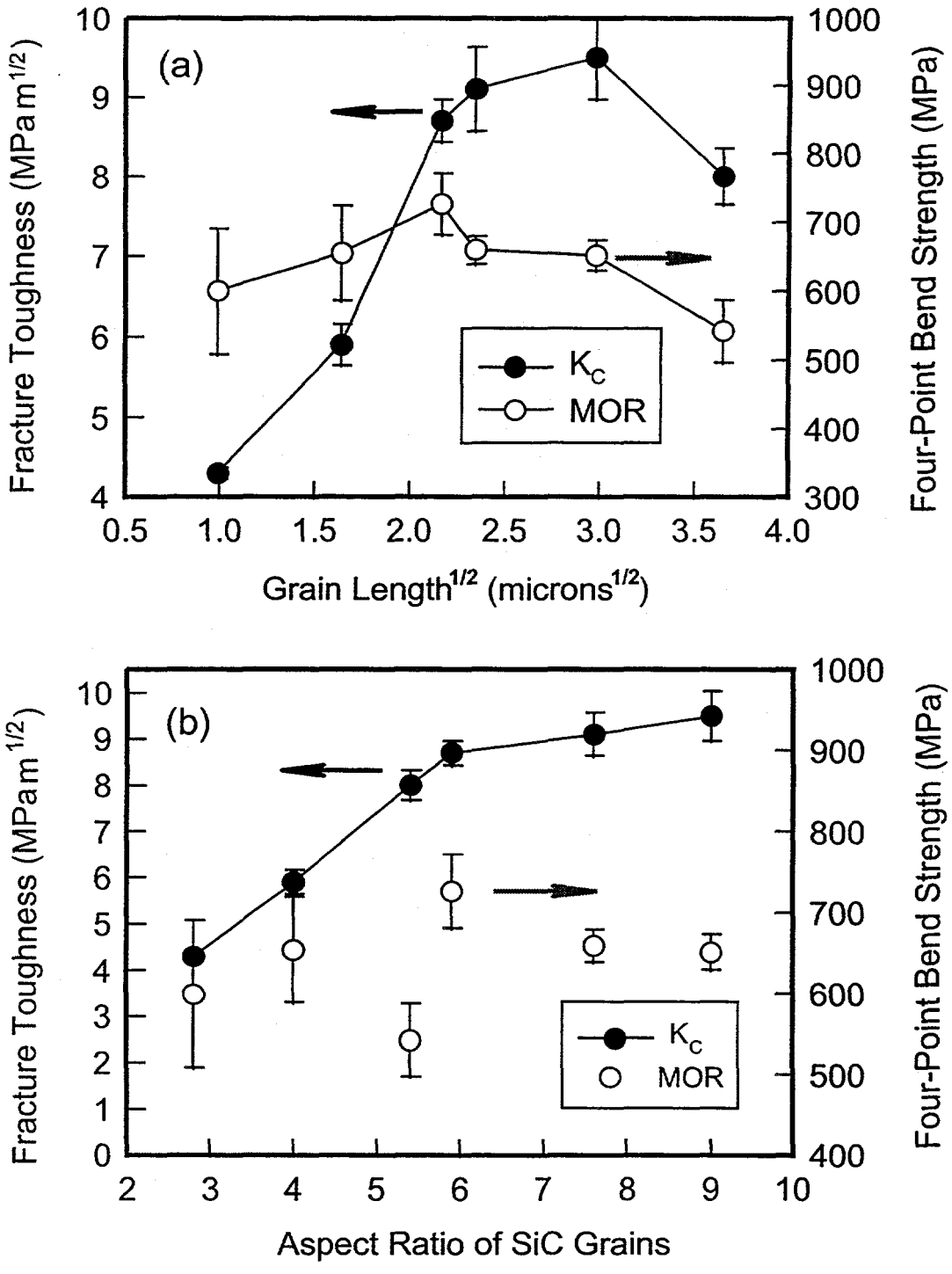

Fig. 3-5 Fracture toughness, K_c, and four-point bend strength, σ_F, as a function of the square root of grain length (a) and as a function of apparent grain aspect ratios (b) in the hot pressed ABC-SiC ceramics.

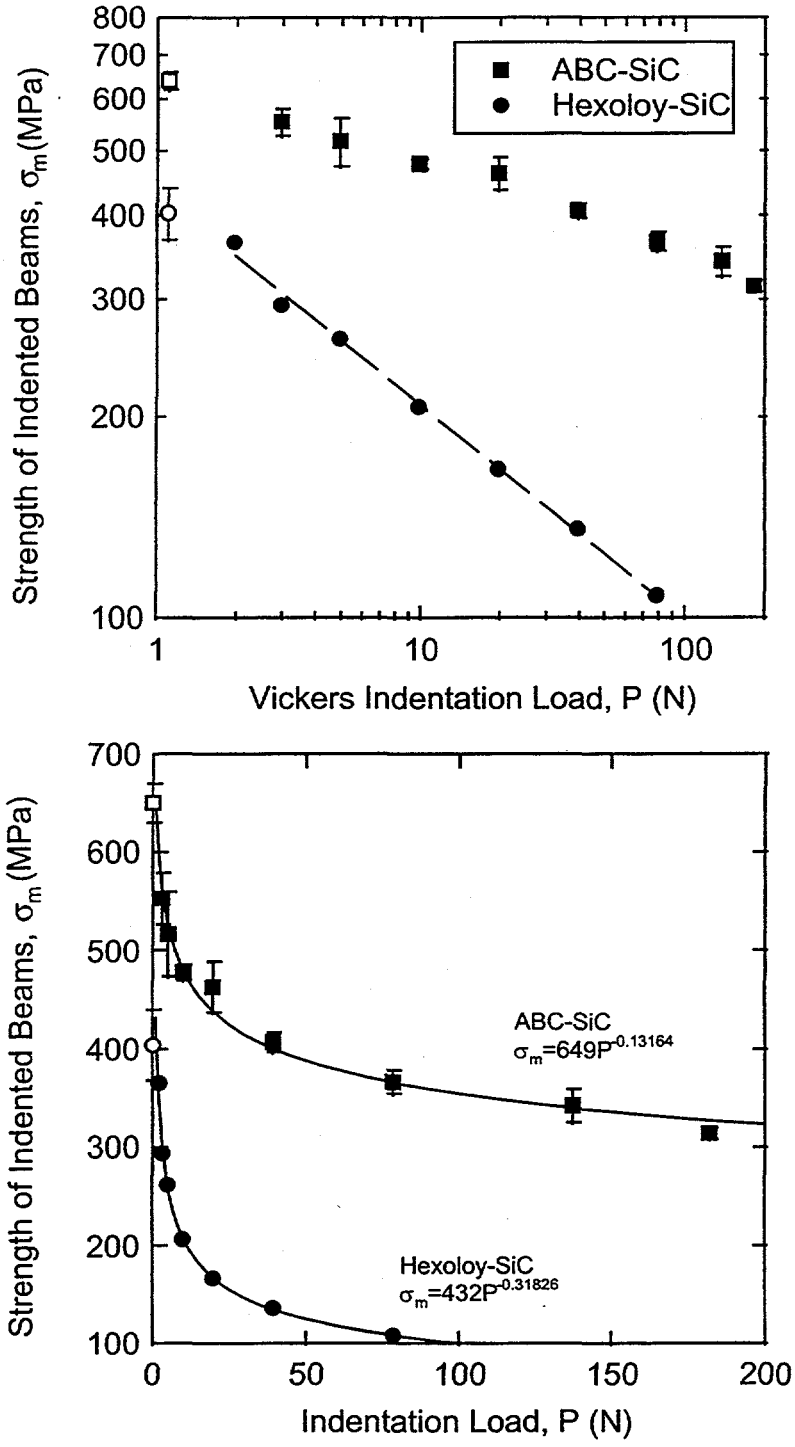

Fig. 3-6 Strength-indentation load relations for Hexoloy-SiC and the ABC-SiC plotted in logarithm scales (a) and in linear scales (b), respectively. Note that for Hexoloy SiC data follow a typical $\sigma_m \propto P^{-1/3}$ response, indicating a single-valued toughness, whereas the ABC-SiC shows strongly enhance flaw-tolerance, indicating a pronounced R-curve behavior.

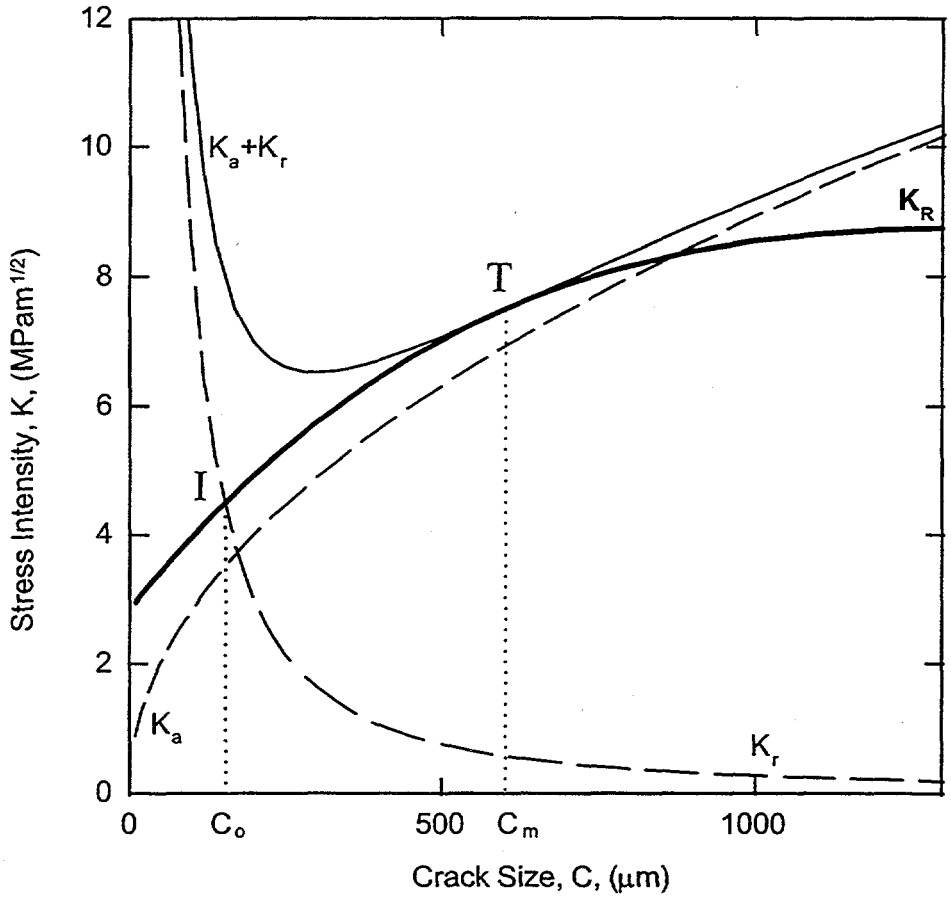

Fig. 3-7 A schematic diagram showing stress intensity factors of the indentation residual stress field, K_{res}, the applied bending stress field, K_a, and the total stress field, $K_{res} + K_a$, as well as the material crack resistance, K_R. Point I at the intersection of K_{res} and K_R represents the initial indentation crack size, C_0. Point T represents crack extension to C_m at the onset of instability. The $K_{res} + K_a$ curve is tangential with the K_R curve at point T.

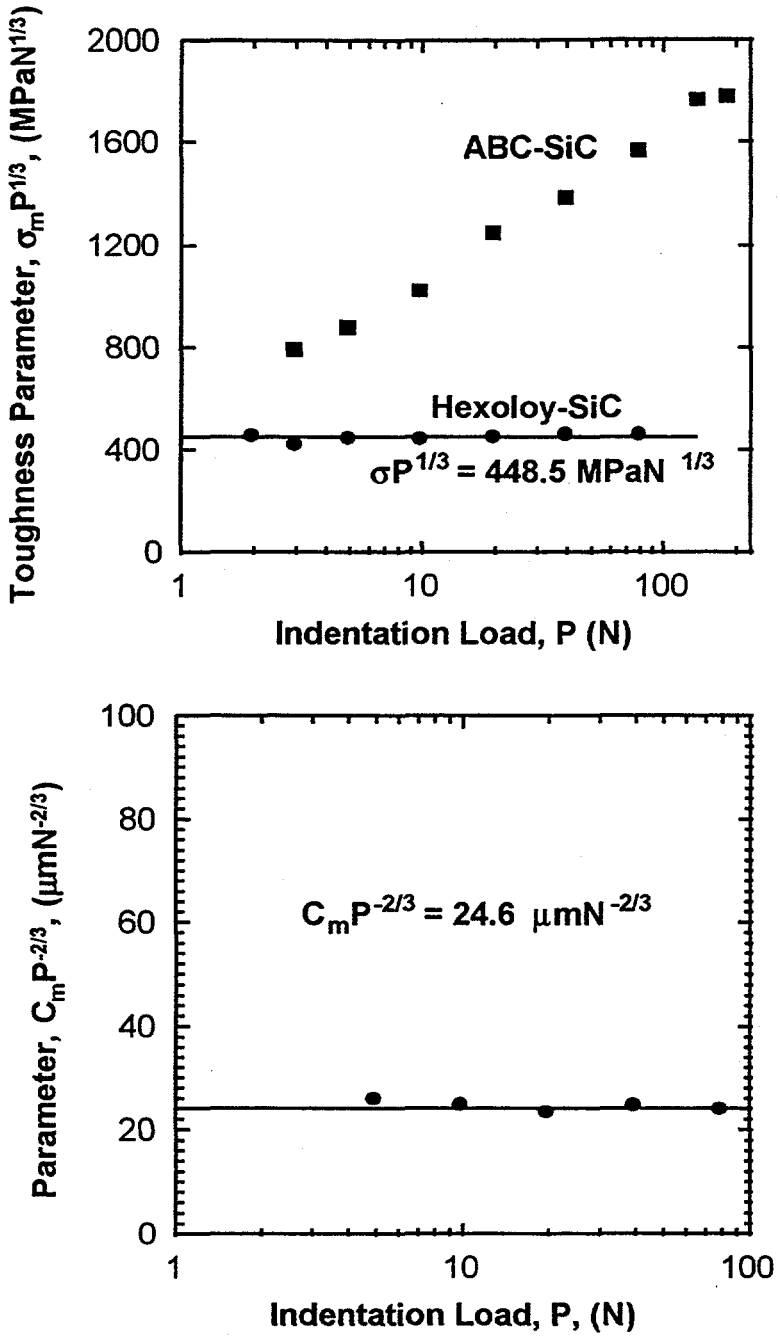

Fig. 3-8 Plots of parameters $\sigma_m P^{1/3}$ (a) and $C_m P^{-2/3}$ (b) versus the indentation load P. The horizontal lines for Hexoloy SiC are used to calibrate the coefficients χ and Y in equations (3-6a) and (3-6b).

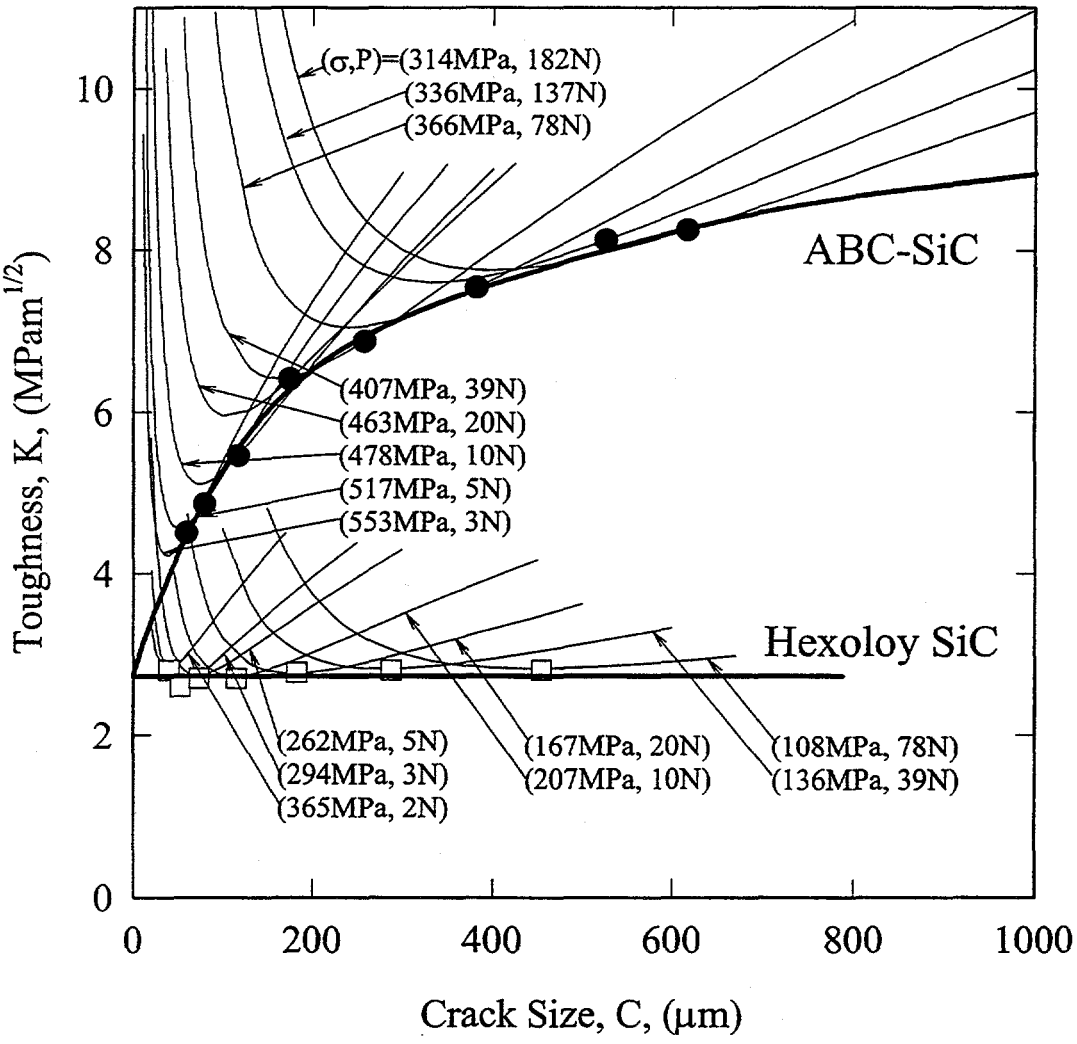

Fig. 3-9 R-curve construction for the ABC-SiC and Hexoloy SiC. The thinner solid curves are plots of the total stress intensities, K_t, versus crack size in Eq. (3-4) using the strength of indented specimens at each indentation load, P, from Fig. 3-6a. The R-curve is an envelop of tangency to the family of K_t curves. The data points here are determined after Ref. [35].

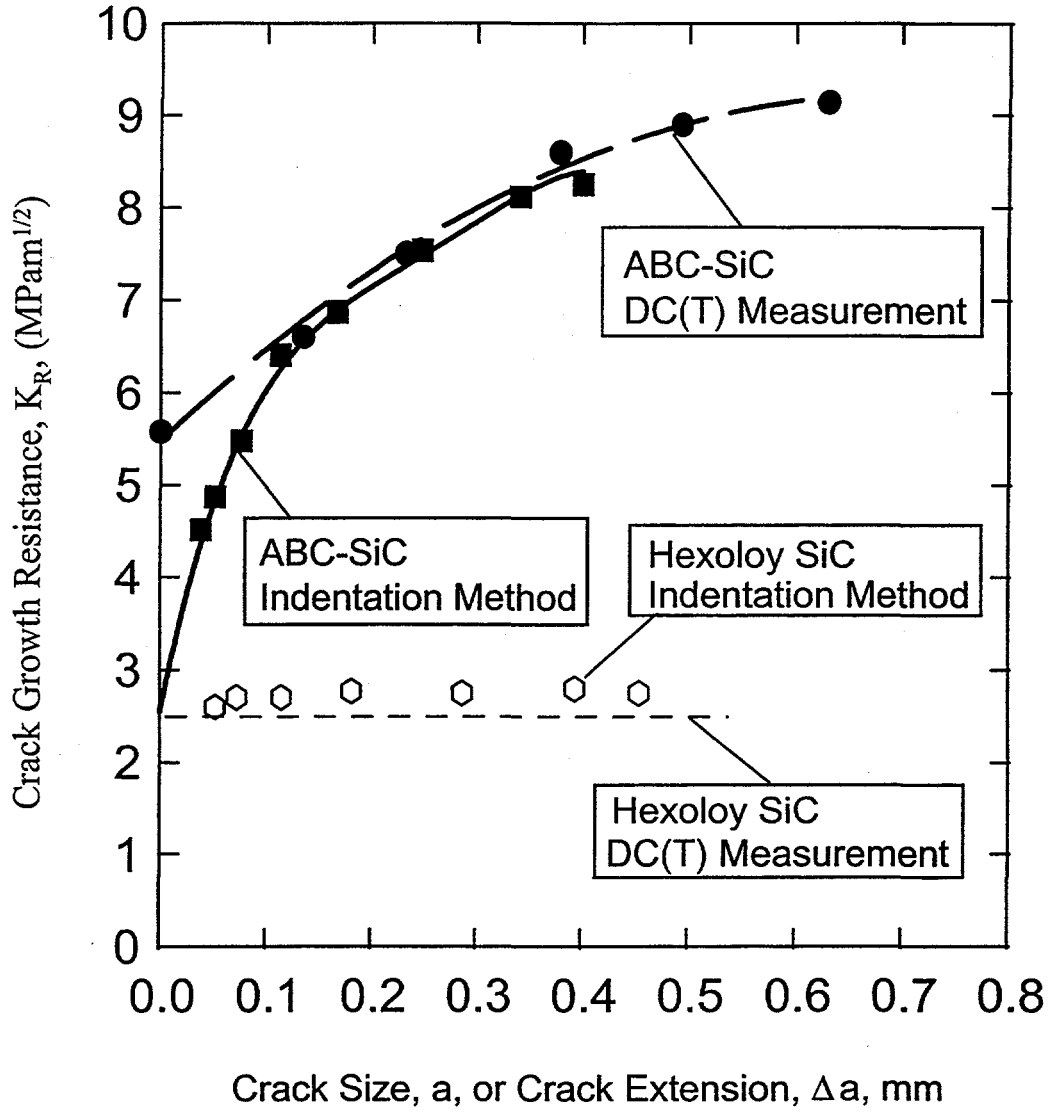

Fig. 3-10 Comparison of the R-curves deconvoluted from the indentation-strength measurements with that directly measured from precracked DC(T) specimens. Note the very high plateau (steady-state) fracture toughness of ~9 MPam$^{1/2}$ for the ABC-SiC in comparison to the single valued toughness below 3 MPam$^{1/2}$ for the Hexoloy SiC. The horizontal axis here is the crack extension in the DC(T) specimens, or the crack depth in the indented beam specimens. (Courtesy of C. J. Gilbert for the DC(T) data)

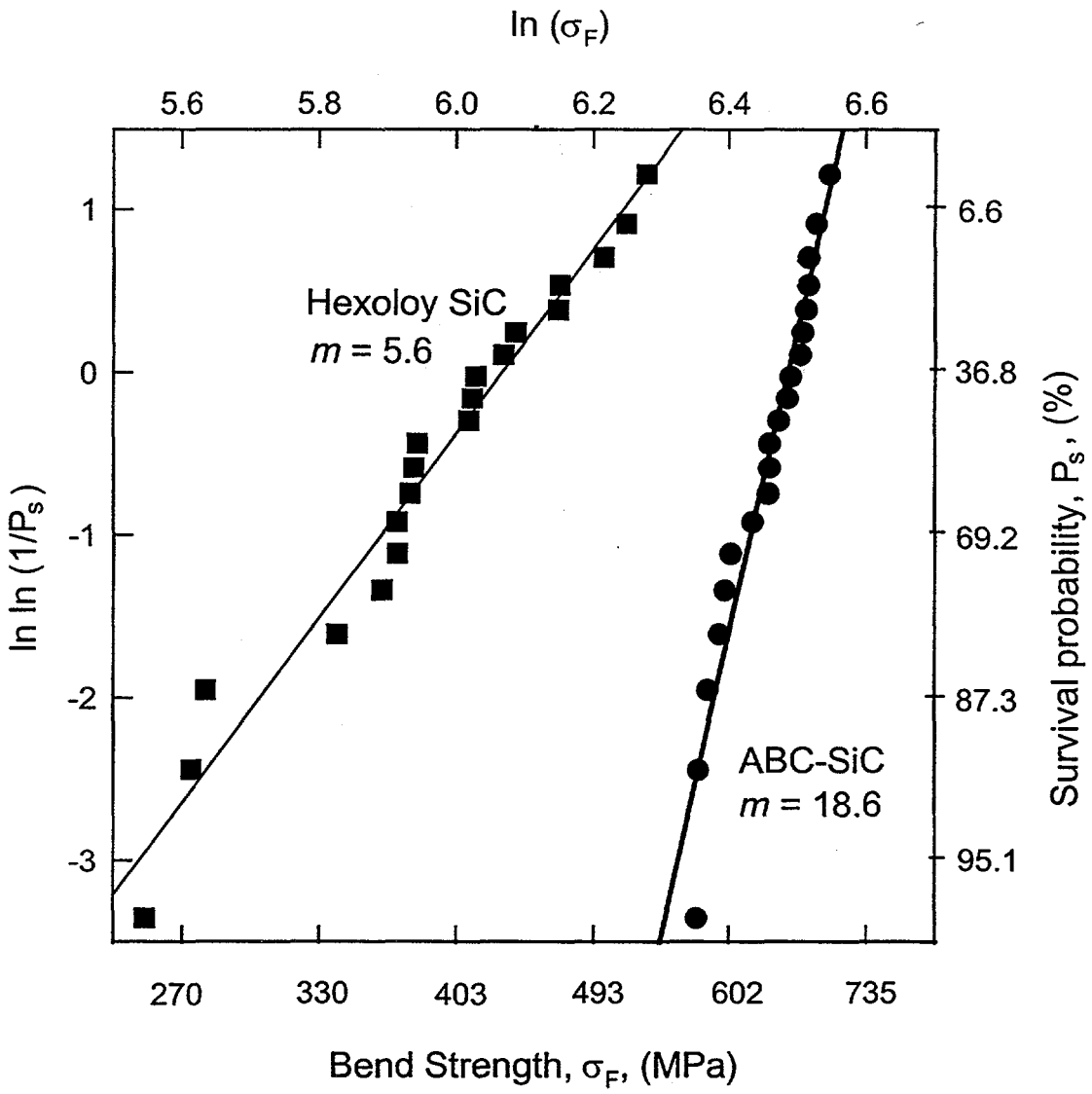

Fig. 3-11 Weibull distributions of flexure strength of the ABC-SiC (processed at 1900°C) and the commercial Hexoloy SiC. Note that the ABC-SiC simultaneously exhibits much better Weibull modulus and mean strength.

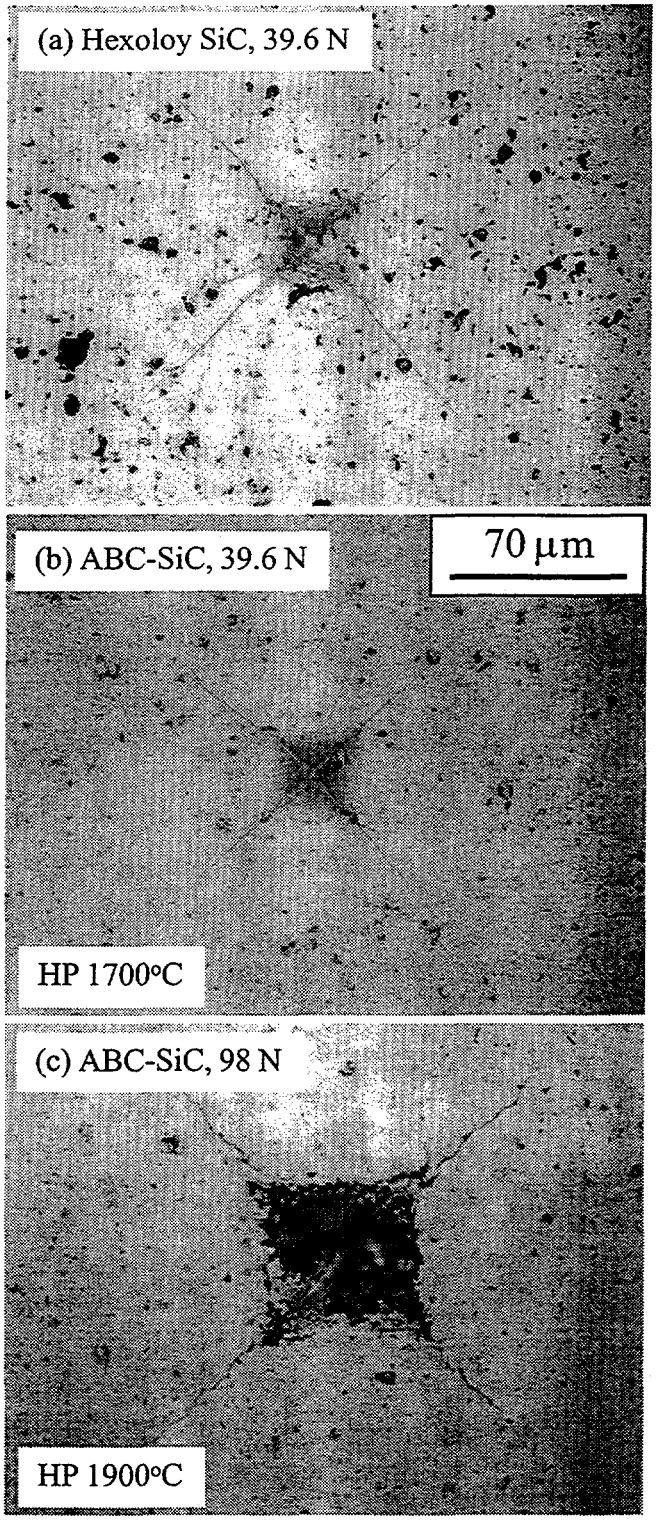

Fig. 3-12 Optical micrographs illustrating the radial cracks from Vickers indentation in Hexoloy SiC (a), an ABC-SiC hot pressed at 1700°C for 1 hour (b), and an ABC-SiC hot pressed at 1900°C for 4 hours (c). The indentation loads are 39.6 N for (a) and (b), and 98 N for (c).

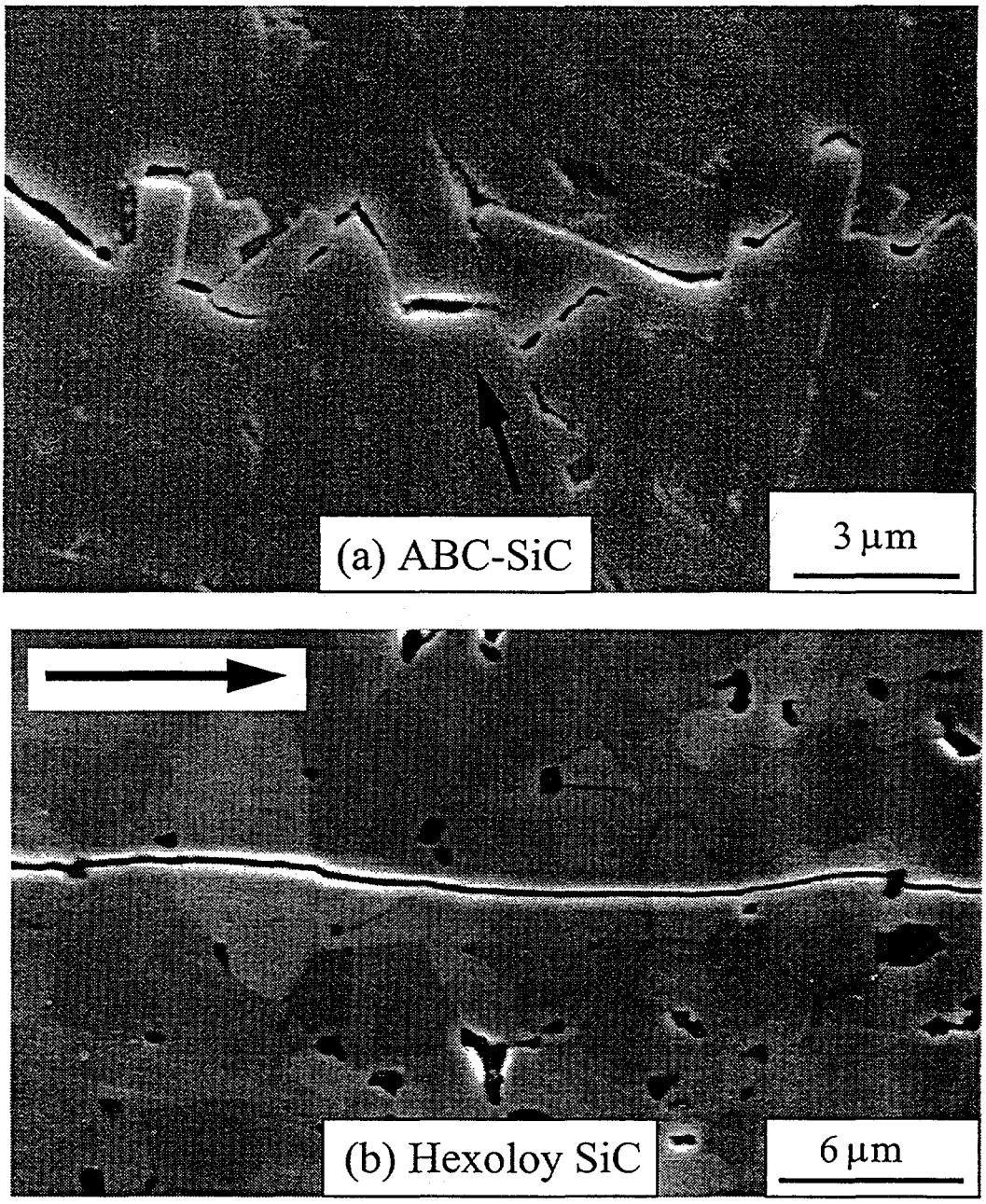

Fig. 3-13 SEM micrographs of crack paths in (a) an *in situ* toughened ABC-SiC (1900°C/4h), and (b) Hexoloy SiC. Note the numerous grain-bridging sites in (a) in contrast to the straight and transgranular path in (b). The horizontal arrow shows direction of crack growth.

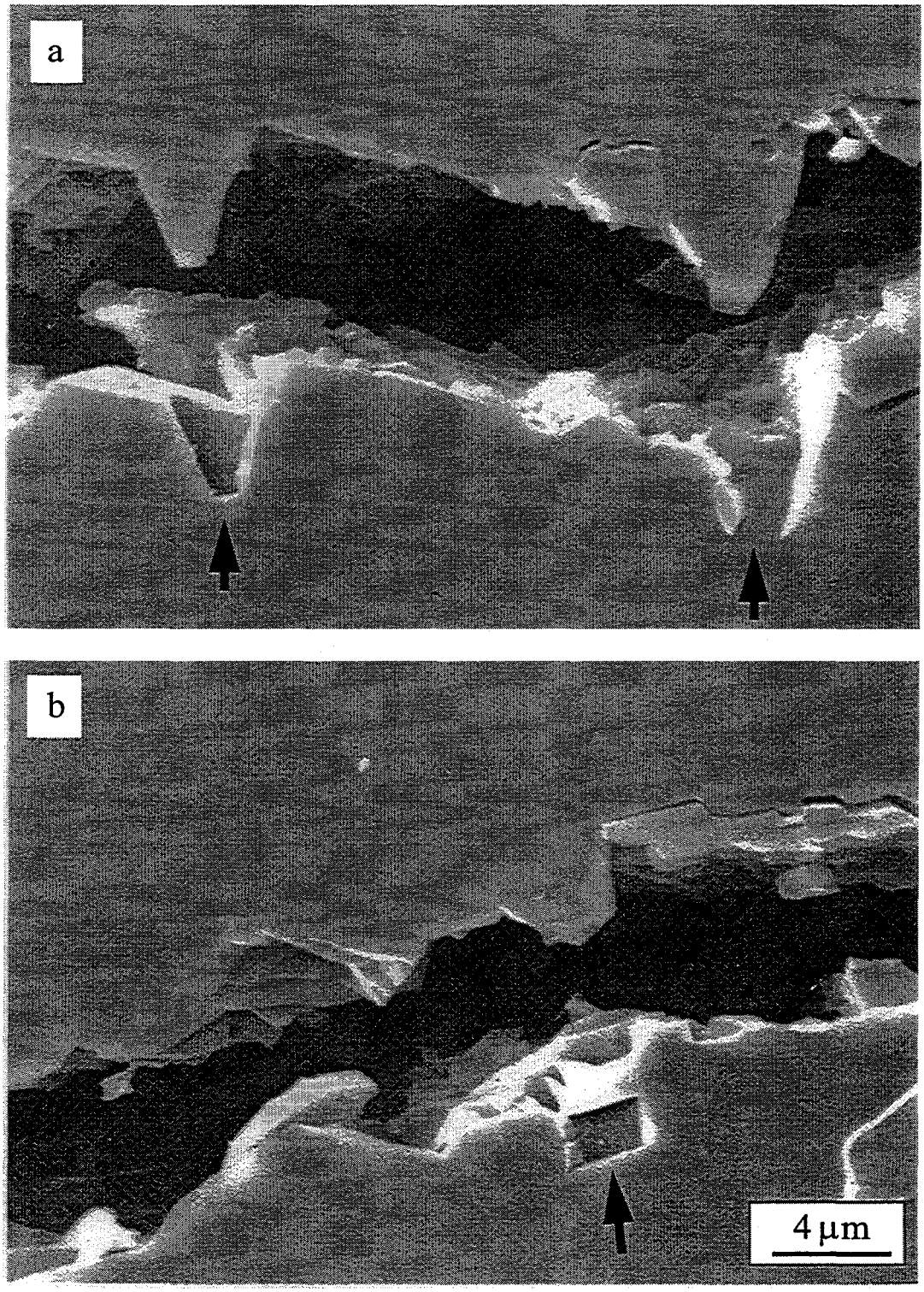

Fig. 3-14 SEM micrographs showing that grains were pulled out (a), a grain fractured after some sliding (b), a group of grains were pulled out (c), and that contacting facets provided additional sliding friction (d).

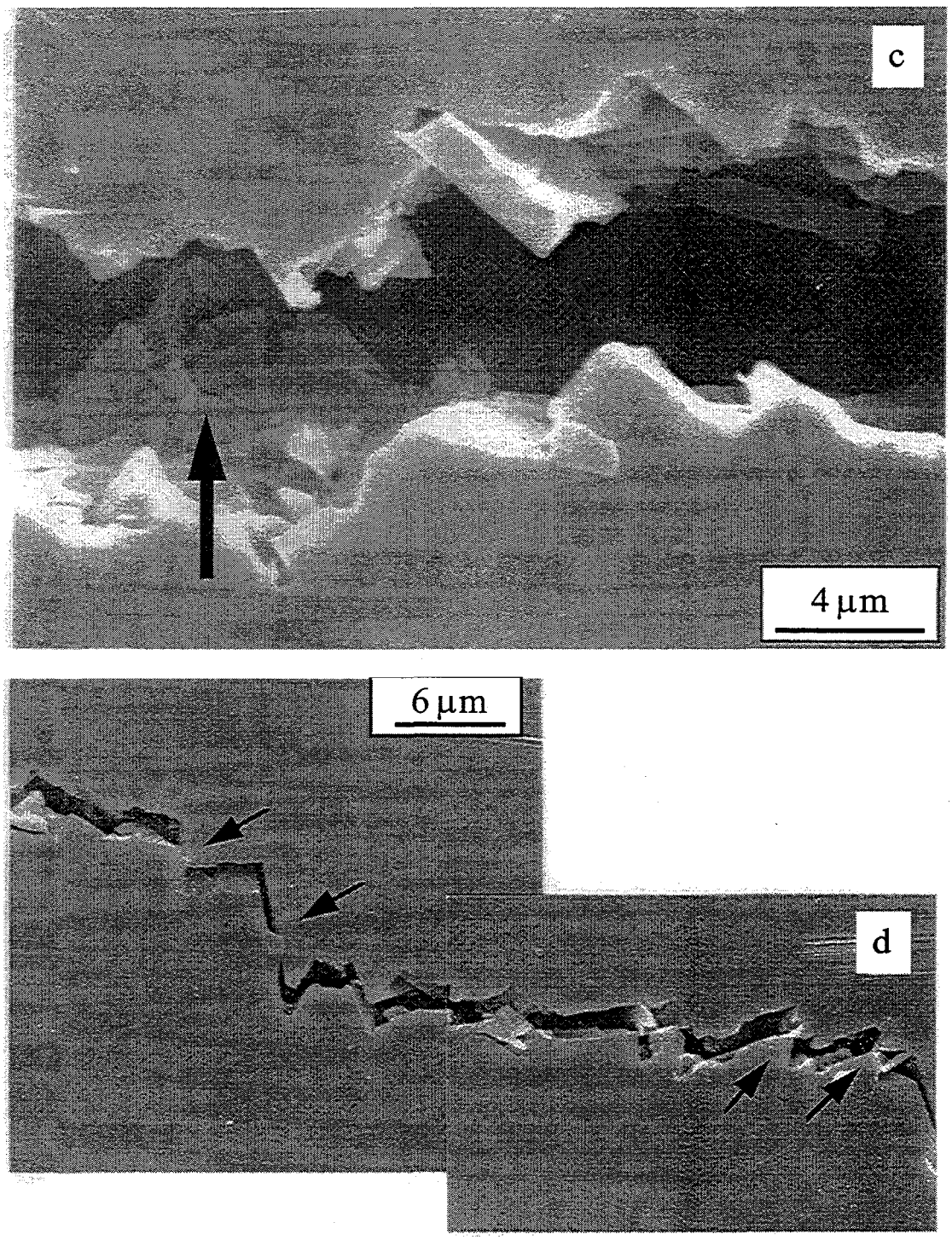

Fig. 3-14 SEM micrographs showing that grains were pulled out (a), a grain fractured after some sliding (b), a group of grains were pulled out (c), and that contacting facets provided additional sliding friction (d).

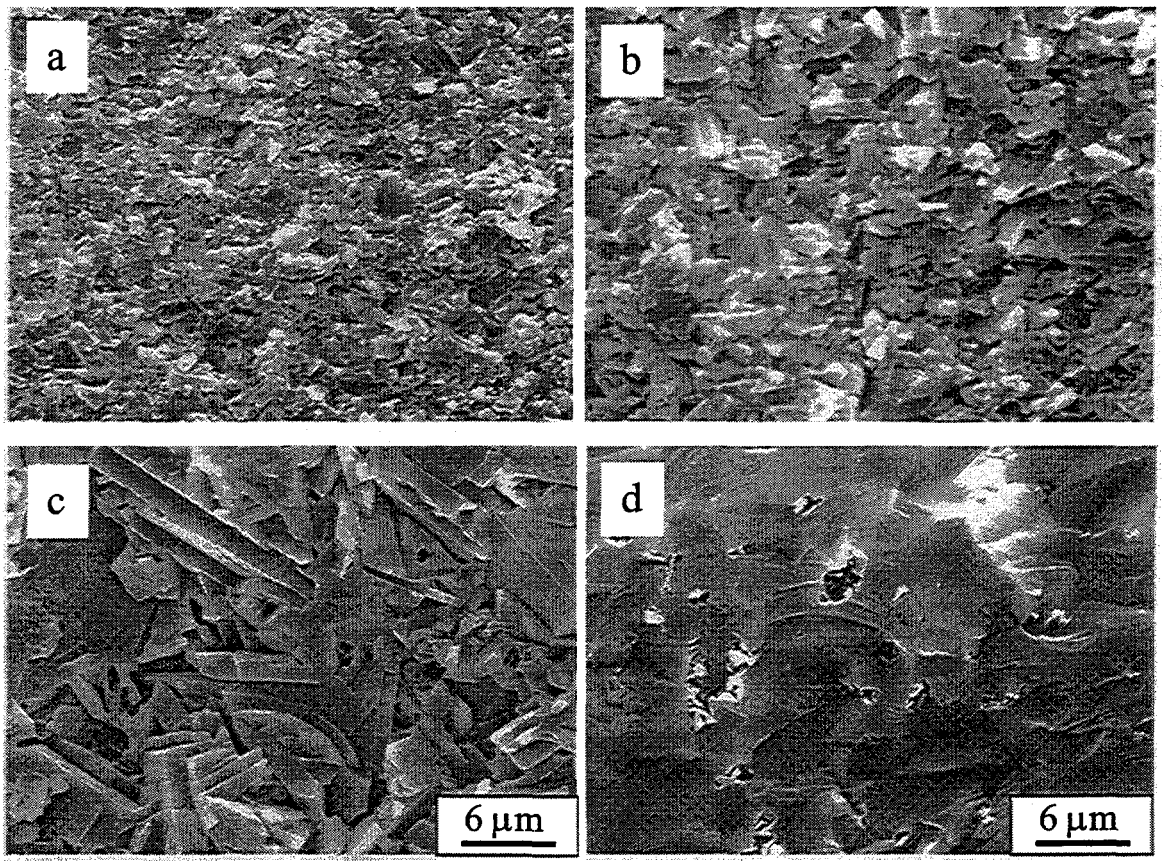

Fig. 3-15 SEM fractographs of the ABC-SiC ceramics hot pressed at various conditions: (a) 1700°C/1h, (b) 1780°C/1h, (c) 1900°C/1h, and (d) Hexoloy SiC. These ABC-SiC materials failed intergranularly, whereas the Hexoloy SiC fractured transgranularly.

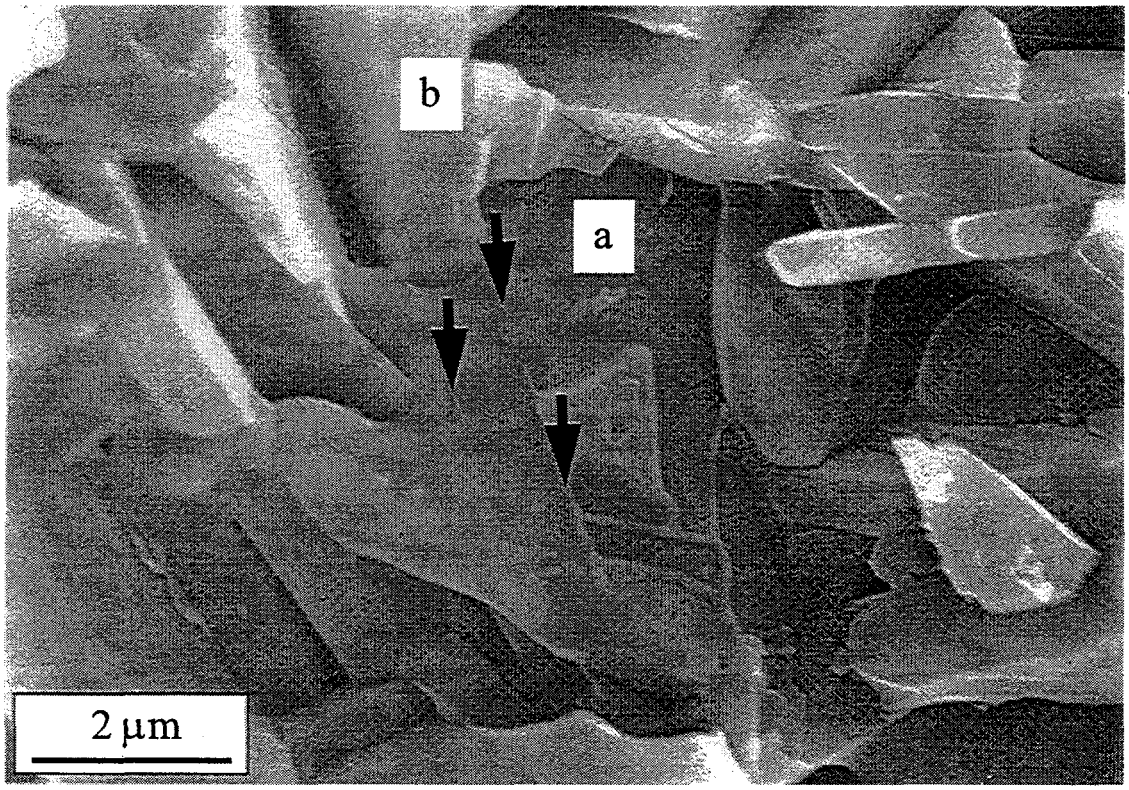

Fig. 3-16 SEM fractograph showing that grain *b* fractured at the interlock with gra
leaving "triple-point" materials as indicated by arrows on the flat surface of grain *a*

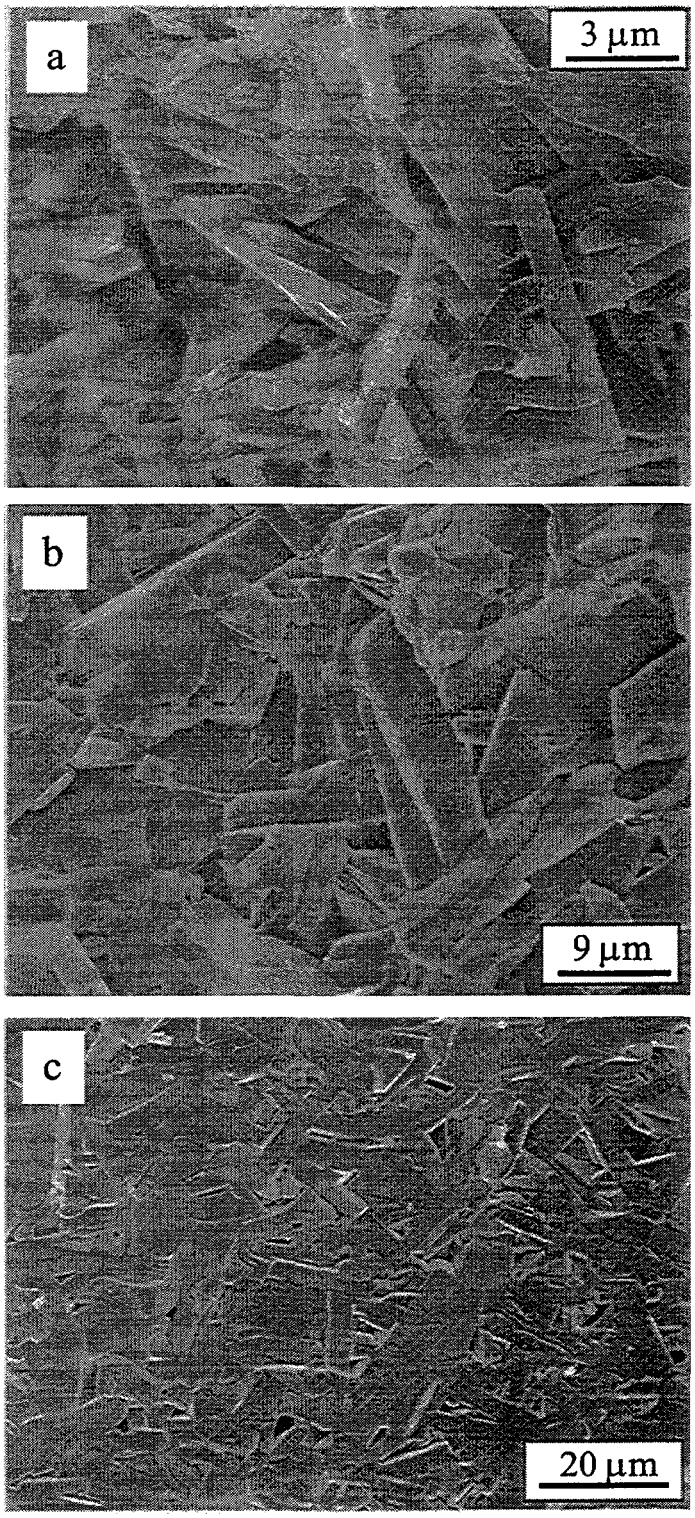

Fig. 3-17 SEM fracture surfaces of three silicon carbides processed at various conditions: (a) hot pressed at 1900°C/1h, (b) hot pressed at 1950°C/1h, and (c) hot pressed at 1900°C/1h and annealed at 2000°C/3 h.

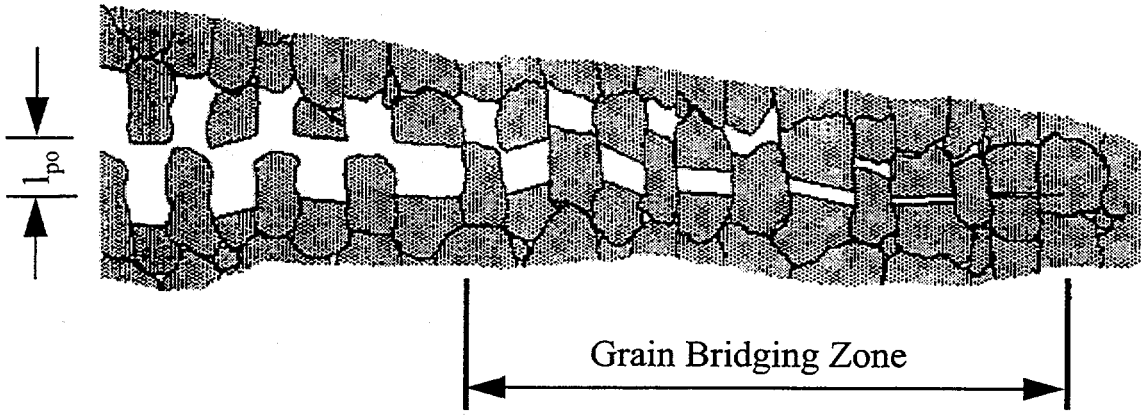

Fig. 3-18 A schematic diagram of a crack with a number of grains pulling out (after Ref. [21]).

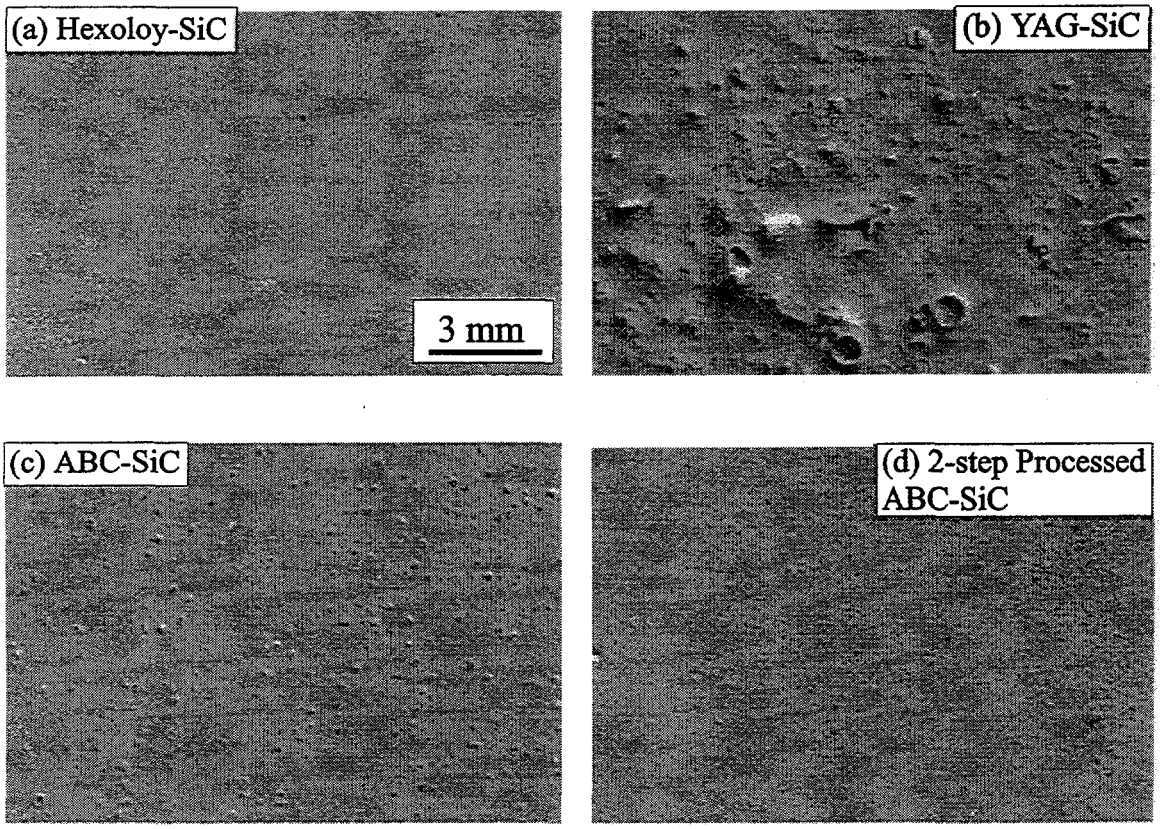

Fig. 4-1 Low magnification SEM images showing the morphologies of the oxidized surfaces of SiCs with various sintering additives. Micrographs (a) through (d) are for samples A through D, respectively.

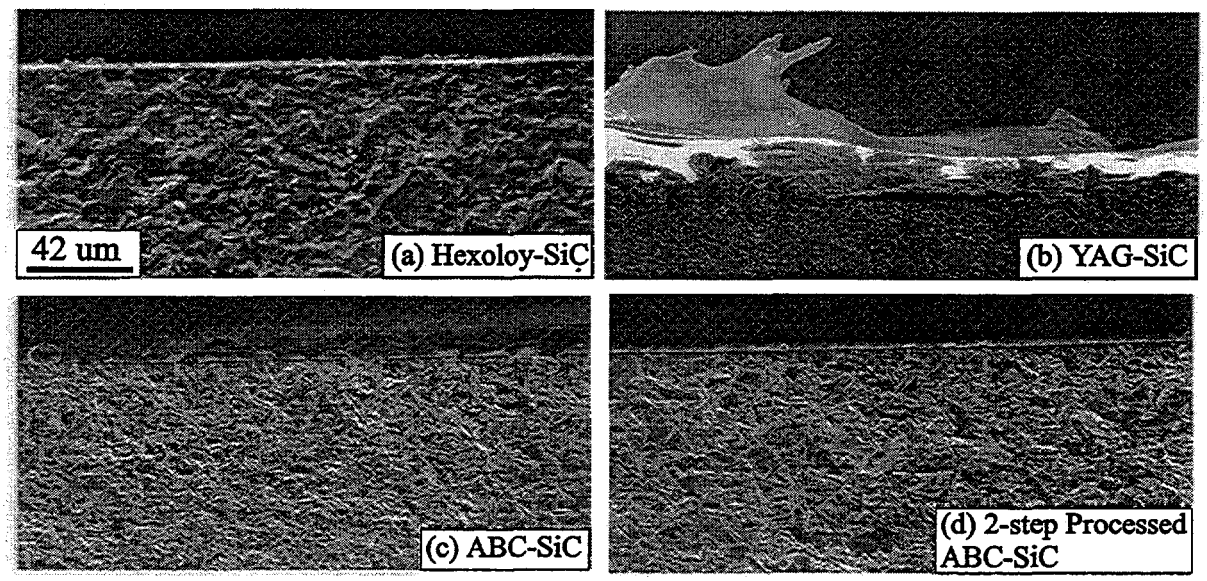

Fig. 4-2 SEM Cross-sectional views of oxidized SiC materials with various sintering additives. Images (a) through (d) are for samples A through D, respectively.

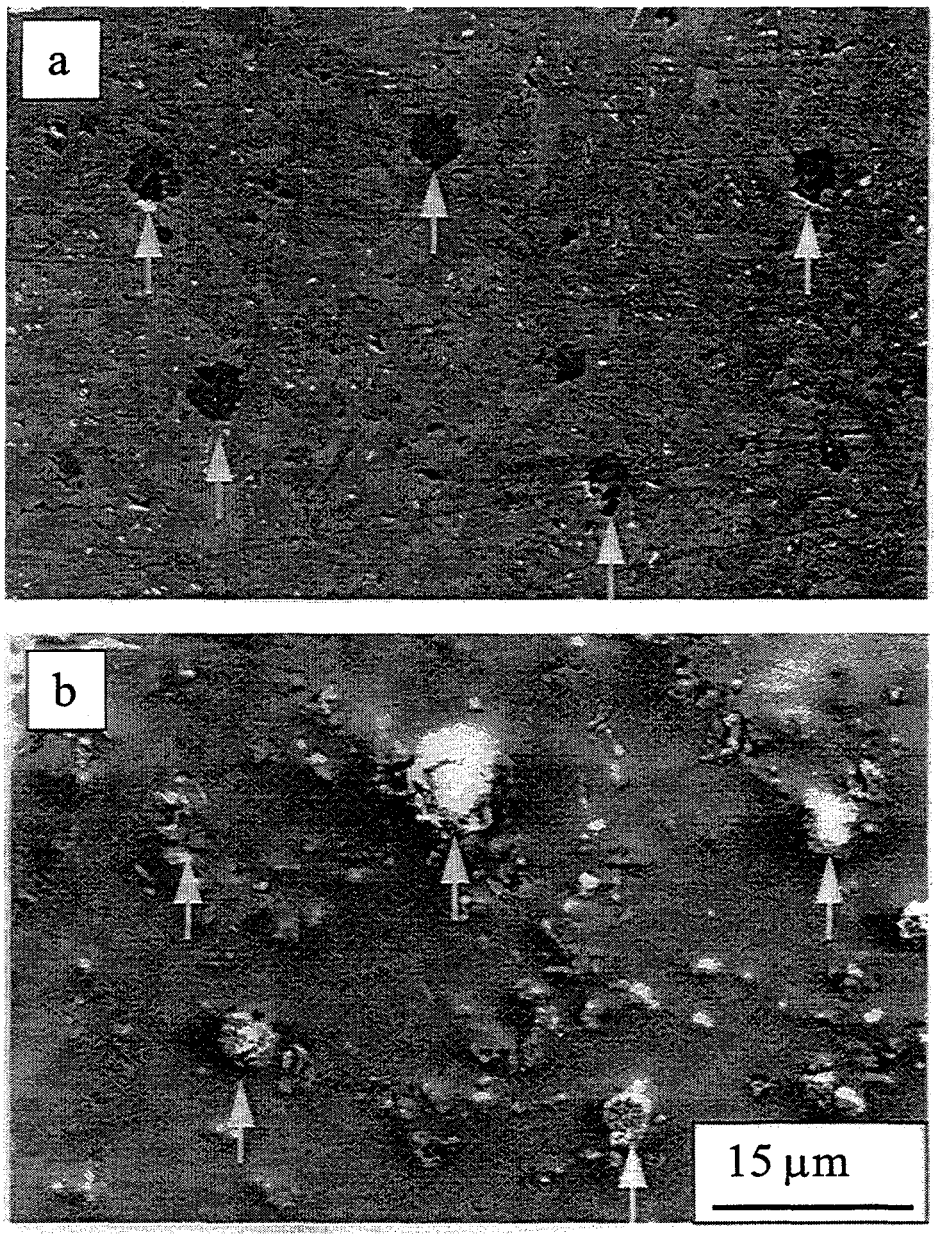

Fig. 4-3 SEM micrographs of the same area of polished and oxidized surfaces of the ABC-SiC (sample C): a polished surface (a) and the oxidized surface (b). Bubble formation correlated to the secondary inclusions.

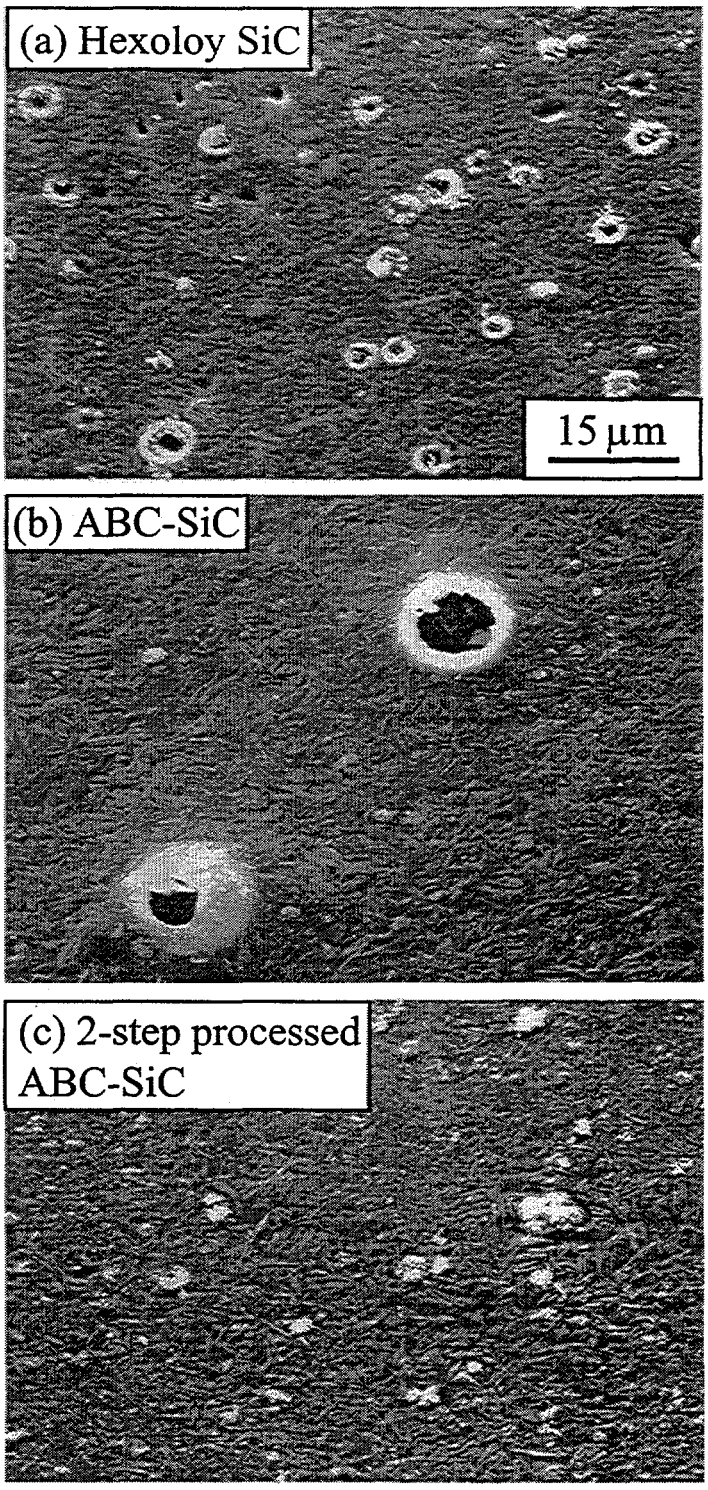

Fig. 4-4 SEM top views of oxidized SiC materials: Hexoloy SiC (a), ABC-SiC (b), and a two-step processed ABC-SiC (c).

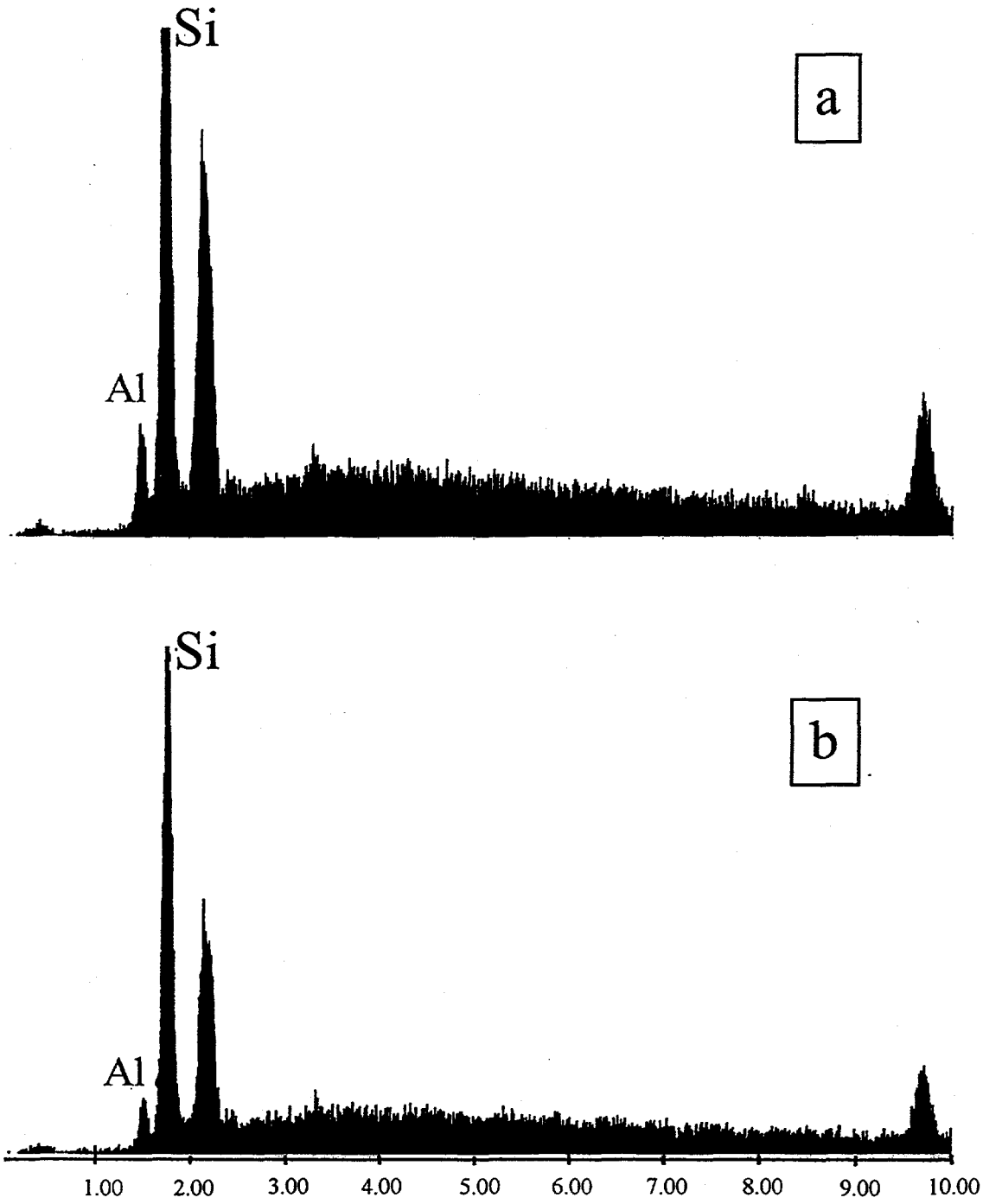

Fig. 4-5 EDS spectra acquired of the oxide scales on a hot-pressed ABC-SiC (a) and on a two-step processed ABC-SiC (b).

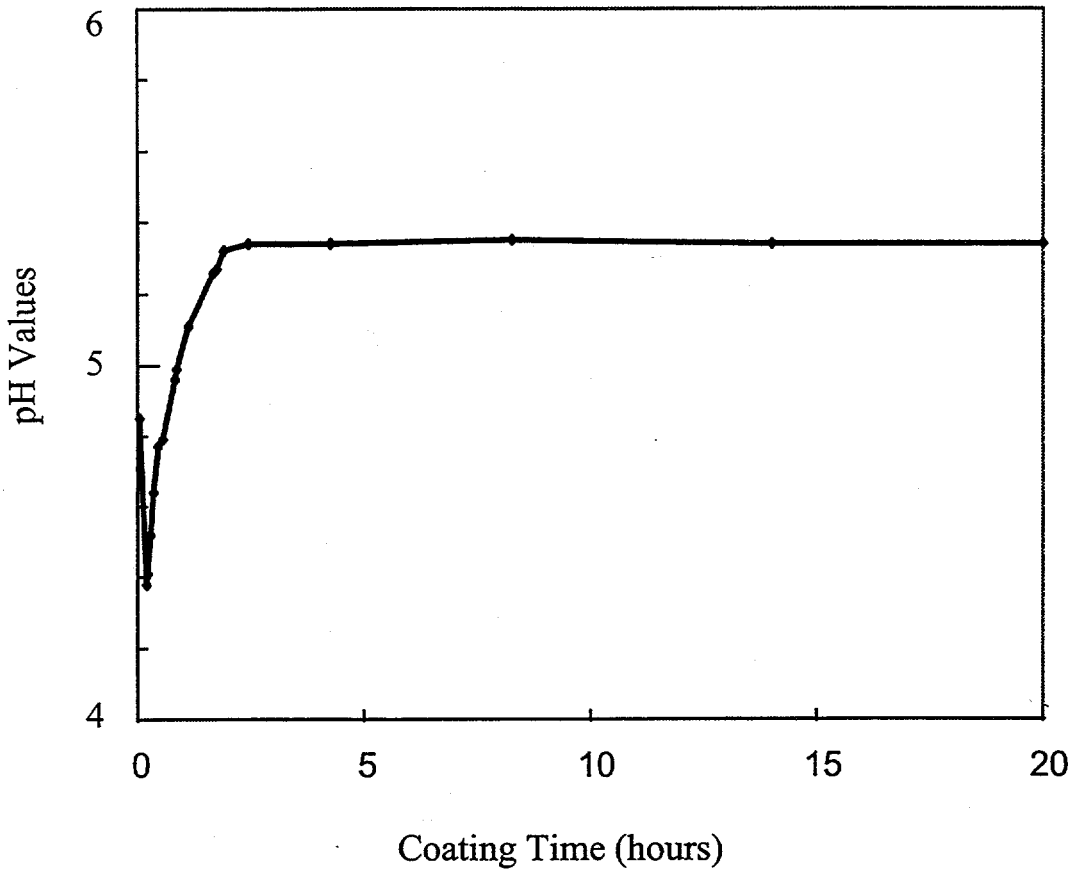

Fig. 5-1 The pH values of the solution in an yttria-precursor coating run.

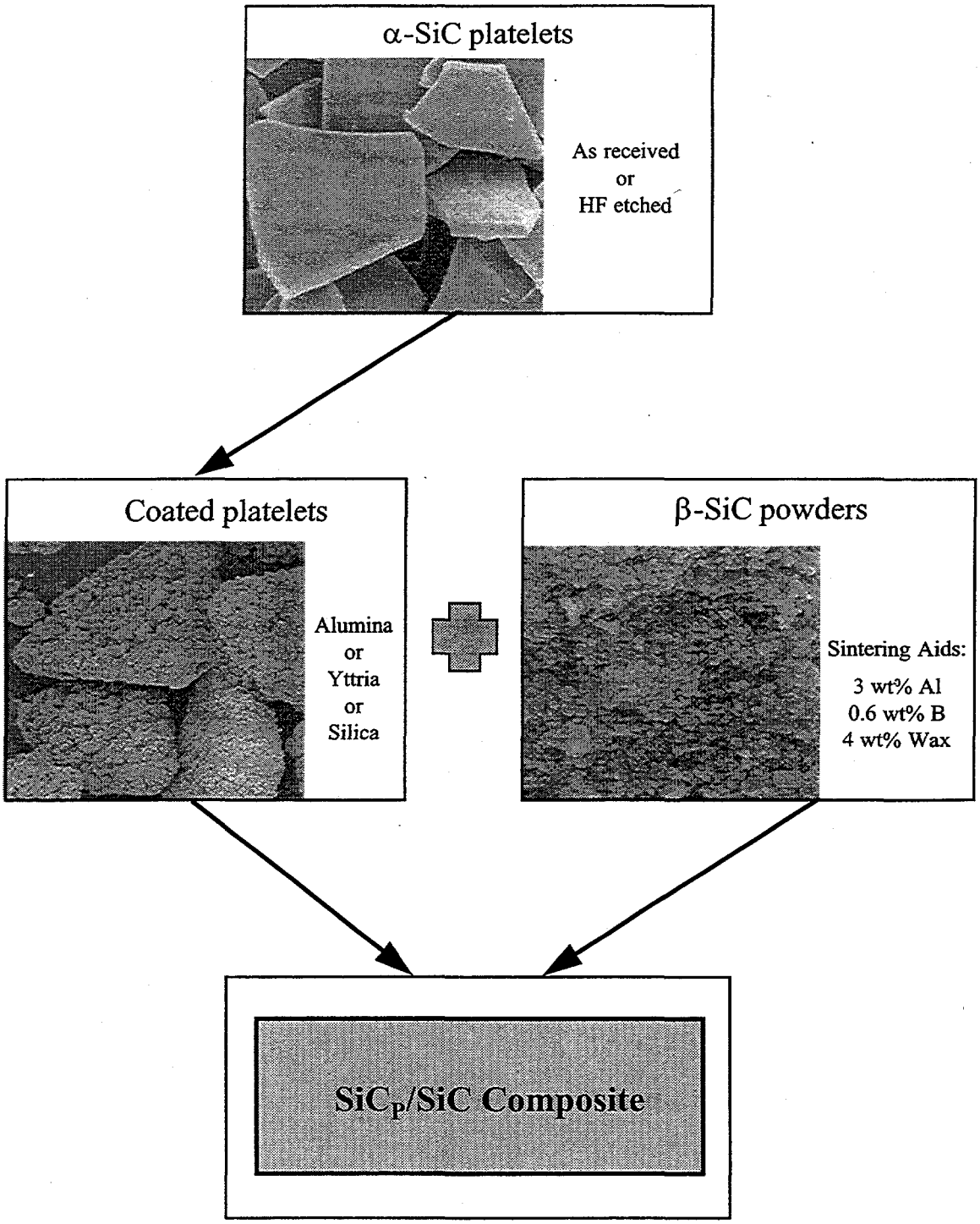

Fig. 5-2 A schematic processing route for oxide-encapsulated SiCp / SiC composites. SiC platelets were encapsulated with either alumina, yttria, or silica. The β-SiC powders were mixtured with 3 wt% Al, 0.6 wt% B, and 2 wt% C snitering aids. After mixing the coated platelets with the β-SiC powders, the composites were hot pressed at various temperatures.

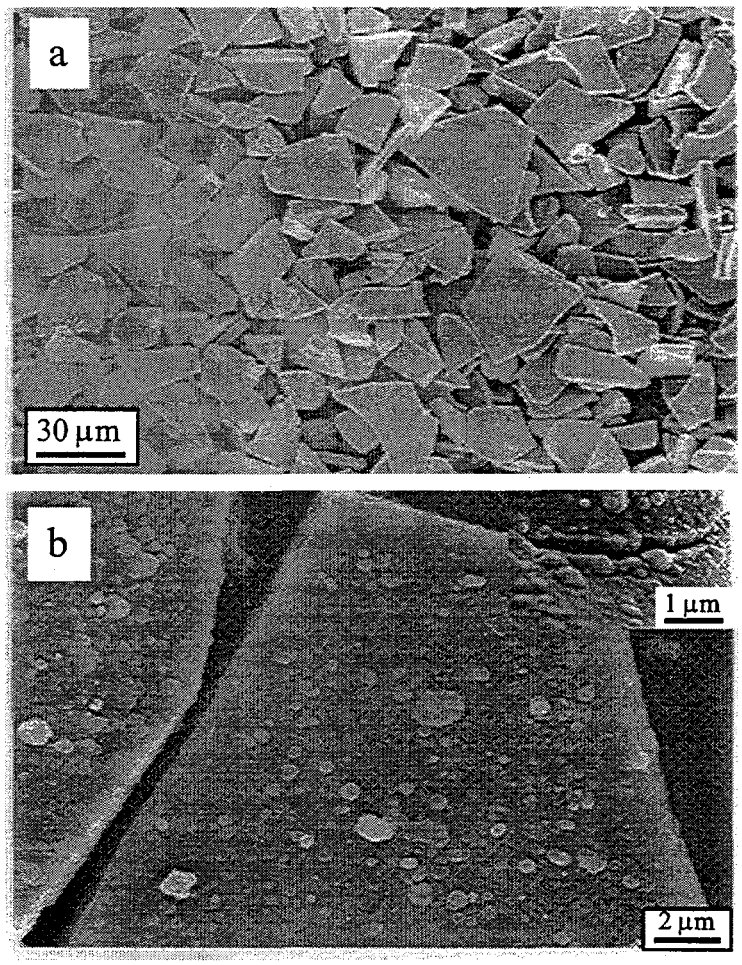

Fig. 5-3 SEM micrographs of the uncoated (a) and yttria-coated (b) SiC platelets. Annealing the coated platelets at an excessive temperature (900°C) induced cracking in the coating (see insert).

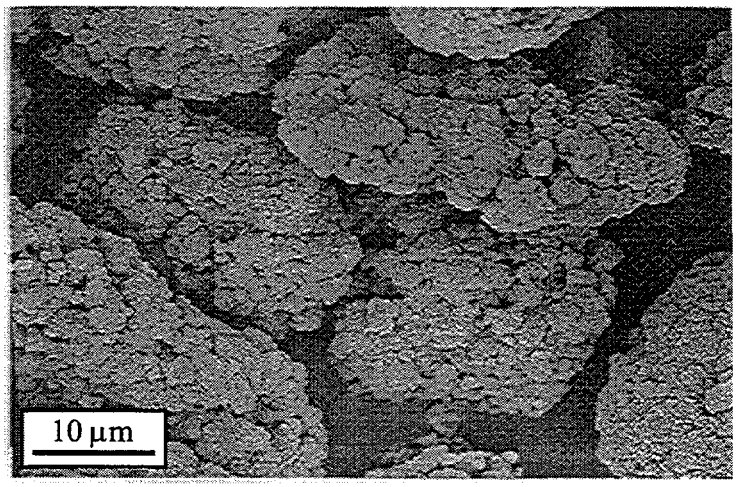

Fig. 5-4 SEM micrograph of alumina-coated SiC platelets.

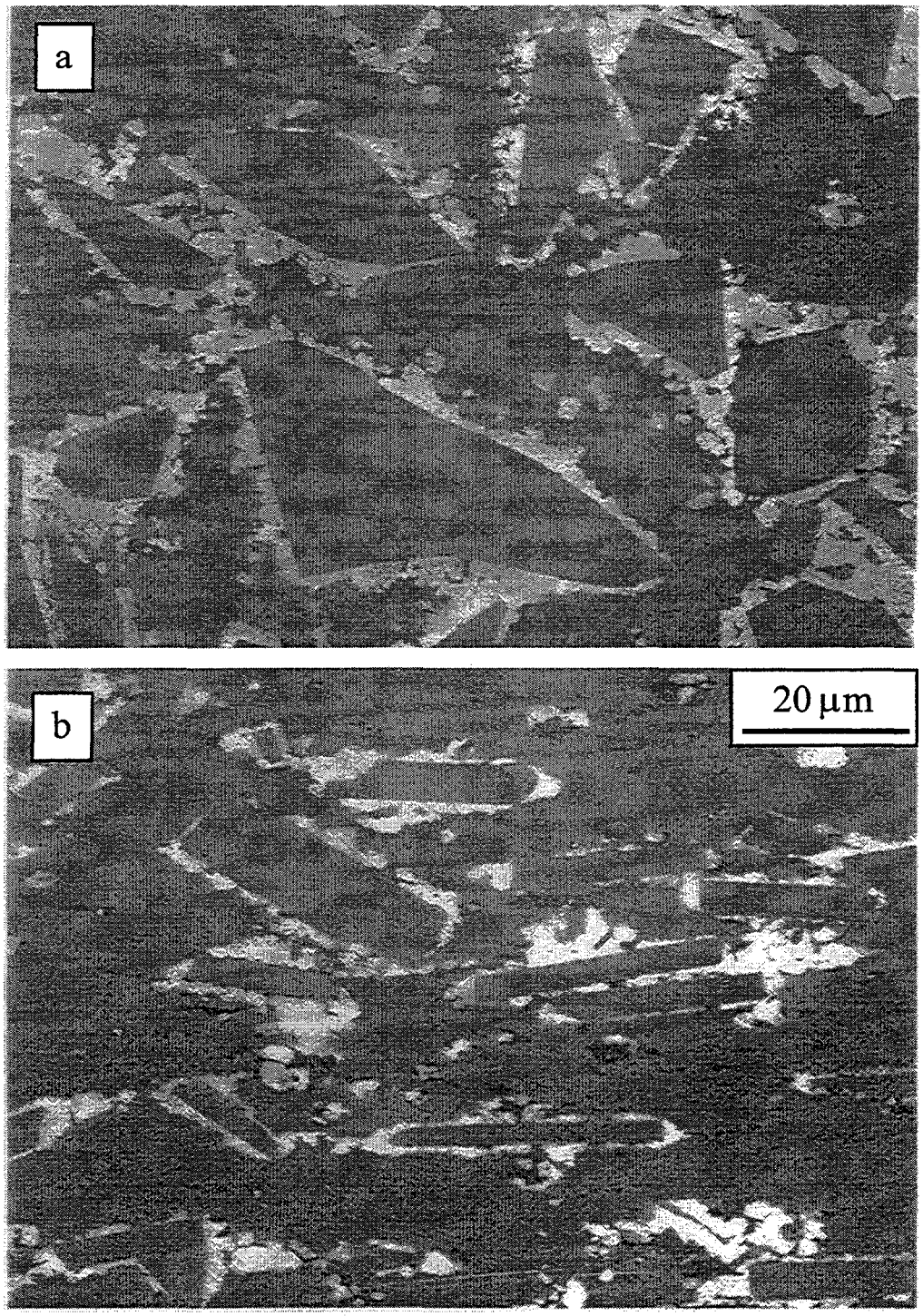

Fig. 5-5 SEM micrographs of polished surfaces of a SiC composite hot pressed at 1700°C: a) of a surface perpendicular to the hot pressing direction and b) of a surface parallel to the hot pressing direction. The composite is near fully dense. The alumina-coating provides a continuous barrier to protect the integrity of the platelets and a weak interphase.

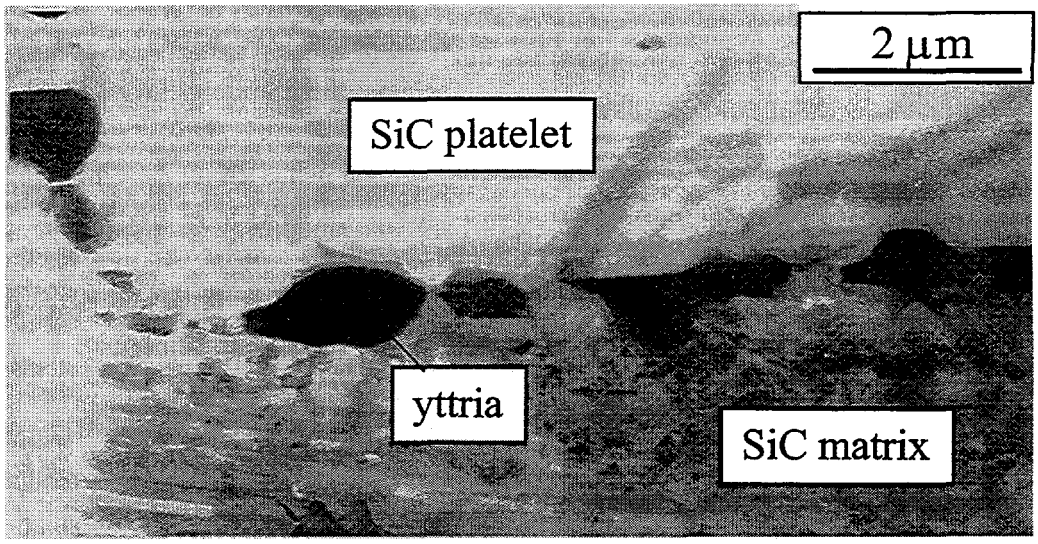

Fig. 5-6 TEM micrograph of a SiC composite with yttria-coated platelets. Note that the yttria coating changed its morphology to discrete islands after hot pressing of the composite (courtesy of M. Niu).

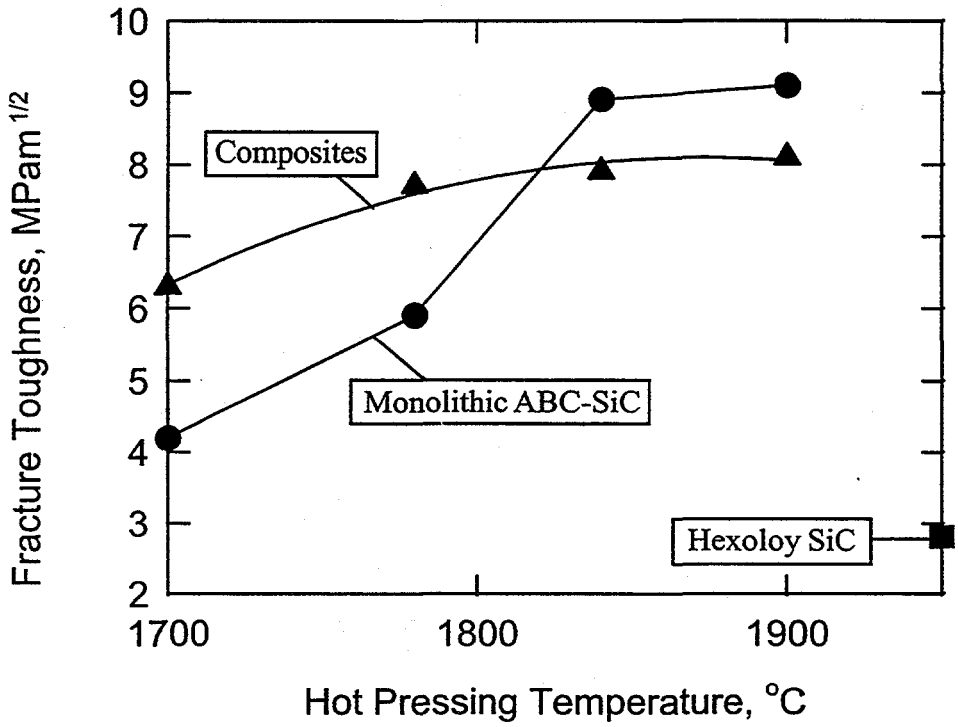

Fig. 5-7 Fracture toughness of monolithic ABC-SiC and alumina-coated SiC platelets reinforced SiC composites hot pressed at various temperatures. The toughness of a commercial Hexoloy SiC, measured under identical conditions, is also shown for comparison.